..noi le accenneremo di volo, ma senza che la brevità nuoca all'intento…

(Sinibaldi, C., 1802)

Università di Bologna

Scuola di Dottorato in Scienze della Terra

Ciclo XXII

Coordinatore

Prof. Roberto Barbieri

Geological and Structural evolution of the Eurasia Africa plate boundary in the Gulf of Cadiz

Central Eastern Atlantic Sea.

Candidato

Filippo D'Oriano

Tutore

Prof.ssa Rossella Capozzi

Cotutore

Dott. Nevio Zitellini

Abstract

Iberia Africa plate boundary, cross, roughly W-E, connecting the eastern Atlantic Ocean from Azores triple junction to the Continental margin of Morocco. Relative movement between the two plate change along the boundary, from transtensive near the Azores archipelago, through trascurrent movement in the middle at the Gloria Fracture Zone, to transpressive in the Gulf of Cadiz area. This study presents the results of geophysical and geological analysis on the plate boundary area offshore Gibraltar. The main topic is to clarify the geodynamic evolution of this area from Oligocene to Quaternary. Recent studies have shown that the new plate boundary is represented by a 600 km long set of aligned, dextral trascurrent faults (the SWIM lineaments) connecting the Gloria fault to the Riff orogene. The western termination of these lineaments crosscuts the Gibraltar accretionary prism and seems to reach the Moroccan continental shelf.

In the past two years newly acquired bathymetric data collected in the Moroccan offshore permit to enlighten the present position of the eastern portion of the plate boundary, previously thought to be a diffuse plate boundary.

The plate boundary evolution, from the onset of compression in the Oligocene to the Late Pliocene activation of trascurrent structures, is not yet well constrained. The review of available seismics lines, gravity and bathymetric data, together with the analysis of new acquired bathymetric and high resolution seismic data offshore Morocco, allows to understand how the deformation acted at lithospheric scale under the compressive regime. Lithospheric folding in the area is suggested, and a new conceptual model is proposed for the propagation of the deformation acting in the brittle crust during this process. Our results show that lithospheric folding, both in oceanic and thinned continental crust, produced large wavelength synclines bounded by short wavelength, top thrust, anticlines. Two of these

anticlines are located in the Gulf of Cadiz, and are represented by the Gorringe Ridge and Coral Patch seamounts. Lithospheric folding probably interacted with the Monchique – Madeira hotspot during the 72 Ma to Recent, NNE – SSW transit. Plume related volcanism is for the first time described on top of the Coral Patch seamount, where nine volcanoes are found by means of bathymetric data. ^{40}Ar-39Ar age of 31.4±1.98 Ma are measured from one rock sample of one of these volcanoes. Analysis on biogenic samples show how the Coral Patch act as a starved offshore seamount since the Chattian. We proposed that compression stress formed lithospheric scale structures playing as a reserved lane for the upwelling of mantle material during the hotspot transit. The interaction between lithospheric folding and the hotspot emplacement can be also responsible for the irregularly spacing, and anomalous alignments, of individual islands and seamounts belonging to the Monchique - Madeira hotspot.

Riassunto

Il limite di placca tra Iberia e Africa nell'oceano Atlantico centrale si estende dalla giunzione tripla delle Azzorre ad est fino all' orogene betico-rifano verso ovest. Il regime tettonico lungo il limite di placca varia da transtensivo nei pressi delle Azzorre, trascorrente lungo la zona di frattura Gloria, a compressivo nell'area del Golfo di Cadice. Qui la velocità di convergenza tra le due placche è attualmente di 4 mm/a (DeMets et al. 1994). Negli ultimi anni il Golfo di Cadice è stato interpretato come un limite diffuso di placca. Recentemente è stata scoperta una serie di lineamenti morfologici (lineamenti SWIM, dal progetto europeo che ha acquisito i dati batimetrici che hanno permesso la loro individuazione) attribuiti a strutture trascorrenti che interessano tutto il Golfo di Cadice. Questi sono stati proposti da Zitellini et al. (2009) come costituire il probabile limite di placca tra Iberia e Africa a partire dal Pliocene Superiore (2 Ma). I lineamenti connettono la zona di frattura Gloria con il margine Marocchino e la catena Betico Rifana. Su questo margine, a seguito di una campagna oceanografica avvenuta nel 2008 è stato possibile caratterizzare i lineamenti tramite batimetria ad alta risoluzione e sismica CHIRP. I lineamenti in questo settore si impostano sul prisma di accrezione di Gibilterra, causando evidenti fenomeni gravitativi nella sua parte superficiale.

Uno degli obbiettivi di questa tesi è stato inoltre lo studio delle deformazioni a scala litosferica a partire dall'Oligocene fino ad oggi. La riattivazione di questo margine in regime compressivo è avvenuta a causa della rotazione antioraria di Iberia a partire dall'Oligocene. Tramite lo studio di linee sismiche e dati gravimetrici è stato proposto che a partire dall'Oligocene l'area del Golfo di Cadice sia stata interessata da piegamenti litosferici. Inoltre è stato possibile proporre un nuovo modello concettuale di come si manifestino nella crosta superiore processi legati a piegamento litosferico. Questo modello prevede che si formino

sinclinali ad ampia lunghezza d'onda (30 – 140 km) seguite da anticlinali con lunghezze d'onda minori (10 – 80 km).

L'area in esame è stata interessata a partire da 72 Ma dal transito del punto caldo Monchique – Madeira. Numerosi monti sottomarini e piccole colline abissali ne segnano la traccia. In questo lavoro per la prima volta viene descritto in dettaglio uno di questi, il monte sottomarino Coral Patch. Nove edifici vulcanici minori sono stati descritti sulla sua sommità e uno di questi, campionato durante una crociera oceanografica nel 2004, è stato datato a 31 Ma. Inoltre è stato ipotizzato che il magmatismo nell'area abbia interagito con i processi di piegamento litosferico. Questa interazione ha portato ad una distribuzione anomala dei vulcani che spesso, come nel caso del Coral Patch, si allineano lungo le zone di debolezza litosferica causate dai processi tettonici.

Table of contents

Table of Figures out of the submitted papers

1 Introduction

1.1 Study area

The Gulf of Cadiz is the portion of the Eastern - Central Atlantic bounded by South Iberia and Northwest Morocco (Fig. 1.1.1). Here is located the Eastern end of the Azores-Gibraltar plate boundary. Nowadays, the kinematic of this plate boundary show a progressive change from extension at the Azores, pure right lateral strike slip in the middle at the Gloria trascurrent fault, compression in the Gulf of Cadiz with a relative plate velocity of about 4 mm/a (Argus et al., 1989, DeMets et al., 1994). To the East, the Azores - Gibraltar plate boundary ends against the Gibraltar accretionary prism (Fig. 1.1.2) formed by the westward motion of the Betic – Rif orogenic arc.
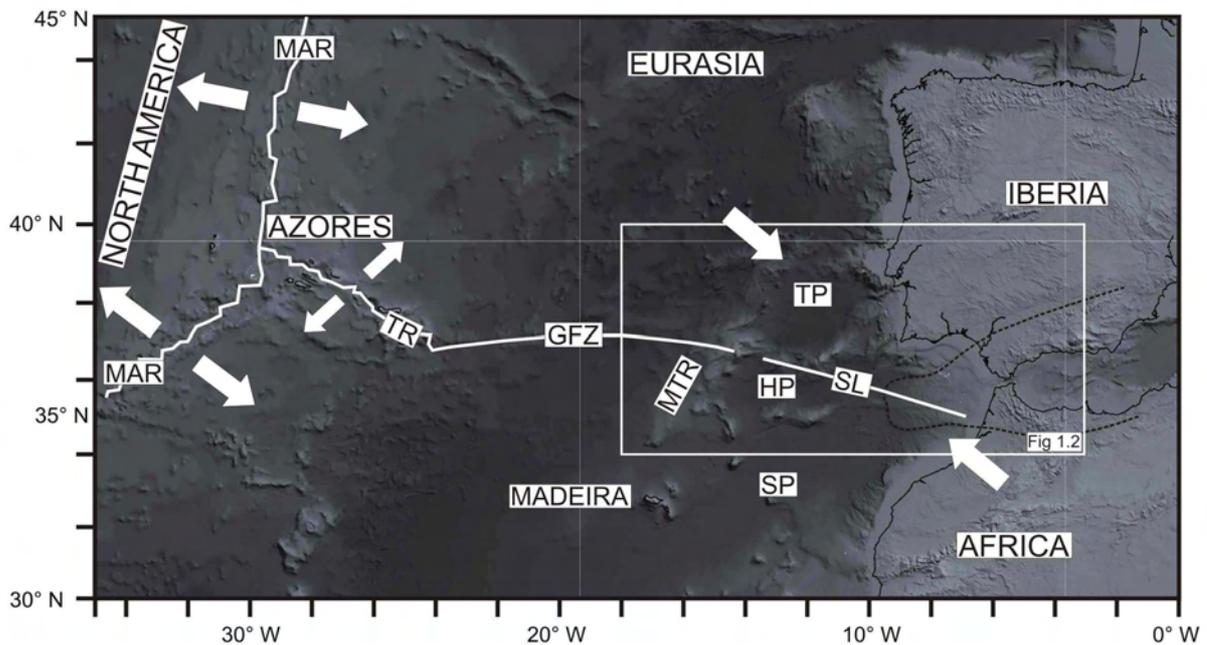
Figure 1.1.1 Central Atlantic Sea. MAR: Mid Atlantic Ridge; TR: Terceira Ridge; GFZ: Gloria Fracture Zone; MTR: Madeira Tore Rise; SL: SWIM Lineaments; TP: Tagus abyssal Plain; HP: Horseshoe abyssal Plain; SP: Seine abyssal Plaine; Dashed line; Betic-Rifean Front; White box outlines area of figure 1.2; White arrows indicate relative plate motion along the plate boundaries.

Several huge seamounts are present offshore in the Gulf of Cadiz, as the Gorringe Ridge and the Coral Patch seamounts. Associated to these seamounts are the greatest geoid anomaly in

9

the Atlantic sea with a gravity anomaly of about 400 mGal at the Gorringe and 200 mGal at the Coral Patch (Sandwell and Smith, 1997).
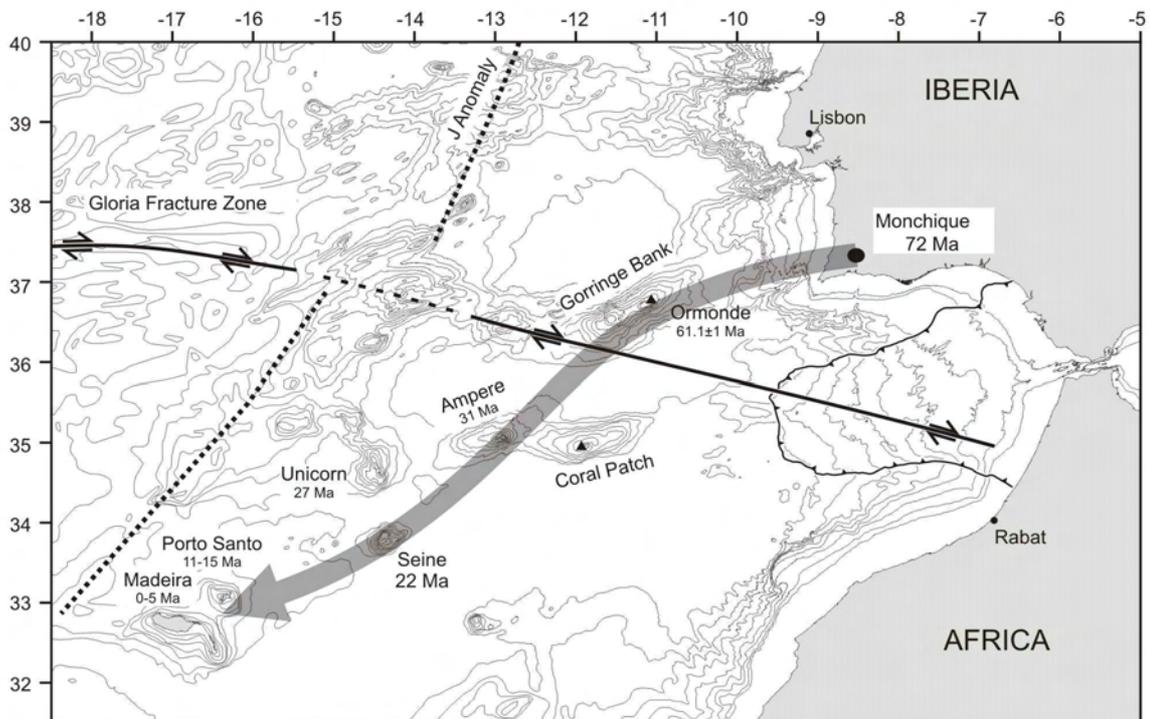
Figure 1.1.2 Study area. Thin solid line, Gibraltar accretionary prism; thick solid line Gloria fracture zone and SWIM lineaments; grey arrow, track of the Monchique – Madeira hotspot.

Natural seismicity is heavily concentrated along the Gloria Fracture Zone, while it becomes scattered in the Gulf of Cadiz and Gibraltar region (Fig 1.1.3). In this area the seismicity is located preferentially offshore South Iberia and it is not focused on some particular structures (Grimison and Chen, 1986).

In the last 15 years, this sector of the Eurasia – Africa plate boundary was interpreted as a diffuse plate boundary (Sartori et al., 1994, Hayward, 1996). In particular, Sartori et al. (1994) showed that the compressional deformation is NW-SE trending, and distributed over a wide region. The Gulf of Cadiz is also the source area of several high- magnitude earthquakes, as the 1755 Great Lisbon earthquake with an estimate magnitude of M=8.5 to 8.7 (Martinez-Solares and López Arroyo, 2004). The earthquake was followed by the largest tsunamis ever

experienced in the Western Europe Atlantic margin and was observed as far as the Caribbean and North American coasts. In the past twenty years several international project were focused on the area. Thanks to these efforts a huge geophysical and geological dataset was collected.
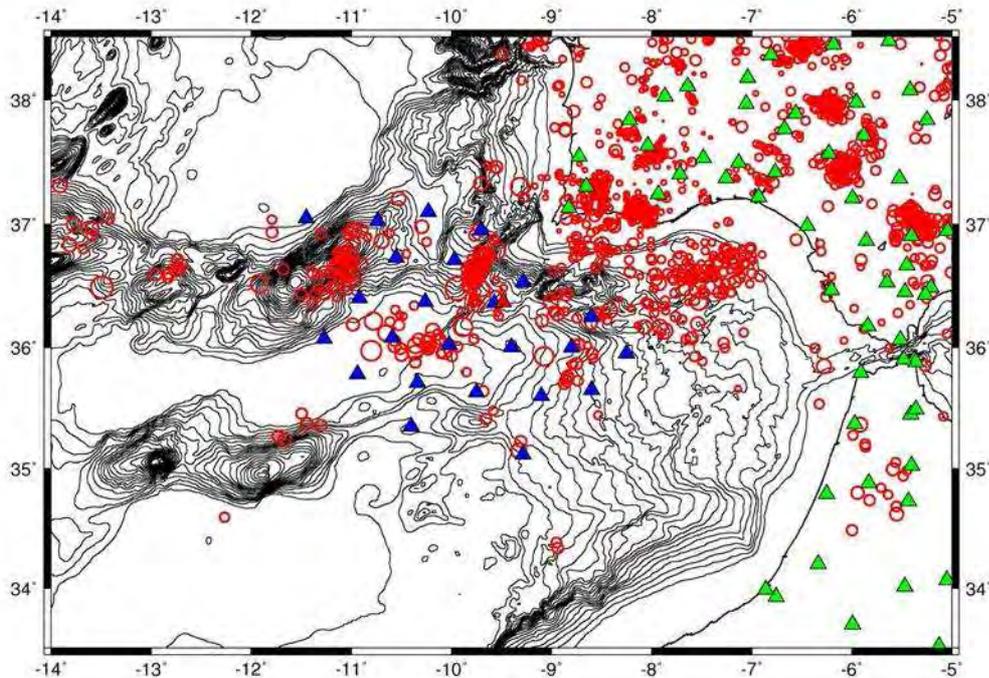
Figure 1.1.3 Natural seismicity of the Gulf of Cadiz and surrounding area, from August 2007 to April 2008, recorded during the NEAREST project. Blue triangle, OBS station; green triangle, land seismometers station

The Gulf of Cadiz was almost completely mapped by means of high-resolution bathymetry and geophysical seismic data during the ESF SWIM project to constrain the major active structures of the area (Gracia et al., 2003; Zitellini et al., 2004). After the SWIM project new bathymetric compilation is now available (*The SWIM multibeam compilation,* Zitellini et al., 2009). The SWIM compilation revealed a new set of lineaments, that were called the *SWIM lineaments*, cross cutting the Gulf of Cadiz from the eastern termination of the Gloria fault to the NW Moroccan offshore. Zitellini et al. (2009) proposed this structures to be the recent plate boundary between Iberia and Africa (Fig 1.1.4) and Rosas et al. (2009) showed how, in the last 2 Ma, the deformation was active on these trascurrent structures.

11
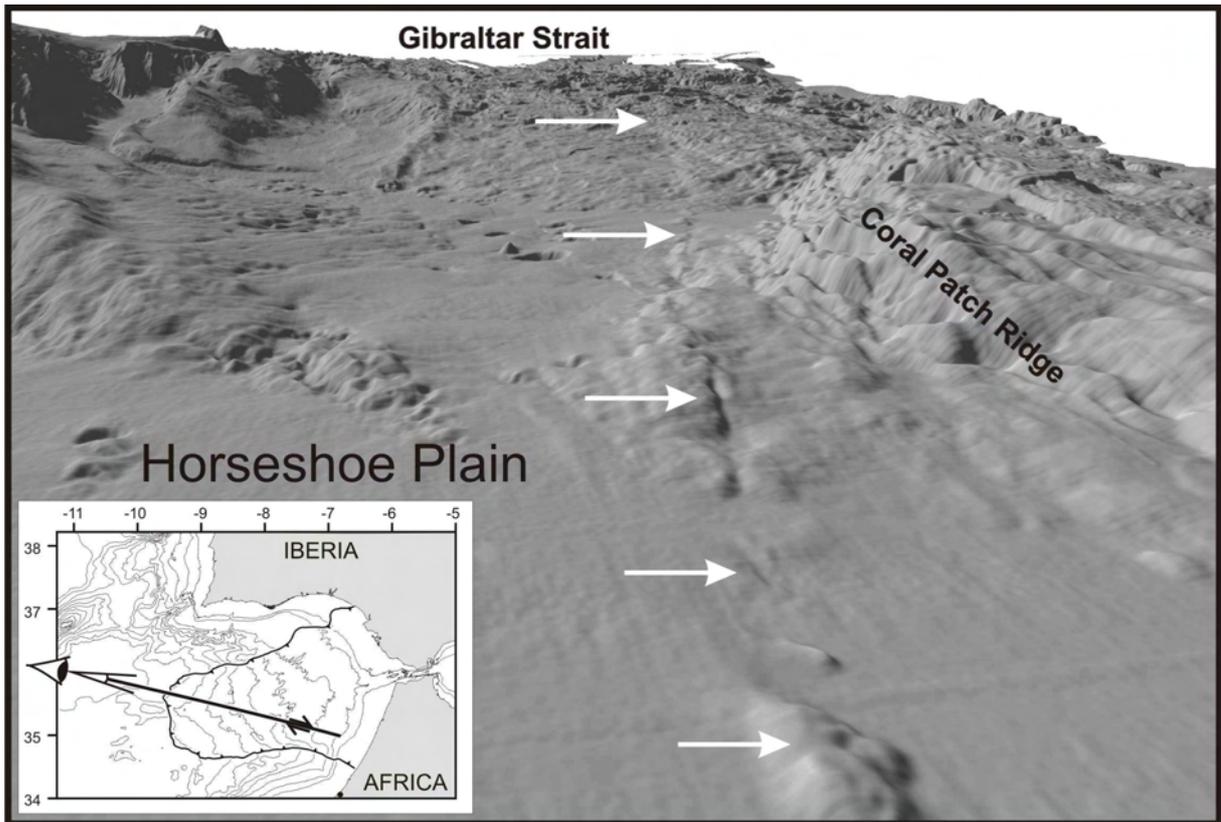
Figure 1.1.4 SWIM lineaments cross-cutting Horseshoe Abyssal plain and the Gibraltar accretionary prism. West to East view. Vertical exaggeration 5X.

The Gulf of Cadiz evolution was also influenced by the transit of the Madeira – Monchique hotspot. The track of this hotspot is underlined by a 700 km long, 200 km wide chain of volcanic abyssal hills and seamounts (Fig. 1.1.2). The hotspot volcanism spans in age from the 70-72 Ma at the Monchique volcanic field, in South Portugal, to 14-0 Ma volcanism at Madeira archipelago (Morgan, 1981; Geldmacher et al., 2000). Up to day several aspect of this volcanism are still matter of debate: for example the alignment of seamounts such as the Coral Patch and Ormonde offsets the trace axis (Geldmacher et al., 2005). This anomalous feature of the Monchique – Madeira hotspot track is explained either as related to (1) a volcanism locally controlled by lithospheric discontinuities or (2) magmatism, possibly related to a weak pulsating plume (Merle et al, 2006; Geldmacher et al., 2005). In addiction,

the interaction of volcanism with tectonic processes nearby the plate boundary is still not yet well understood because of the scarce information about its submerged part.

1.2 Objectives

Aim of this work is to understand the tectonic processes, at crustal and lithospheric scale, acting in the area from the onset of the counterclockwise rotation of Iberia, during Oligocene, and the consequent reactivation of the Azores Gibraltar plate boundary between Iberia and Africa. The rotation of Iberia caused extension in the Bay of Biscay and the reactivation of a compressive stress regime offshore SW Iberia and in the Gulf of Cadiz. This study intend mainly to enlighten the processes that were active during this compressive stage.

In this work, the interaction between tectonic setting and the alkaline hotspot volcanism belonging to the Madeira – Monchique volcanic province, is also analyzed. This volcanism is present in the area from Late Cretaceous in South Portugal to Recent at the Madeira archipelago.

Furthermore, in this study the deformation associated to the WNW-ESE-oriented dextral strike-slip movement across the Gibraltar accretionary prism in the vicinity of the Moroccan coast is analyzed.

1.3 Structure of the work

This thesis is constituted by seven chapters. After a general introduction on the study area (chapter 1), the principal data and methodology used during this work are shown in chapter 2. Geological and Geomorphological setting of the study area are treated in chapter 3. Chapter 4 presents a paper "submitted to Geology" focused on the mode of deformation acting near the Plate boundary, from Eocene to Pleistocene, while Chapter 5, contains a work on the tectonic process acting in this sector from Pleistocene to Recent, along and in the vicinity of the WNW

– ESE SWIM faults, on the plate boundary offshore Morocco. The following chapter 6, presents a paper concerning volcanism episodes not related to the opening of the Atlantic Ocean and examine the interaction of this volcanism with the tectonic processes acting in the area. This paper is submitted to Terra Nova. The main conclusions of this work are discussed in Chapter 7.

2 Data and methodology

2.1 Swath bathymetry

In the last decade the Gulf of Cadiz has been intensively investigated. One of the major outcomes of these researches was the publication of the *"Bathymetry of the Gulf of Cadiz, North-East Atlantic: the SWIM multibeam compilation"* (Zitellini et al., 2009). This map is the result of a collaboration with several European and Italian scientific partners, 19 surveys for more than 200 days (Enclosure 1). The map was built from a dtm with 100 m x 100 m cells resolution and the digital data are available on line as supplementary material with cells resolution of 250 m x 250 m.

Model	RESON SeaBat 8160
Operating frequency:	50 KHz
Swath angle:	150°
Operating Depth:	5 – 3000 mt
Beam number:	126
Vertical resolution:	1.4 cm with range until 750 m 2.9 cm with range between 1000 m and 1500 m 8.6 cm with range between 1500 m and 2500 m

TABLE 2.1 Technical parameter of the RESON multibeam system of the R/V *Urania* during the NEAREST cruises.

Two of the surveys mentioned above were the Nearest 2007 and Nearest 2008 cruises carried out in the frame of the European project NEAREST (*http://nearest.bo.ismar.cnr.it*). Two bathymetric surveys were acquired and began part of the compilation. The research cruise was carried out with the 61 meter R/V *Urania*, owned and operated by SO.PRO.MAR. and on long-term lease to CNR. I had the opportunity to be on board and to acquire and reprocess the data at the *Centro di Calcolo* facilities in ISMAR-Bo.

R/V *Urania* was equipped with a RESON 8160 multibeam systems and a DGPS FUGRO positioning system. The navigation and the bathymetric acquisition was done with the PDS2000 software by RESON. During the acquisition CTD casts were performed to calibrate the Sound velocity values on the acquisition software (Table 2.1).

The data was stored in SIMRAD binary format (*.all) to be reprocessed by the most common bathymetric processing software. To reprocess the data I used the: NEPTUNE / Konsgberg, CARAIBES / Ifremer and MB system / Columbia University (Caress and Chayes, 2009) softwares. After reprocess classical digital terrain model (dtm) are built using GMT (Wessel and Smith, 1995 & 1998) to make bathymetric map.

NEAREST 2007 survey was done on the South Portuguese continental shelf offshore Portimao (Fig. 2.1.1). This survey covers 400 km^2 of the external continental shelf and the first part of the continental slope at depth between 100 m bsl and 300 m bsl. The shelf is characterized by a general flat morphology, somewhere interrupted by meter scale high hundreds meters long, bedrock ridges. The southern margin of the continental shelf and the slope characterized by the head of three small arcuate canyons. These develop on a 11° dip slope and connect to the continental shelf through a structural flat area at 300 m bsl.

The results of NEAREST 2008 survey offshore Morocco are presented and discussed on chapter 5.
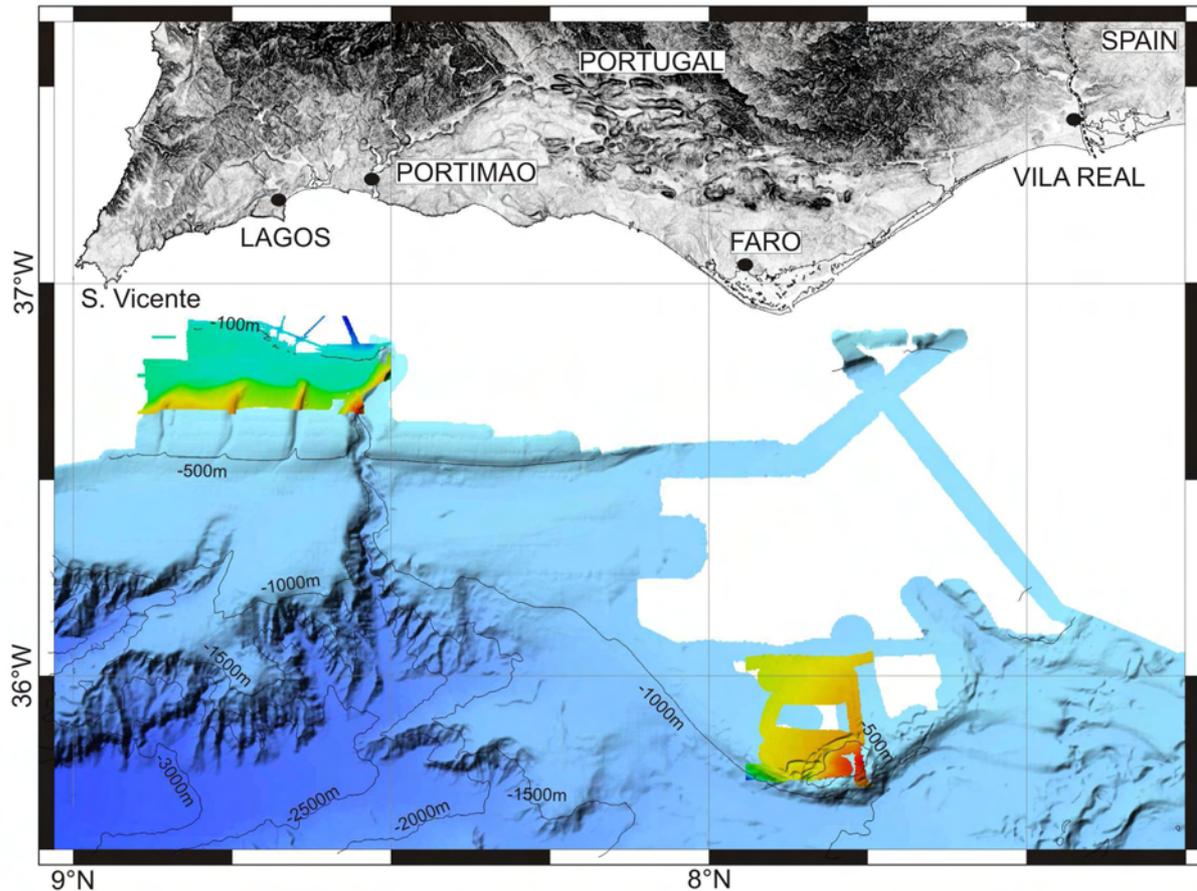
Figure 2.1.1 NEAREST 2007 survey, bathymetric shaded relief map (Coloured area: 25 m x 25 m cell size resolution). Blue bathymetry from Gulf of Cadiz Multibeam Compilation (Zitellini et al., 2009) 100 m x 100 m grid resolution.

2.2 High-resolution CHIRP seismic

Hull-mounted and towed sub-bottom profilers have become common within the academic community and are typically acquired during high-resolution multibeam bathymetric surveys. Sub-bottom profilers emit a chirp signal that characterized by frequencies of 3-7 KHz which often penetrates the bottom 100 meters or more. Sub-bottom profilers get more deep penetration with low frequency, thus a chirp center frequency near the "old" 3.5 kilohertz is generally used (Henkart, 2009).

The high-resolution sub-bottom seismic data, acquired during NEAREST 2007 and 2008 cruises with a BENTHOS CHIRP II (Table 2.2), were processed with SeisPrho (ISMAR) software (Gasperini and Stanghellini, 2009). The program allows the users to handle SEG-Y

data files (and other non-standard formats) carrying out a processing sequence over the data to obtain, as a final result, bitmap images of seismic sections. The resulting images have been interpreted on screen or printed, then the interpretation was reported on cartographic software as QGis or GMT. During this three years a large database of sub bottom lines acquired during several oceanographic cruises has been created using GIS software.

Factory	Benthos
Model	Chirp II
Installation	Hull mounted
Number of transducers	16
Transducers type	AT 471
Signal generator / DSP	CAP-6600 Chirp II Workstation
DSP Sonar Signal Processing	16 bit A/D, continuous FFT
Operating sweep frequency	2 – 7 kHz
Ping rate	Variable, operator selectable (max 12 ping/sec)
Sweep Length	Variable, operator selectable
Multiping option	yes
Gain	Automatic gain control
Bottom tracking	Interactive
Navigation / Annotation	NMEA 0183
Data format	SEG Y
Printer	Alden
Acquisition software	SwanPRO / ChirpScan II
Processing software	SeisPRO / SwanPRO
Location controller / recorder	Recording room (room # 525)

Table 2.2 CHIRP seismic sub bottom profiler on board R/V *Urania* during NEAREST cruises.

During this period I had the chance to take part in two oceanographic surveys, the Nearest 2007 and Nearest 2008 cruises, in the area of the Gulf of Cadiz and to acquire directly Chirp data helpful to my study. In particular CHIRP data have been used for the geo-morphological interpretation of the NEAREST08 Morocco bathymetric survey (chapter 5) and for the geological interpretation of the Coral Patch seamount (chapter 6).

2.3 Seismic reflection data

2D seismic multichannel (MCS) data have been the main dataset used in this work. ISMAR-BO participated in the last 20 years to several international and national scientific projects during which a large dataset of seismic lines was acquired (Fig. 2.3.1). Data available and interpreted during this thesis belong to several survey: RIFANO 1992 (Sartori et al., 1994), BIGSET 1998 (Zitellini et al., 2004 a), VOLTAIRE 2004 (Zitellini et al., 2004 b), IAM 1993 (Banda et al., 1995), SWIM 06, SISMAR 2001 (Contrucci et al., 2004) and ONHYM-ONAREP 1987 (Flinch, 1993).
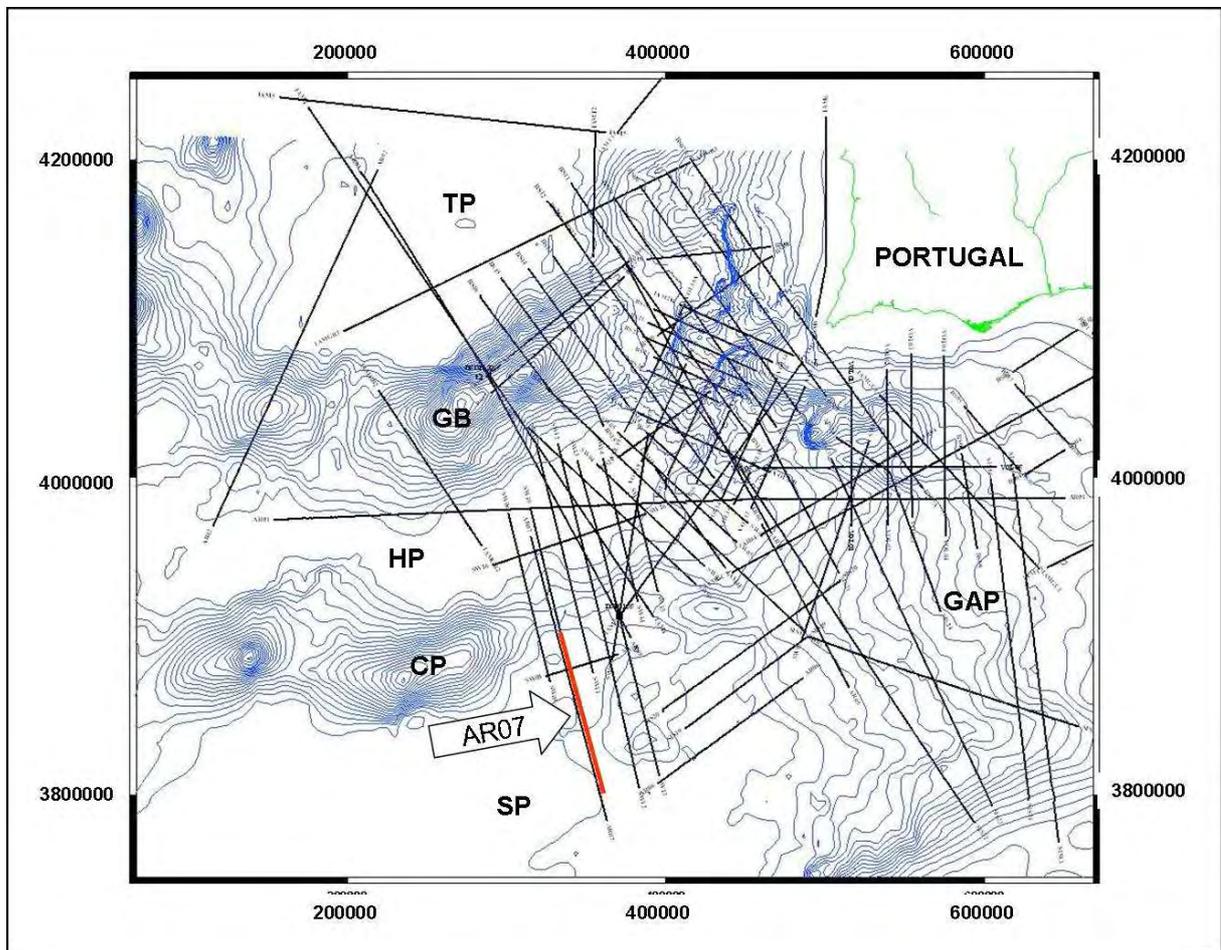
Figure 2.3.1 Seismic lines dataset collected in the last 15 years at ISMAR for the area offshore SW Iberia. TP: Tagus abyssal Plain; GB: Gorringe Bank; HP: Horseshoe abyssal Plain; CP: Coral Patch; SP: Seine abyssal Plain; GAP: Gibraltar Accretionary Prism. Red line: Seismic AR07 line in Fig. 2.4.2.

Seismic interpretation is based on the recognizing of faults and unconformities, seismic facies and reflectors termination (Payton, 1977). Seismic facies are defined on the basis of change in reflection style including continuity, wavelength and amplitude (Mitchum et al., 1977; Bally 1987).
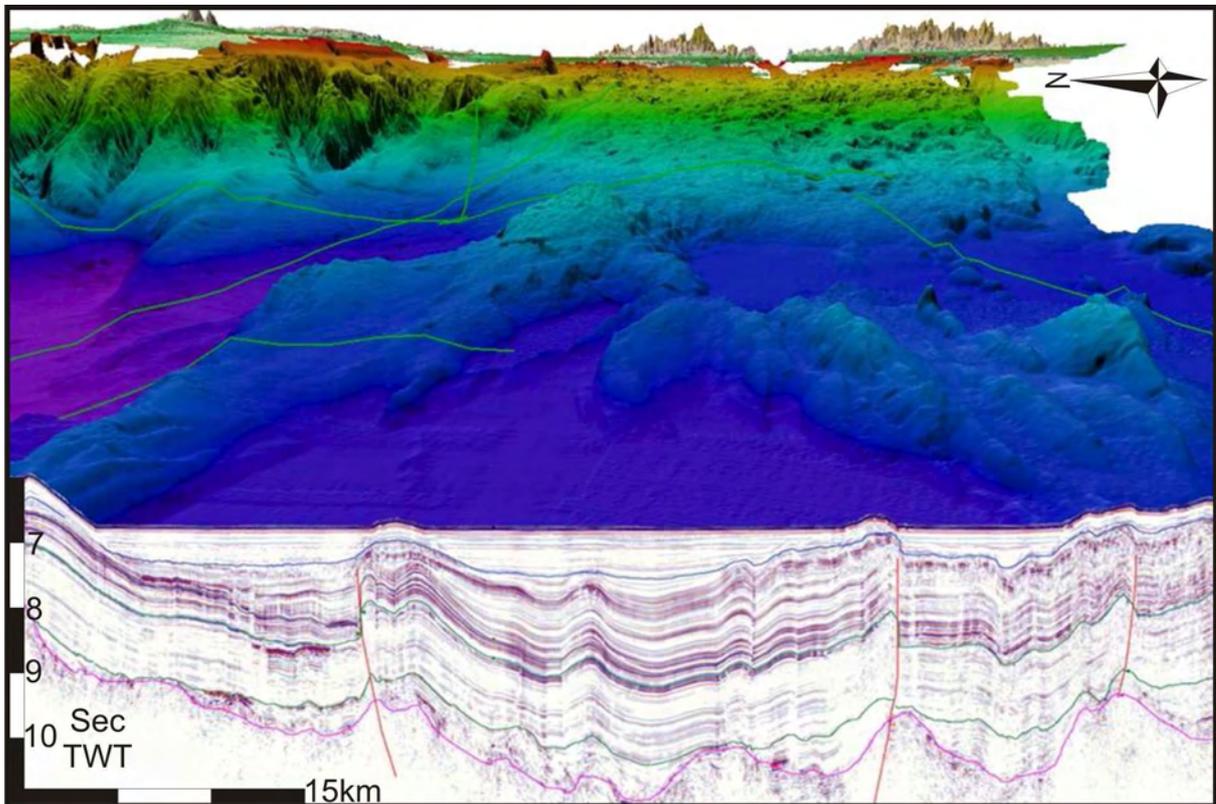
Figure 2.3.2 Seismic line AR 07 and 3D view bathymetry of the Gulf of Cadiz. (SW to NE view). Vertical scale in second Two way Time. For location see Fig. 2.4.1.

In particular for this thesis about 5000 km of MCS were interpreted. The review of these seismic dataset collected in the last 15 years at ISMAR-BO permits to directly correlate, for the first time, the principal regional unconformity in the three main basins of the area, Seine, Horseshoe and Tagus Abyssal plains. In turn, this allows to correlate the main tectonic events and their temporal development on the whole oceanic domain of the Gulf of Cadiz. The constraining of the temporal evolution of the main tectonic events, at regional scale, permits to better understand the events responsible of the main geological structures in the area at lithospheric scale.

3 Geomorphological, structural and geophysical setting of the Gulf of Cadiz

3.1 Structural Settings

Kinematic model proposed in the last 10 years (Rosembaun et al., 2002; Schettino & Scotese 2005) shows that the Gulf of Cadiz area was characterized by a poliphasic tectonic regime from the onset of Atlantic oceanization to Recent.

Palinspastic restoration, based on the study of oceanic magnetic anomaly lineations (Srivastava et al., 1990), show how the Eurasia - Africa plate boundary (Fig. 3.1.1) owns the present day configuration only since Late Oligocene times. Since first continental break-up, the region recorded complex plate interactions outlined in Fig.3.1.2.
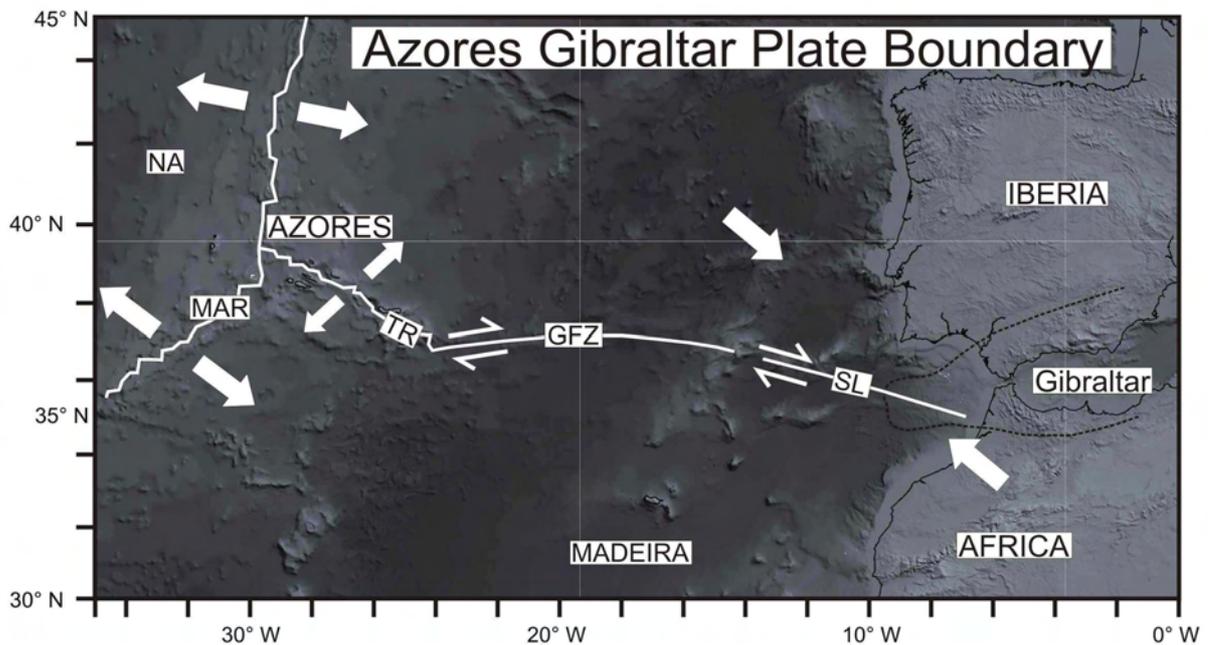
Figure 3.1.1 The Azores Gibraltar plate boundary Line (AGL); NA: North America Plate; MAR: Mid Atlantic Ridge; TR: Terceira Ridge; GFZ: Gloria Fracture Zone; SL: SWIM Lineaments; Dashed line mark the Betic Rifean chain.

The continental margins of South Iberia and Morocco formed during Jurassic continental break-up between North America and Africa while the western continental margin of Iberia formed as a result of the Cretaceous separation of from North America. As a consequence, the Tagus, Horseshoe and Seine Abyssal Plains correspond to oceanic crust of Late Jurassic-Early

Cretaceous age. Starting approximately from Chron M0 (~125 Ma) Iberia moved

independently until Chron 34 (~85 Ma) when appeared welded to Africa. At Chron 13 (~34

Ma), contemporaneously with the Pyrenean continental collision, the boundary jumped again

South of Iberia and only at Chron 6 reached the present day plate-tectonic configuration.
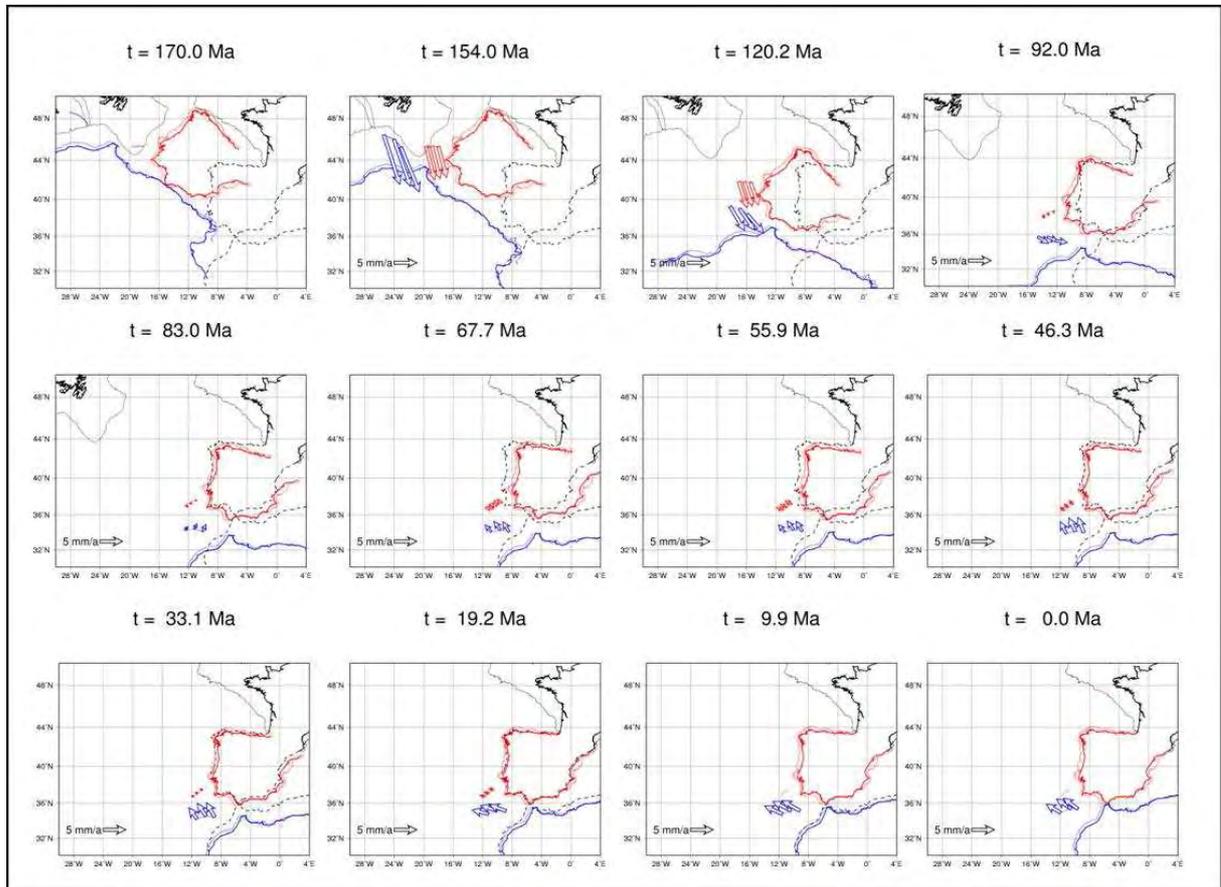
Figure 3.1.2 Plate kinematics reconstruction after Rosembaun et al., 2002, (in a fixed Eurasia references). Blue arrows: movement vectors for the Coral Patch Seamount; red arrows: movements vector for the Gorringe Bank. These two seamounts are chose to enlighten the stress field acting in the Horseshoe abyssal plain between them. Seismic lines permit to consider the Coral Patch as part of Africa plate and Gorringe Bank as part of Iberia plate since the Jurassic breakup.

The Europe-Africa plate boundary now trends roughly E-W, connecting the Azores-Triple

Junction to the Gibraltar Strait along the so called Azores-Gibraltar Line (AGL in Fig. 3.1.1).

Along this line the plate motion is divergent East of the Azores with a dextral strike-slip

component, transform in the middle segment, the Gloria fault, and convergent to the East of

the Tore-Madeira Rise where the upper crust appears affected by diffuse compression (Sartori

et al., 1994). At about 2.0 Ma the localization of the deformation offshore Iberia started to be focused along ESE-WNW strike-slip faults (Rosas et al., 2009) controlling the present-day plate interaction between Iberia and Africa.

Further eastward, the eastern part of the AGL is buried by deformed sediments of the accretionary wedge related to westward-trending Miocene emplacement of the Gibraltar orogenic arc.
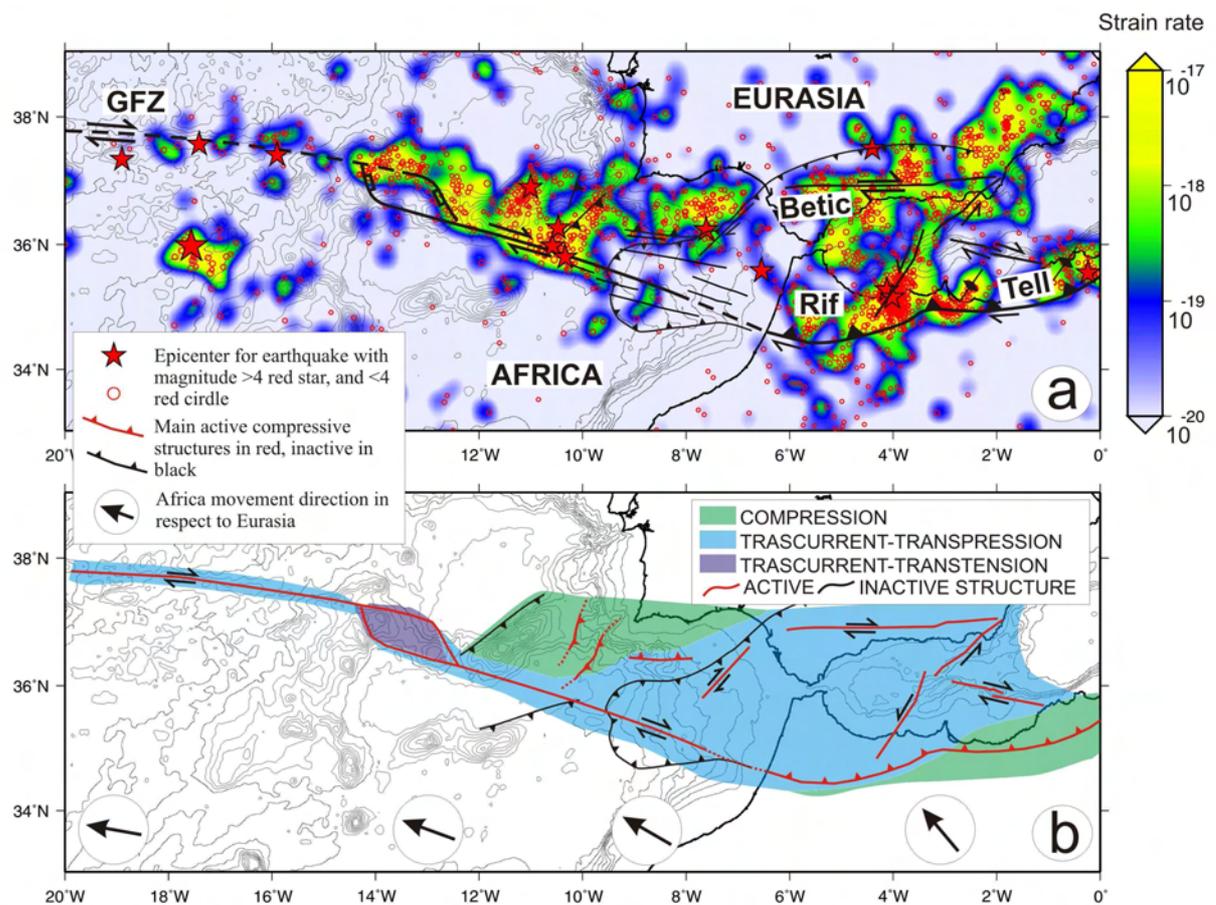
Figure 3.1.3 a) Stress map of the study area, color bar strain rate and b)Recent tectonic setting, (bottom arrow: direction of relative movement of Africa with respect to Iberia). GFZ: Gloria Fracture Zone; Modified after Zitellini et al. (2009).

In the area between the Gorringe Ridge and the Gibraltar Strait, compressive stress trends mainly NNW-SSE with plate convergence rate of 4 mm/y (DeMets et al., 1994). The Gorringe Ridge, the Coral Patch Ridge, and the series of Abyssal hills in the Seine Abyssal

Plain formed by northwest to southeast-trending thrusting during the latest stages of the Eurasia-Africa convergence.

3.2 Main geomorphologic features

The main morphological features of the Gulf of Cadiz (Fig. 3.2.1) are described hereafter from South to North, from the Moroccan offshore to the West Iberia continental margin and abyssal plain systems. The Gibraltar accretionary prism domain is introduced at the end of the chapter.
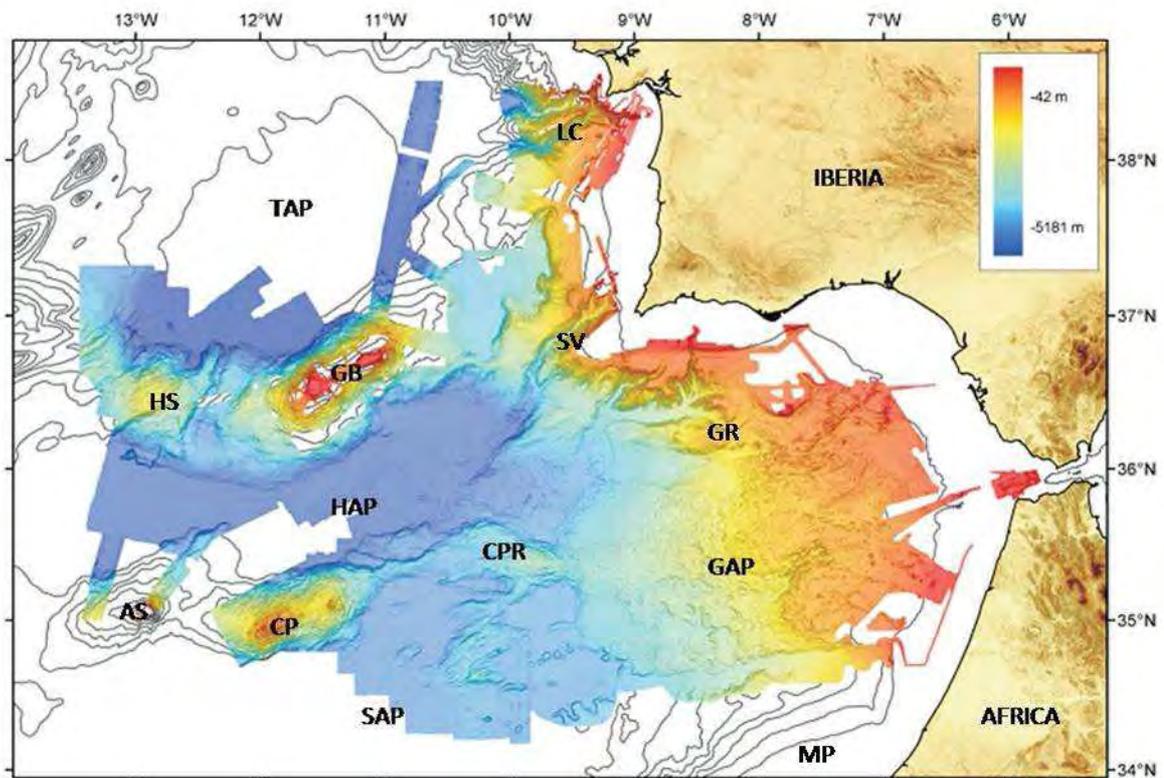
Figure 3.2.1 Morpho bathymetric map of the Gulf of Cadiz, SWIM compilation.
(LC Lisboa Canyon; TAP Tagus Abyssal Plain; SV San Vicente Canyon; GB Gorringe Bank; HS Hirondelle seamount, HAP Horseshoe Abyssal Plain; AS Ampère seamount; CP Coral Patch seamount; CPR Coral Patch Ridge; GAP Gibraltar accretionary prism; SAP Seine abyssal plain; MP Mazagan Plateau).

Zitellini et al. (2009) published a bathymetric compilation map of a great part of the Gulf of Cadiz (Fig.3.2.1 and Plate 1) merging high-resolution bathymetric surveys performed in the

last ten years by several European Oceanographic Institutes. The results is a bathymetric map, (100 m x 100 m grid resolution) that improved the knowledge of the whole area.

The Moroccan Mazagan platform, West of Casablanca, is a 50-60 km wide continental shelf. In this sector four DSDP site (545, 544, 546, 547) (Hinz et al., 1982) reveal the stratigraphy and the evolution of the continental margin showing how the present day continental slope is strongly influenced by the presence of a Cretaceous drowned carbonate platform buried below it. The continental platform gently dips from the coast and is abruptly interrupted by a highly inclined slope connected to the Seine Abyssal plain. The slope, with a mean inclination about 5°, presents a classical canyon - ridge - canyon morphology. In several parts this escarpment can reach slope values around 30°-40°, this steepness resulting by erosive process acting on the old carbonate platform buried below this escarpment.

Northwest of the Moroccan shelf there is the Seine Abyssal Plain. This plain, about 400 km long x 250 km wide, has a mean depth of 4400 m and can be divided in two parts. Toward the West, there is a starved flat basin with only few abyssal hills on the northern side. East of 10°30' W the plain is interrupted by ridges and hills that arise up to 3500 m bsl. Seismic data show how these hills and ridges are of two types: the first one is formed by a regular, sub-parallel top-thrust anticlines, the second one is formed by isolated to aligned diapiric hills. Ridges are commonly 10 to 20 km wide, with a maximum length about 50 km. Diapiric domes are generally of rounded in shape, 5 km wide, rising about 200-300 m from the flat plain. On the western margin a series of rounded shape hills arise for about 200 m from the 4400 m deep, flat abyssal plain. Seismic data reveal that these structures are the morphological expression of deep diapiric structures flowing up to the sea-bottom (Fig. 3.2.2). These diapiric domes are aligned ENE – WSW. Some of these hills are also present eastward, on the top of the Gibraltar accretionary prism.

The presence of these diapiric structures cutting all the sedimentary layers of the accretionary prism, without sign of tectonic lateral displacement, testify the inactivity of the accretionary prism at least at the toe of this structure.
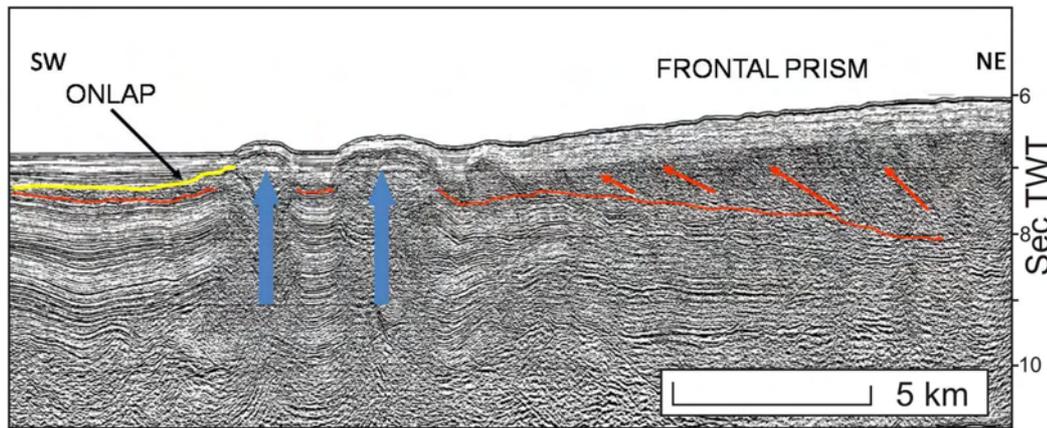
Figure 3.2.2 MCS line AR06 in the Seine Plain, Blue arrow: diapirs; Red arrow: thrust in the accretionary prism; Yellow line: onlap unconformity.

The northern part of the Seine abyssal plain ends at the toe of the 200 km long, WSW-ENE oriented Coral Patch Ridge. This long chain of ridges and seamount starts from the North, at 9°30' W - 35° 30'N, with a 1000 m high seamount and ends to the South with the Coral Patch seamount. On the top of this ridge, halfway between the Coral Patch seamount and the northern Coral Patch Ridge, is located the site of DSDP 135 (see chap. 3.4). The Coral Patch seamount, well described in chapter 6, is a large seamount rising 3800 m from the surrounding abyssal plains. On the top at least nine well preserved volcanic edifices are present. The slopes of the seamount are steep and characterized by gully-like scours and gravitative phenomena. To the west, the Coral Patch is connected through a thin saddle to the Ampere seamount. This is a volcanic seamount rising up to 250 m bsl with a classical conic volcanic shape down to 1000 m bsl. The basal part of the Ampere seamount is elongated in a WSW-ENE direction as the Coral Patch. The Ampere and Coral Patch Ridge separates the Seine abyssal plain from the Horseshoe Abyssal Plain. This is long 300 km with a mean width of 65 km, is elongated toward NE with depth ranging from 4750 m and 4900 m bsl. Only few

abyssal hills rise from the HAP in the eastern sector. These hills seem to be aligned from WNW to ESE; they have been interpreted by Rosas et al. (2009) and Zitellini et al. (2009) as the morphological expression in the area of a set of trascurrent faults, the SWIM lineaments, crosscutting all the Gulf of Cadiz from the Gloria fault to the Moroccan coast. The Western termination of the Horseshoe Abyssal Plain corresponds to the Tore Madeira Rise, formed by a series of seamounts and abyssal hills, roughly aligned N-S.
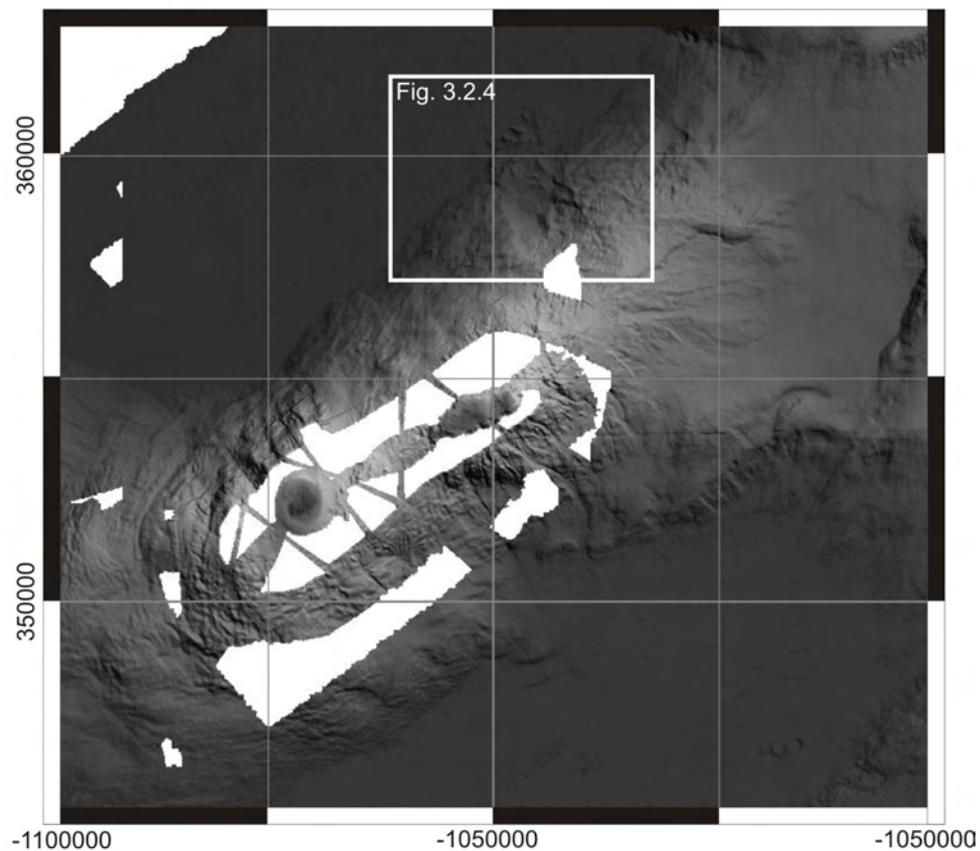
Figure 3.2.3 Gorringe Bank shaded relief map, Mercator Projection, coordinates in meters. White box location of Figure 3.2.4.

The Horseshoe Abyssal Plain is bounded to the North by the impressive slope of the Gorringe Bank and Hirondelle Seamount. The Gorringe Bank is a 4800 m high seamount elongated SW - NE, 200 km long and 80 km wide. The top is made up of two main reliefs, the Gettisburg seamount on the southwestern part, and the Ormonde seamount on the northeastern end, both rising up to 50 m bsl. In between it is located the sites of DSDP 120 (see chap. 3.4), the two

peaks have a flat top surface because of winnowing process during last glaciations; observed morphologies suggest the presence of outcrops of the substratum. The North flank of the Gorringe is characterized by a slope with a mean inclination varying between 7° ad 10°. On this slope a giant landslide is present, with the head escarpment at 2500 m bsl, 20 km wide (Fig. 3.2.3, 3.2.4). The toe deposit of the slide is 20 km wide on the northern abyssal plain, at 5000 m bsl. The slide surface is around 350 km^2 and it is long 45 km from the hinge of the head escarpment to the toe of the accumulation zone. The source area is 20 km long and is from 15 to 20 km wide.
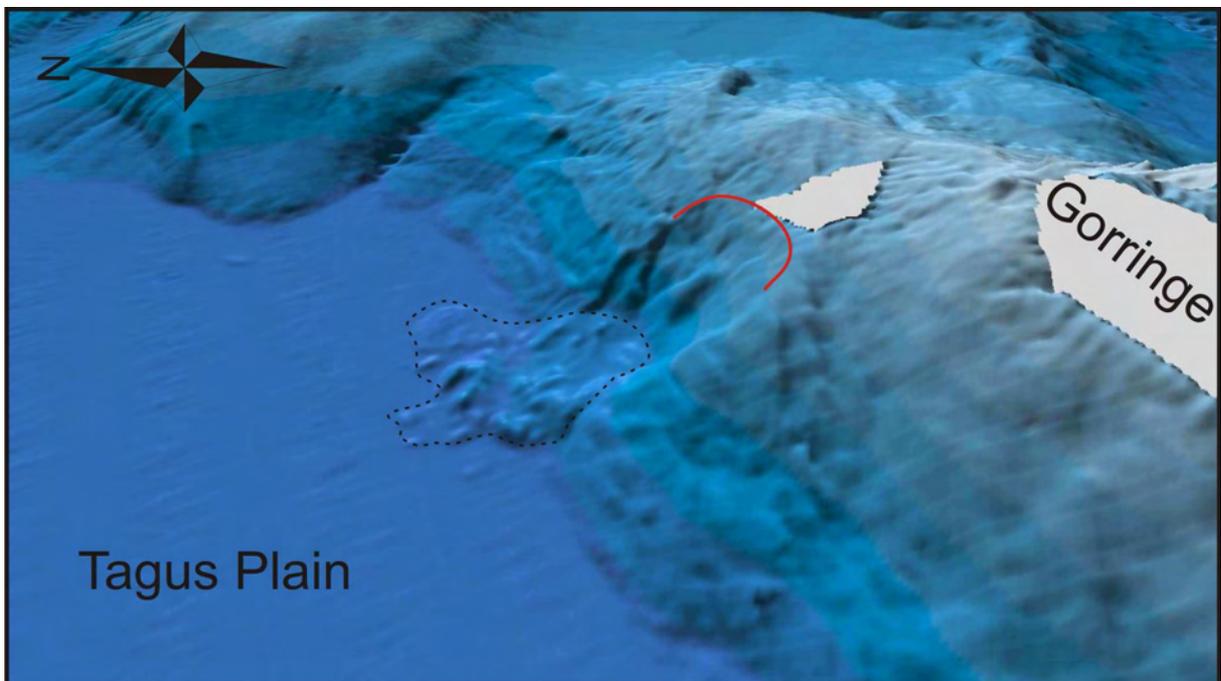
Figure 3.2.4 Giant Slide on the Northern flank of the Gorringe Bank. Red line: headwall; Black dashed line: Toe deposit. Vertical exaggeration 5X, location on figure 3.2.3.

The Hirondelle seamount, bounds the North western sector of the Horseshoe Abyssal Plain West of the Gorringe Bank, it arises 2000 m from the adjacent abyssal plains and is characterized by elongated SW-NE small ridges, probably due to the accretion of new oceanic crust during the initial stage of the oceanization (Rovere et al., 2004). Moreover, the Hirondelle is crosscut by a linear depression extended from the NW sector to ESE, this

depression is interpreted as part of the SWIM trascurrent lineaments (Zitellini et al., 2009). Unfortunately, westward to the Hirondelle, the unique bathymetric data are the Gebco predicted topography (Sandwell and Smith, 1997) that do not have the resolution sufficient to check the westward continuation of the SWIM lineaments.

North of Gorringe Bank and Hirondelle seamounts, the deepest abyssal plain of the area, the Tagus Abyssal Plain, is present. This plain has a mean depth of 5000 m bsl and is bounded to the East by the Iberian continental slope. No particular features are detected at the sea-bottom on this extremely flat plain. The West Iberia Continental margin, instead, shows many of different morphological structures. In this work, is taken into consideration the part comprised between the Lisbon Canyon to the North and the S. Vicente Canyon to the south. Lisbon Canyon, as well as the Cape S. Vicente Canyon, starts on the continental platform and reaches the abyssal plain acting as a connector for the silicoclastic sediment transport from land to the distal abyssal systems (Purdy, 1975).

The South Iberian continental platform starts East of Cape S. Vicente. It can be divided into two main levels at different depth. From the coast, often represented by high-cliffs and Ercinian basements outcrops, a first gently sloping platform extends for ten to twenty kilometers to a depth of 120 m, then, below, a second sub-horizontal platform at depth between 200 and 700 m is present (Terrinha et al, 1998; Rovere et al, 2002). The continental shelf morphology down to -120 m bsl is influenced by Ercinian substratum outcrops between Cape S. Vicente and Faro lagoon. The two set of plateau are formed by prograding neogenic units and then influenced by the strong Mediterranean Outflow Water (MOW) current.

Both the Iberian and the Moroccan platforms terminate to the East against the Gibraltar Accretionary Prism. This is the offshore continuation of the Betic-Rifean arc. Overall, the accretionary wedge is characterized by a mean moderate slope (<2° in general). However, along its external and internal boundaries the seafloor can locally reach slopes up to 10°. The

surface appears scattered by large sub-circular scours and depressions (Rosas et al., 2009). Seismic data show that this morphology is the surface expression of the geological thrust and fold structures of the wedge, covered by few meters of recent sediments. The North-Eastern sector of the Gibraltar Accretionary Wedge is also affected by the Mediterranean Outflow Water current that models and control the local sediment fabric and transport, in fact many conturite fields are present. The central sector of the prism shows two lobes. The lower boundary of these two lobes corresponds approximately to the -2000 m bathymetric contour, and they are marked by arcuate bands of steep (around 10°) slopes. The southern lobe presents several elongated WNW-ESE lineaments cutting the sea-bottom. These lineaments are part of the SWIM lineaments of Zitellini et al. 2009. They cut all the prism from the HAP to the Moroccan margin. Lineaments in this sector influenced and drove the gravitational bodies that in several place are confined by these WNW – ESE oriented lineaments.

3.3 Gravimetric data

Gravity data have been used to investigate crustal density variation. The Sandwell and Smith altimetry derived Free Air Anomaly (Sandwell and Smith, 1997) and the Multibeam topographic data have been used for the gravity inversion. The gravimetric processing was done at *INGV La Spezia* institute. First the gravity-bathymetric correlation was determined using the Nettleton approach in order to compute the best crustal density for Parker inversion; this method gave a 2600 g/cm^3 as mean crustal density. Next, the predictable signal due to water/crust and crust/mantle boundaries were removed from the Free Air Anomaly.
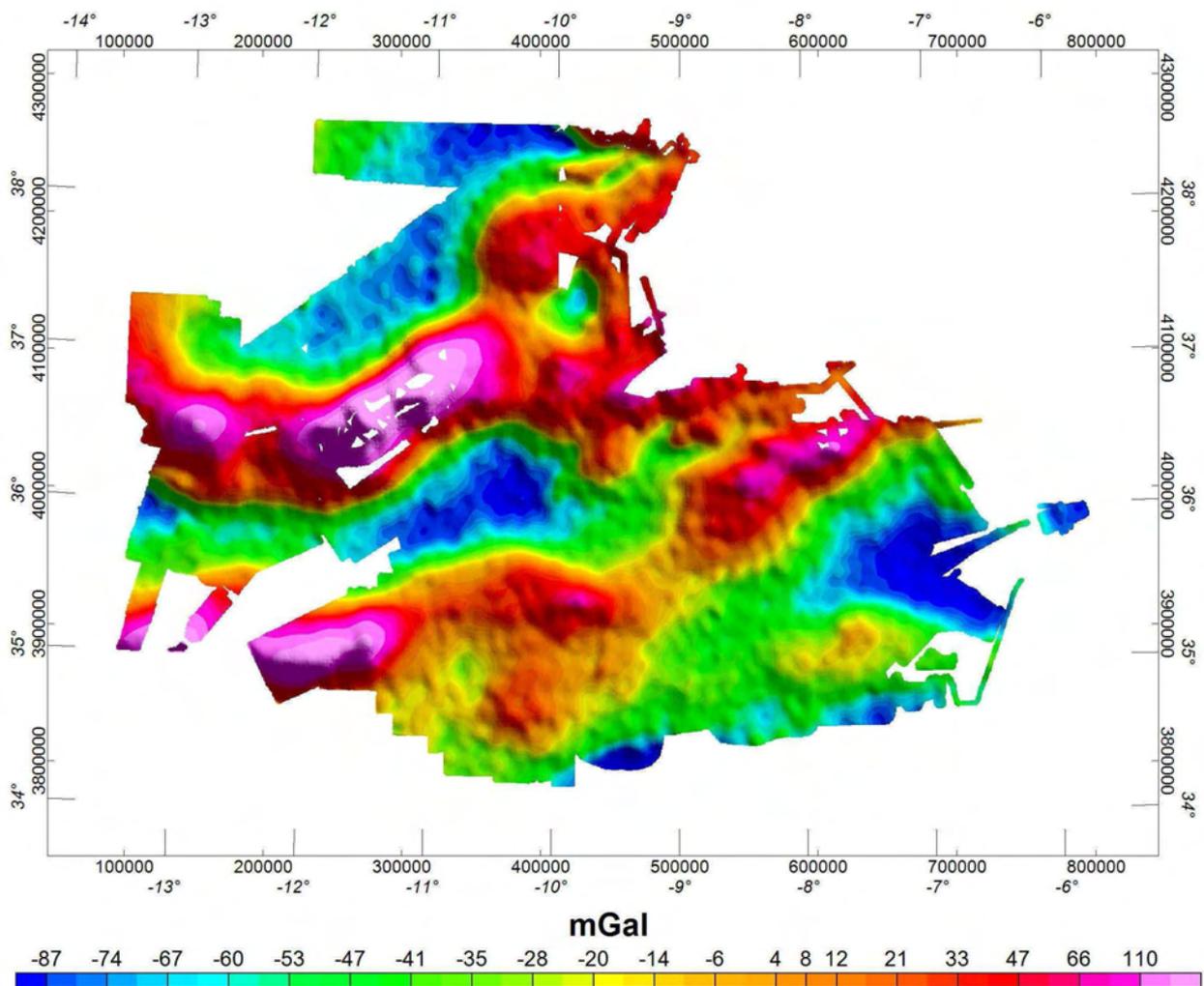
Figure 3.3.1 Free Air Anomaly (Sandwell and Smith, 1997), for the multibeam compilation area

This was done by using a crustal layer bounded by the topography and by a flat 14 km depth Moho. Finally a modified Parker algorithm (Caratori Tontini et al., 2008) was used to compute crustal lateral density variation. The range in density variation is between 2.0 and 3.1 g/cm^3.These are preliminary results. In fact seismic line will be used to constrain sediment/basement and crustal/mantle bounderies in order to perform new gravity inversion.

The gravimetric data are used to validate the lithospheric folding model presented on chapter 4.
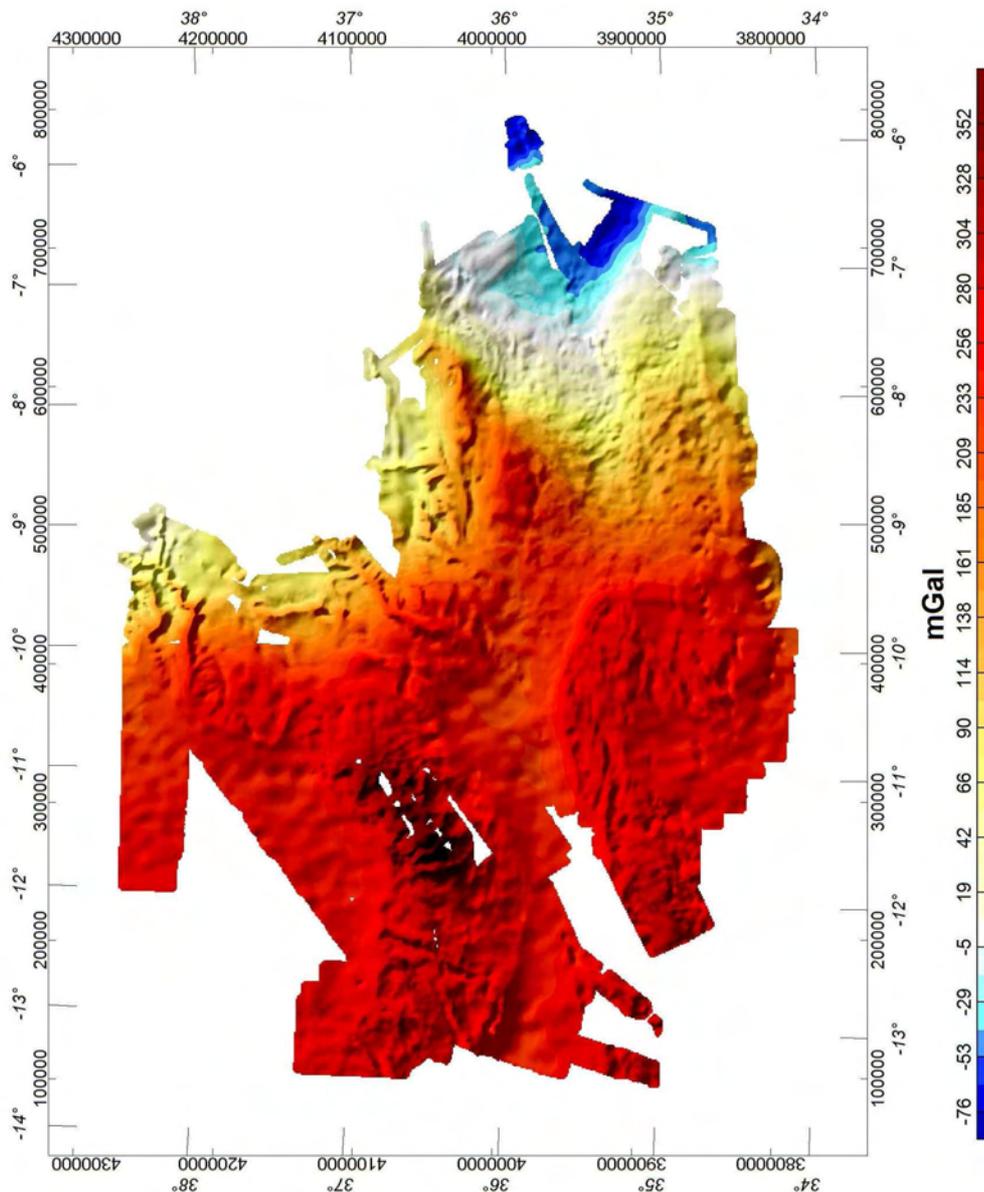
Figure 3.3.1: Bouguer anomaly, corrected for the Gulf of Cadiz Bathymetric Compilatio, UTM 29 Projection.
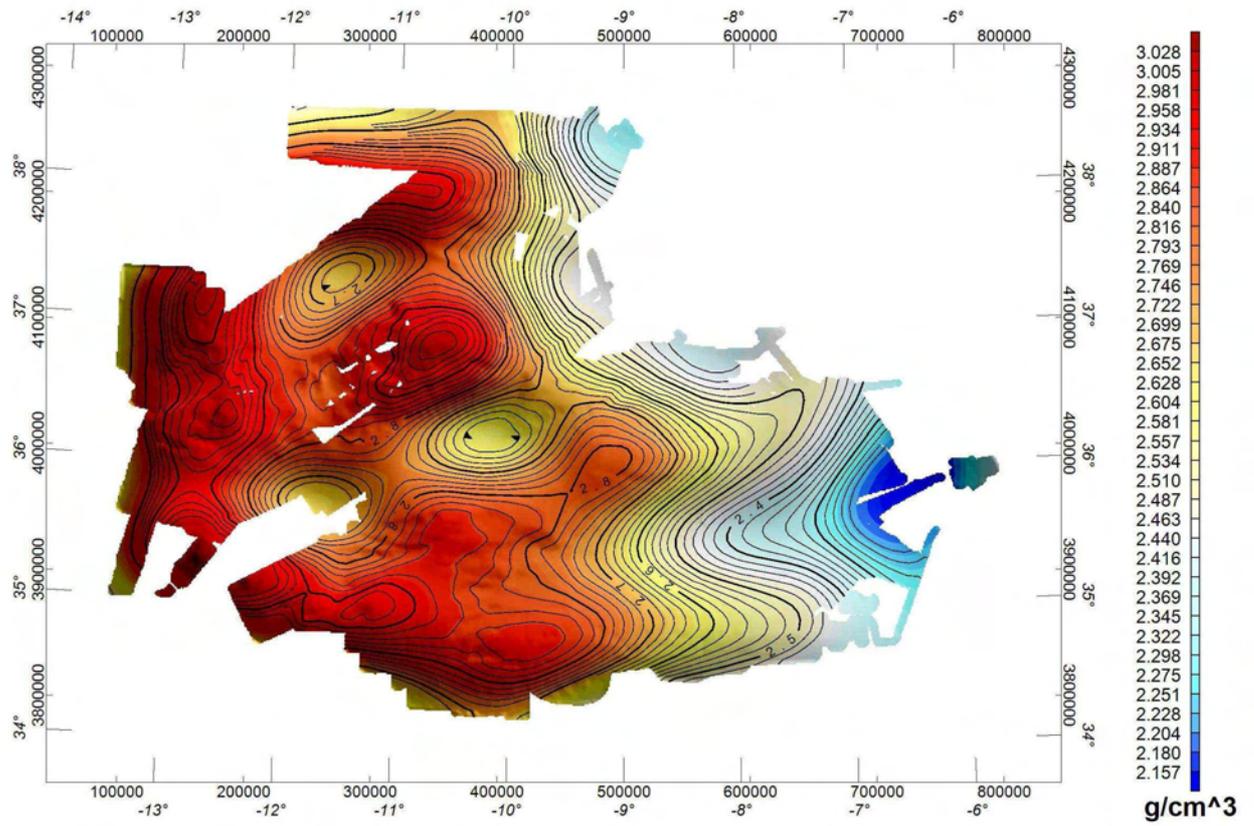
Figure 3.3.3: Crustal density variation computed using the Caratori & Tontini (2008) algorithm.

3.4 DSDP

The Atlantic continental margin between North Iberia and Morocco was matter of several studies implying ODP, IODP and DSDP project. In particular 4 zones were drilled on 27 sites during several leg of this projects.
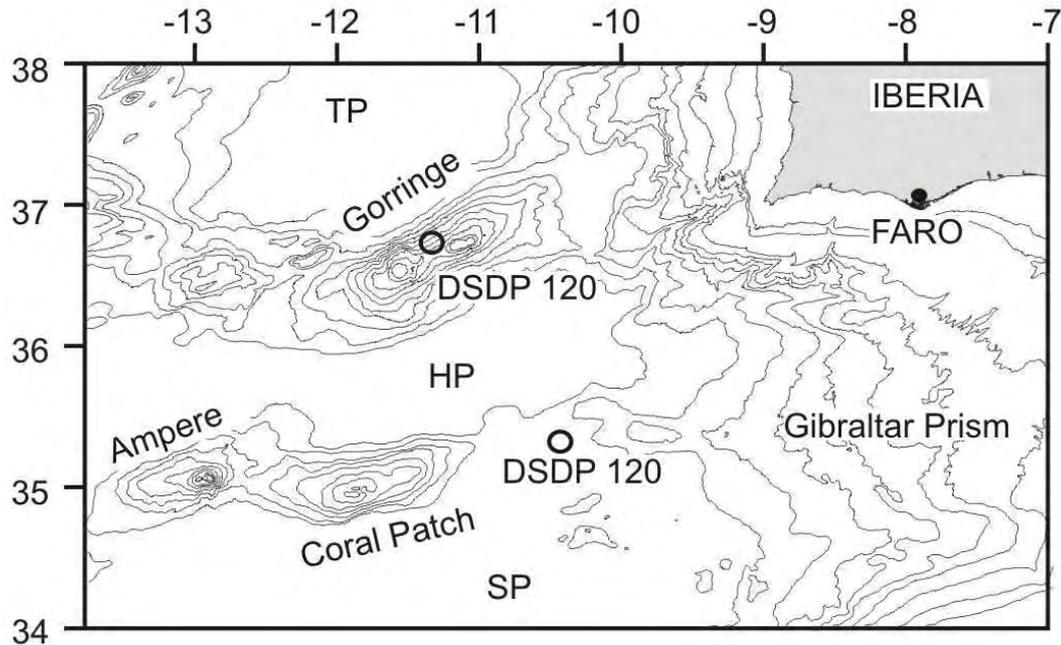
Figure 3.4.1 Location map of DSDP drilling sites: DSDP 120 and DSDP 135; TP: Tagus abyssal Plain; HP: Horseshoe abyssal Plain; SP: Seine abyssal Plain.

The main topic of the drilling project was to study the mode of rifting, subsequent drifting and complete oceanization of the Atlantic Sea, that occurred from the late Jurassic to middle Cretaceous. In particular from North to South the Galizia Margin (ODP sites 103, 149, 173, 637, 638, 639, 641, 398, 897, 898, 899, 900, 901, 1065, 1067, 1068, 1069, 1070, 1276, 1277 Boillot et al., 1985; Sawyer et al., 1994; Whitmarsh et al., 1998), the Gorringe Bank (DSDP 120) the Coral Patch Ridge (DSDP 135) and the Moroccan Margin (DSDP sites 370, 544, 545, 546, 547) were drilled between 1970 and 2001.

Two DSDP (120 and 135) wells drilled in the Gulf of Cadiz (Figures: 3.4.1, 3.3.2, 3.4.3) are used in this work to calibrate and correlate seismo – stratigraphic interpretation.
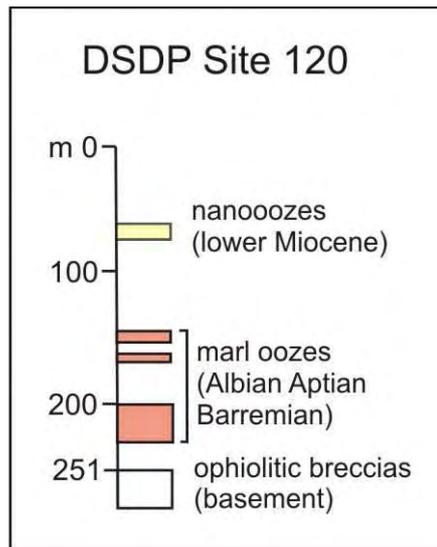
Figure 3.4.2 schematic stratigraphy.

The well DSDP 120 (Ryan et al. 1973), located at 36°41.388'N 11°25.938'W on the northern flank of the Gorringe Bank, reach a depth of 253.4 m from the sea bottom (Fig 3.4.2). During the drilling, because of technical problem, only 8 core fragments were recovered, so the sampled material was only the 19.8% of the total length of the well.

At DSDP 120, Lower-Middle Miocene and Lower Cretaceous (Albian, Aptian, Barremian) gray and green, partly silicified nannofossil oozes were cored. The inferred stratigraphic section (Fig. 3.4.2) contains two significant unconformities: (l) a hiatus in bathypelagic sedimentation between Cretaceous and Miocene; (2) an abrupt change in sediment facies across this unconformity, silicified nannofossil ooze yielding poor assemblages of planktonic foraminifera (suggestive of original deposition near or below the lysocline) and younger chalks and oozes unaffected by solution with rich, diverse assemblage.

The well reached the basement at 251.7 m below the sea bottom, the basement rocks consist of spilitic basalt, serpentinite, and meta-gabbro. This ophiolitic rock give a radiometric Giurassic age.
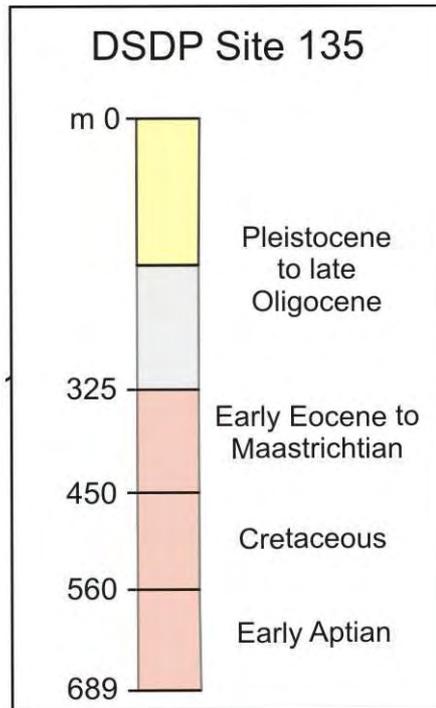
Figure 3.4.3 DSDP 135 schematic stratigraphy.

The well DSDP 135 (Hayes et al. 1972), located at 35°20.802'N 10°25.458'W on the Coral Patch Ridge, drilled 687 m of recent to Aptian sediments (Fig 3.4.3) and did not reach the basement.

The upper part of the core consist of 325 m of calcareous mud from Pleistocene to Recent in age. Under this unit pelagic sediments with little carbonate fraction and terrigenous quartz dominated sediment are recovered. The bottom part of the DSDP 135 is characterized, below 560 m, again by calcareous sediments, Aptian in age. A major unconformity is represented by a hiatus in the sedimentation between Oligocene and Upper Eocene.

4 Structural Evolution Eocene-Pleistocene

Paper submitted to Geology

TITLE

Synclines as prime expression of compressional deformation of the lithosphere: the Central Atlantic segment of the Iberia-Africa Plate Boundary

AUTHORS

N. Zitellini, Istituto di Scienze Marine, Sede di Bologna (ISMAR), Via Gobetti 101, 40129, Bologna, Italy.

S. Cloetingh, Faculty of Earth and Life Sciences, VU University (ISES), De Boelelaan 1085, 1081 HV Amsterdam, The Netherlands.

F. D'Oriano, Dipartimento Scienze della Terra e Geologico Ambientali, Via Zamboni n.67, 40127, Bologna, Italy

E. Burov, Lab. Tectonique UMR7072, Case 129, University of Paris 6, 4 Place Jussieu, Paris 75252, France.

ABSTRACT

Quantitative analysis of deep penetrating multi-channel seismic (MCS) lines, supplemented by gravity data, documents the fine structure of intra-plate deformation adjacent to the convergent Europe-Africa plate boundary offshore Gibraltar, Central Atlantic. In the brittle lithosphere, the deformation is expressed by crustal folding with the development of 30-190 km wide large wavelength synclines, bounded by short wavelength anticlines. The synclines

are almost symmetrical with wavelengths characteristic either for coupled or decoupled lithosphere. The spatial characteristics of the deformation show a striking similarity with the intraplate deformation in the northeastern Indian Ocean in terms of inferred mantle wavelengths. In contrast, the observation that in the Gulf of Cadiz only syncline structures are well expressed, suggests that gravity prevents the formation of anticlines of the same wavelength during the first stages of plate convergence, and only later one vergence will prevail, as in the Indian Ocean.

INTRODUCTION

Since the discovery of intraplate deformation in the form of oceanic lithospheric folding in the Northeastern Indian Ocean, numerous studies have provided evidence in support of this style of deformation in several areas around the globe (e.g. Stephenson and Lambeck, 1985; Stephenson and Cloetingh, 1991; Burov et al., 1993; Burg and Podlachikov, 1999; Cloetingh et al., 1999). Most of these studies have addressed folding in continental lithosphere since, due to its mechanical stratification, continental lithosphere is in general more prone to folding than oceanic lithosphere (Sokoutis et al., 2005). However, studies of continental lithosphere folding have been hampered by sub-aerial erosion removing part of the record of associated vertical motions and wiping out much of the high-frequency, short-wavelength records of folding (Cloetingh et al., 1999). Oceanic lithosphere and offshore rifted margin lithosphere has no such drawbacks, allowing the determination of the full spectrum of intraplate wavelengths due to folding. Due to its high strength, folding of oceanic lithosphere requires high stress levels such as observed in the Indian plate (see also Cloetingh and Wortel, 1985, Stein et al, 1989). Similar high stress levels are likely generated also in the proximity of plate boundaries in contrast to the interiors of oceanic plates where exceptionally high stress levels are generally not observed. Lithosphere regions adjacent to plate boundaries may thus be likely candidates for folding in oceanic domains. We present the results of a new quantitative

analysis of a set of MCS profiles offshore SW Iberia (Fig.1), acquired parallel to the motion vector of Africa with respect to Iberia. The data set, collected during the AR92 R/V Explora Cruise (Sartori et al., 1994), provides new evidence for folding of continental and oceanic lithosphere.

GEOLOGICAL SETTING

Palinspastic restorations (Plate 1), based on oceanic magnetic anomaly lineations (Srivastava et al., 1990), show that the Eurasia/Africa plate boundary underwent complex plate interactions, acquiring its present configuration only since late Oligocene times (Plate 1h). The continental margins of South Iberia and Morocco formed during Jurassic continental break-up between North America and Africa while the western continental margin of Iberia formed as a result of the Cretaceous separation between Iberia and North America (Plate 1c). As a consequence, the Tagus, Horseshoe and Seine Abyssal Plains correspond to oceanic crust of Late Jurassic-Early Cretaceous age.

In the Atlantic, the Europe-Africa plate boundary (Plate 1h) now trends roughly E-W, connecting the Azores-Triple Junction to the Gibraltar Strait along the so-called Azores-Gibraltar Line (AGL). Along this line, plate motion is divergent east of the Azores, transform in the middle segment (Gloria fault), and convergent to the east of the Tore-Madeira Ridge where the upper crust appears affected by diffuse compression (Sartori et al., 1994) with plate convergence of 4 mm/y (DeMets et al., 1994). Further eastward, the termination of the AGL is buried by the deformed sediments related to westward Miocene emplacement of the Gibraltar orogenic arc (Fig.1). During the Eocene-Late Pliocene stages of Eurasia-Africa convergence, northwest and southeast directed thrusting originated the Gorringe Ridge, the Coral Patch Ridge and the series of abyssal hills in the Seine Abyssal Plain (Zitellini et al., 2009). At about 2.0 Ma (Rosas et al., in press) the localization of the deformation offshore

Iberia started to be focused along ESE-WNW strike-slip faults controlling the present-day plate interaction between Iberia and Africa (Zitellini et al., 2009).

DEFORMATION OFF SW IBERIA: CONSTRAINTS FROM MCS DATA

The seafloor off SW Iberia and in the Gulf of Cadiz has attracted considerable attention during the last decade (Sartori et al. 1994; Hayward et al. 1999; Gutscher et al., 2002; Terrinha et al., 2003; Gracia et al., 2003; Medialdea et al., 2004; Zitellini et al. 2001, 2004) due to the occurrence of pronounced anomalous topography. The area is also considered to be the source area of the 1755 Lisbon earthquake (Plate 1a). Spectacular features include the Gorringe Bank, a large uplifted block of oceanic mantle characterized by shallow-depth peridotite outcrops, and by one of the largest geoid anomalies of the oceans (Bergeron and Bonin, 1991).

Figure 1 displays line drawings of three parallel MCS lines exhibiting the spatial variation of the deformation pattern of the area. Line AR10 encompasses the deformation of the thinned continental margin offshore SW Iberia. Lines AR03-08 and AR07 comprise the full deformation zone of the oceanic domain, situated between the undeformed sediments of the Tagus and Seine Abyssal Plains.

Line AR10 (Fig.1 and Plate 1j) shows the deformation due to Europe-Africa convergence of Late Jurassic-Early Cretaceous thinned continental crust of the rifted SW Iberia margin that began in the Eocene. The seismic line shows the presence of a large syncline bounded by two top thrust anticlines with opposing, outward verging, thrust planes. The width of this structure measured from the two opposite bounding faults is 90 Km (Fig.1) with peak to peak distance between the bounding anticlines of 63 km. The two bounding faults, as shown in Plate 1, are at high angle throughout the sediment cover and are blind thrusts, not reaching the surface. In

41

the upper crust however, they propagate at lower angle with a dip of 24° (Zitellini et. al., 2001). The bounding faults merge on a common, almost horizontal, detachment fault at 11 sec. TWT depth, at approximately 18 km, where the earthquake activity of the structure is concentrated. Zitellini et al. (2001) interpreted this horizon as an intra-crustal decoupling level.

Within the sedimentary cover, which is approximately 3 sec TWT thick and which records presently active shortening (Zitellini et al., 2004), the unconformity that marks the onset of compression can be recognized (Plate 1, shot point 1500, 5s depth). Most of the deformation is concentrated on the bounding anticline structures while the intervening syncline, once formed, remained practically undeformed, becoming an important regional basin depocenter. At present, however, no clastic sedimentation occurs as a result of compression induced uplift that triggered the formation of the San Vicente Canyon within the syncline axis (Plate 1j).

Line AR03-08 connects the Gorringe Bank with the Coral Patch Ridge (Fig. 1i). These two parallel ridges can be regarded as analogues, at a larger scale, of the anticline structures described above. The Gorringe/Coral Patch ridges show shortening accommodated mainly by two, inward directed faults bounding a less deformed, wide, syncline. The peak to peak distance of the anticlines is about 165 Km. At the Gorringe Bank the bounding thrust exposes mantle rocks, implying lithospheric, low angle decoupling whereas at the Coral Patch Ridge the bounding fault increases its dip upward, without reaching the surface, similar to the previous AR10 line case. The occurrence of mantle rocks at the Gorringe Ridge can be explained if the seafloor was floored by peridotite, exhumed during the initial stages of Cretaceous separation between Iberia and North America, as in the Galicia Bank (Rovere et al., 2004). Deformation across the Gorringe-Coral Patch ended during Middle-Late Miocene as indicated by the on-lapping sedimentary units of the Tagus and Horseshoe (HS) Abyssal Plains (Zitellini et al., 2004). As in line AR10, the syncline become a basin depocenter,

storing 3 km of syn-post deformation sedimentary deposits. Once more, we observe that most of the brittle deformation is concentrated at the bounding anticline structures while the syncline did not experience important deformation. The vertical set of faults cross-cutting the HS Plain are related to later dextral strike-slip motion (Zitellini et al., 2009) that started later, at the end of Pliocene time (2.0 Ma).

Line AR07 illustrates the deformation that occurred on the 160 Ma old (Srivastava et al.,1990), Late-Jurassic, oceanic crust of the Seine plain, 200 km offshore Morocco. Expressed as a set of parallel folds emerging from the Seine Plain, the deformation took place from Eocene until Late Pliocene. In section, the presence of a large syncline is observed which encompasses and contains a smaller one. As in the previous cases, the synclines are confined laterally by a set of opposite verging high angle inverse faults, marked by anticlines (Fig.1 and Plate 1l). The spatial separation between two bounding anticlines of the same order is 82 km and 34 km. The onset of folding and faulting is recorded by a regional unconformity for the larger structure and by a local unconformity for the smaller one. The relations between these unconformities show that deformation moved toward the centre (centripetal) in time. However, once formed the larger and the smaller structures grow together. In this sector the onset of the compressional stage is synchronous with the onset of deformation in the HS area, as shown by the good correlation of a region-wide, pre-folding unit. A regional unconformity marks the end of the major stage of compression, at about 2 Ma, when deformation focused in the HS plain transcurrent structures (Zitellini et al. 2009).

DISCUSSION AND CONCLUSIONS

The seismic sections reveal that deformation in the brittle lithosphere is expressed as a set of large synclines possessing variable wavelengths (Fig. 1). These are bordered by short wavelength anticlines generated above two antithetic thrust faults dipping inward, towards the

syncline axis. Deformation of synclines with relatively shorter wavelengths involve the Late Jurassic continental crust of the Iberian continental margin (Line AR10) and the Jurassic oceanic crust offshore the Moroccan margin in the Seine Plain (Line AR07). Larger wavelength deformation appears to be restricted to the oceanic lithosphere of the Gorringe/Coral Patch region (Lines Ar03-08). Table 1 summarizes the main characteristics of these structures. We term these structure "Drakkar" given their close similarity with the hull of the Viking ships.

Gravity data furnish the means to explore the lithosphere character of the Drakkar structures. In particular, lateral density variations are mirrored by the long wavelength of the gravity field (Cloetingh et al., 1999). Free-air gravity anomalies of the region (Plate 1b) appear directly correlated with the longer wavelength topographic structures of the area (Plate 1a). In fact, the pronounced positive gravity anomalies over the Gorringe Bank and the Coral Patch ridge are separated by a gravity low, corresponding to the syncline that connects them. In contrast, the shorter wavelength Drakkar structures such as the set of folds in the Seine plain do not display any direct gravimetric correlation. This is an indication that the Drakkar structures of the Gorringe/ Coral-Patch pair are conformable with the deep lithosphere deformation, while the short wavelength tectonic deformation occurring in the Seine Plain implies decoupling between the upper oceanic crust and the mantle.

Figure 2 displays folding wavelengths against the thermal ages of the lithosphere as observed offshore SW Iberia together with other documented studies. There is a good correlation between the wavelengths and the thermal ages of the Drakkar structures for different decoupling levels that have been inferred from MCS data. Besides the 18 km deep intra-crustal decoupling level along the continental margin of SW Iberia, Figure 2 reveals that two decoupling levels act in the Seine Plain, one within the crust and one deeper at the crust-mantle transition. The Gorringe-Coral patch structure instead resides in the coupled crust-mantle field.

Despite the general agreement between field data and previous theoretical models for the lithospheric folding wavelength in the upper crust, a substantial divergence is observed between folding models and the Drakkar structures. Classical models, in fact, predict deformation made up of synclines and anticlines with constant wavelength (Fig. 3a,c). We observe only the syncline development with deformation focused on the bounding top thrust anticlines with slight deformation within them as sketched in Fig. 3b,d. In the Gulf of Cadiz this occurs both in coupled and in mechanically decoupled lithosphere (Fig.2), suggesting that syncline development forms the principal mode by which the upper lithosphere responds to lithospheric folding during the initial stage of compressional deformation. This is also shown by Burov and Cloetingh (2009) (Figure DR-1) which presents the results of a numerical model for folding of a weak lithosphere similar to the case of the offshore Iberian margin (i.e. Line AR10); although generalized in terms of adopted timing, erosion and sedimentation rates, the model predicts that, in this rheologically state, asymmetric anticlines-synclines structures can develop similar to those observed in the study area.

The most obvious force preventing the full development of anticlines is gravity, both for mechanically coupled and uncoupled lithosphere. Meanwhile, the sedimentary load of this basin can, as gravity, enhance the development of the synclines. An immediate consequence of this mechanical behavior of the upper lithosphere is the generation of almost symmetrical, barely deformed basins, of particularly large dimensions in cases of mechanically coupled lithosphere, which are predicted to occur during the first stage of plate convergence.

Solid Earth Science (ISES). Istituto di Scienze Marine, Sede di Bologna (ISMAR-BO) contribution n. **XXX** .

REFERENCES CITED

Bergeron, A., and Bonnin, J., 1991, The deep structure of Gorringe Bank (NE Atlantic) and its surrounding area: Geophysical Journal International, v. 105, p. 491-502.

Bonnet, S., Guillocheau, F., Brun, J.-P., and Van den Driessche, J., 2000, Large-scale relief development related to Quaternary tectonic uplift of a Proterozoic-Paleozoic basement: The Armorican Massif, NW France: Journal of Geophysical Research, v. 105, p. 19273-19288.

Burg, J.P., and Podladchikov, Y., 1999, Lithospheric scale folding; numerical modeling and application to the Himalayan syntaxes: International Journal of Earth Sciences, v. 88, p. 190-200.

Burov, E., Lobkovsky, L., Cloetingh, S., Nikishin, A., 1993. Continental lithosphere folding in Central Asia. Part 2: constraints from gravity and topography. Tectonophysics 226, 73-87.

Burov, E. and Molnar, P., 1998. Gravity anomalies over the Ferghana Valley (central Asia), and intracontinental deformation. Journal of Geophysical Research 103, 18137-18152.

Burov, E., and Cloetingh, S., 2009, Interactions of mantle plumes and lithospheric folding: impact on intra-plate continental tectonics. Geophysical Journal International, in press.

Cloetingh, S., Burov, E., Beekman, F., Andeweg, B., Andriessen, P.A.M., Garcia-Castellanos, D., De Vicente, G., and Vegas, R., 2002, Lithospheric folding in Iberia: Tectonics, v. 21, p. 1041 doi:10.1029/2001TC901031.

Cloetingh, S., Burov, E., and Poliakov, A., 1999, Lithosphere folding: primary response to compression? (from Central Asia to Paris Basin): Tectonics, v. 18, p. 1064-1083.

Cloetingh, S., and Wortel, R., 1985, Regional stress field of the Indian Plate: Geophysical Research Letters, v. 12, p. 77-80.

DeMets, C., Gordon, R. G., Argus, D. F., Stein, S., 1994, Effect of recent revisions to the geomagnetic reversal time scale on estimates of current plate motions: Geophysical Research Letters, v. 21, p. 2191-2194.

Gracia, E., Danobeitia, J., Verges, J., Zitellini, N., Rovere, M., Accetella, D., Ribeiro, A., Cabral, J., Matias, L., Bartolome, R., Farran, M., Casas, D., Maldonado, A., Pazos, A., Cordoba, D., and Roset, X., 2003, Mapping active faults offshore Portugal (36 degrees N-38 degrees N); implications for seismic hazard assessment along the Southwest Iberian margin: Geology (Boulder), v. 31, p. 83-86.

Gutscher, M.A., Malod, J., Rehault, J.P., Contrucci, I., Klingelhoefer, F., Mendes-Victor, L., and Spakman, W., 2002, Evidence for active subduction beneath Gibraltar: Geology, v. 30, p. 1071-1074.

Hayward, N., Watts, A.B., Westbrook, G.K., and Collier, J.S., 1999, A seismic reflection and GLORIA study of compressional deformation in the Gorringe Bank region, eastern North Atlantic: Geophysical Journal International, v. 138, p. 831-850.

McAdoo, D.C., and Sandwell, D.T., 1985, Folding of oceanic lithosphere: Journal of Geophysical Research, v. 90, p. 8563-8569.

Medialdea, T., Vegas, R., Somoza, L., Vazquez, J.T., Maldonado, A., diaz del Rio, V., Maestro, A., Cordoba, D., and Fernandez-Puga, M.C., 2004, Structure and evolution of the "Olistostrome" complex of the Gibraltar Arc in the Gulf of Cadiz (eastern Central Atlantic):evidence from two long seismic cross-section: Marine Geology, v. 209, p. 173-198.

Nikishin, A.M., Cloetingh, S., Lobkovsky, L.I., Burov, E.B., and Lankreijer, A.C., 1993, Continental lithosphere folding in Central Asia; Part I, Constraints from geological observations: Tectonophysics, v. 226, p. 59-72.

Rosas, F.M., Duarte, J.M., Terrinha, P., Valadares, V., and Matias, L., 2009. Morphotectonic characterization of major bathymetric lineaments in NW Gulf of Cadiz (Africa-Iberia plate boundary): insights from analogue modelling experiments: Marine Geology, in press, doi:10.1016/j.margeo.2008.08.002.

Rovere , M., Ranero, C. R., Sartori, R., Torelli, L., and Zitellini, N., 2004. Seismic images and magnetic signature of the Late Jurassic to Early Cretaceous Africa–Eurasia plate boundary off SW Iberia, Geophysical Journal International, v. 158, p. 554-568.

Sandwell, D. T., W. H. F. Smith, 1997, Marine gravity anomaly from Geosat and ERS 1 satellite altimetry: Journal of Geophysical Research, v. 102 , No. B5, p. 10039-10054.

Sartori, R., Torelli, L., Zitellini, N., Peis, D., and Lodolo, E., 1994, Eastern segment of the Azores-Gibraltar line (central-eastern Atlantic); an oceanic plate boundary with diffuse compressional deformation: Geology (Boulder), v. 22, p. 555-558.

Sokoutis, D., Burg, J.-P., Bonini, M., Corti, G., and Cloetingh, S., 2005, Lithospheric-scale structures from the perspective of analogue continental collision: Tectonophysics, v. 406, p. 1-15.

Srivastava, S.P., Roest, W.R., Kovacs, L.C., Oakey, G., Levesque, S., Verhoef, J., and Macnab, R., 1990, Motion of Iberia since the Late Jurassic; results from detailed aeromagnetic measurements in the Newfoundland Basin: Tectonophysics, v. 184, p. 229-260.

Stein, C.A., Cloetingh, S., and Wortel, R., 1989, Seasat-derived gravity constraints on stress and deformation in the northeastern Indian Ocean: Geophysical Research Letters, v. 16, p. 823-826.

Stephenson, R.A. and Cloetingh, S., 1991, Some examples and mechanical aspects of continental lithospheric folding: Tectonophysics, v. 188, p. 27-37.

Stephenson, R., and Lambeck, K., 1985, Isostatic response of the lithosphere with in-plane stress; application to central Australia: Journal of Geophysical Research, v. 90, p. 8581-8588.

Terrinha, P., Pinheiro, L.M., Henriet, J.P., Matias, L., Ivanov, M.K., Monteiro, J.H., Akhmetzhanov, A., Volkonskaya, A., Cunha, T., Shaskin, P., and Rovere, M., 2003, Tsunamigenic-seismogenic structures, neotectonics, sedimentary processes and slope instability on the Southwest Portuguese Margin: Marine Geology, v. 195, p. 55-73.

Zitellini, N., Gràcia E., Gutscher M.A., Matias L., Masson D., Mulder T., Terrinha P., Somoza L., DeAlteriis G., Henriet J.P., Dañobeitia J.J., Ramella R., Abreu M.A. and Diez S., 2009. The quest for the Iberia-Africa Plate boundary west of Gibraltar. Earth and Planetary Science Letters, v. 280, p. 13-50.

Zitellini, N., Mendes, L.A., Cordoba, D., Danobeitia, J., Nicolich, R., Pellis, G., Ribeiro, A., Sartoi, R., Torelli, L., Bartolome, R., Bortoluzzi, G., Calafato, A., Carrilho, F., Casoni, L., Chierici, F., Corela, C., Correggiari, A., Della Vedova, B., Gracia, E., Jornet, P., Landuzzi, M., Ligi, M., Magagnoli, A., Marozzi, G., Matias, L., Penitenti, D., Rodriguez, P., Rovere, M., Terrinha, P., Vigliotti, L., and Ruiz, A.Z., 2001, Source of 1755 Lisbon earthquake and tsunami investigated: Eos, Transactions, American Geophysical Union, v. 82, p. 285.

Zitellini, N., Rovere, M., Terrinha, P., Chierici, F., Matias, L., and Team, B., 2004, Neogene through Quaternary Tectonic reactivation of SW Iberian Passive Margin: Pure and applied Geophysics, v. 161, p. 565-585.

FIGURE CAPTIONS

Figure 1. Sketch map of the studied area with line drawing of deep seismic reflection profiles showing the major compressional structures. The lines are located parallel to plate motion

direction active from Eocene to Late Pliocene. Inset shows the bathymetry of the studied area (Data from GEBCO97 Digital Atlas Web site:www.gebco.net) with toponyms.

Figure 2. Comparison of observed (solid square, circle and triangle) wavelengths of folding offshore Iberia with theoretical predictions for oceanic lithosphere (McAdoo and Sandwell, 1985) in the absence (solid line) or presence (dotted line) of a thick sedimentary column (representative for the intraplate area in the NE Indian Ocean) and continental lithosphere (gray bands) (Cloetingh et al., 1999). Also shown for comparison are other estimates (open squares, circles and triangles) for wavelengths documented from geological and geophysical studies (Arctic Canada: Stephenson and Cloetingh, 1991; Central Asia: Nikishin et al., 1993; Britany: Bonnet et al., 2000; Mainland Iberia: Cloetingh et al., 2002, NE Indian Ocean: McAdoo and Sandwell, 1985; Stein et al., 1989). Both offshore Iberia (solid square and circle) and mainland southern Iberia (open solid square and circle) are characterized by separate dominant wavelengths for crust and mantle folds, reflecting decoupled modes of lithosphere folding. Note the similarity in wavelength of the inferred folding in the Gorringe Bank and Ampere Patch area (solid triangle) and the Central Indian Ocean (open triangle).

Figure 3. Four modes of continental folding: a) Folding of coupled oceanic lithosphere, typical for the NE Indian Ocean (McAdoo and Sandwell, 1985; Stein et al., 1989); b) Folding of partially decoupled oceanic lithosphere, with a possible decollement between crust and upper mantle at oceanic Moho depths. Activation depends on the degree of shortening and the magnitude of horizontal stress, which can lead to the development of large-scale synclinal deformation as observed in the Gorringe-Coral Patch area in the far field of the Africa-Iberia plate boundary (see Figs 1 and 2, line AR03-08) as well as to decoupled crustal scale folding in the area offshore Morocco closer to the Africa-Iberia plate boundary (see Figs 1 and 2, line AR07); c) Decoupled continental lithosphere folding with separate wavelengths for crustal

50

and upper mantle folding such as observed in mainland Southern Iberia (Cloetingh et al., 2002); d) Folding of decoupled rifted Cretaceous continental margin lithosphere characteristic for offshore Iberia (see Figs. 1 and 2, line AR10).

Table 1

Constraints on timing, shortening rate and thermo-mechanical age of lithosphere in the Gulf of Cadiz.

Plate 1 (a) Bathymetry of the Gulf of Cadiz and offshore SW Iberia (Data from GEBCO97 Digital Atlas Web site:www.gebco.net). Solid thick lines mark the locations of deep penetration seismic profiles shown in Fig.1 and Plate 1, solid thin line marks the boundary of Gibraltar accretionary prism. Arrows show the relative motion between Europe and Africa. Star shows location of the 1755 Lisbon Earthquake epicenter. (b) Free-air gravity map of the area (Sandwell and Smith,1997), color bar in mgal. (c-h) Jurassic to Present Plate tectonic reconstruction modified after Srivastava et al. (1990). (i-l) Time-migrated seismic lines AR92-3, AR92-8, AR92-7 and AR92-10, and interpretation, modified after Sartori et al. (1994).

Repository Data Figure Captions:

Figure DR-1. A numerical model (Burov and Cloetingh, 2009) of folding of weak lithosphere of thermo-tectonic age and initial structure resembling the case of the line AR10 (visco-elastic-plastic rheology) with quartz-dominated crust and olivine-dominated mantle. Note initially harmonic character of deformation that evolves in asymmetric folding during later stages. Note that these results should be considered as illustrative only for the key features of

the observed intraplate deformation as the adopted sedimentation rates and timing are only a first order approximation of the characteristics of the study area.
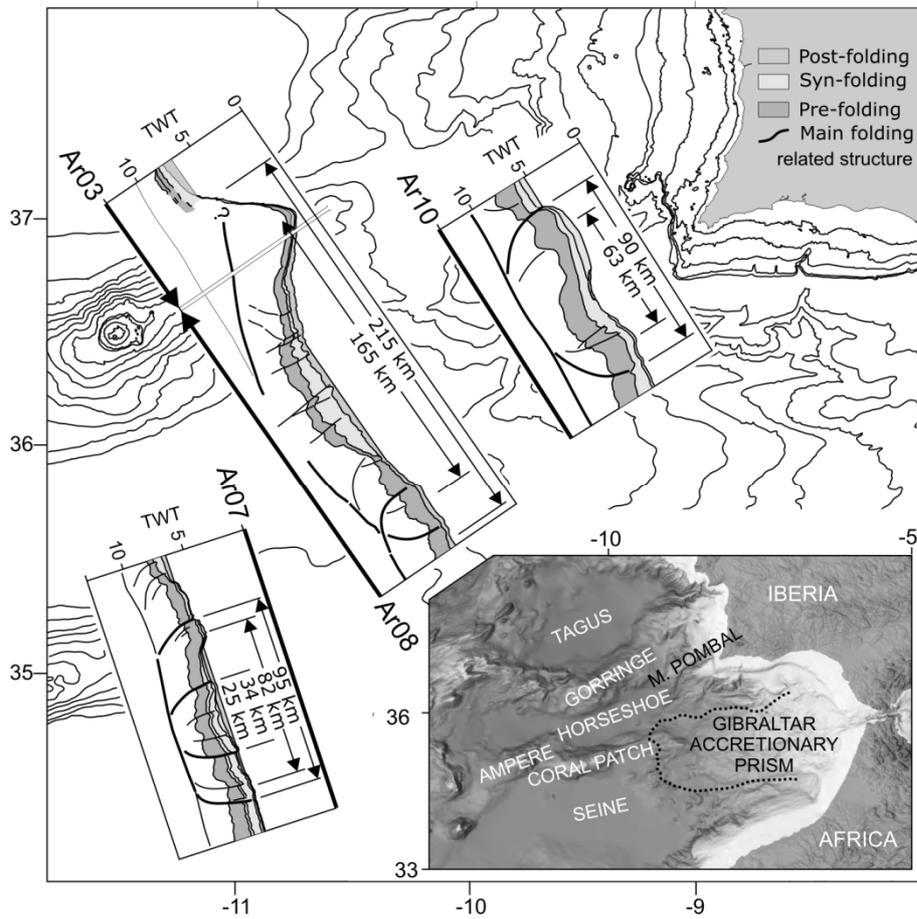
Zitellini et al., Figure 1, Zitellini_Fig_1.tif
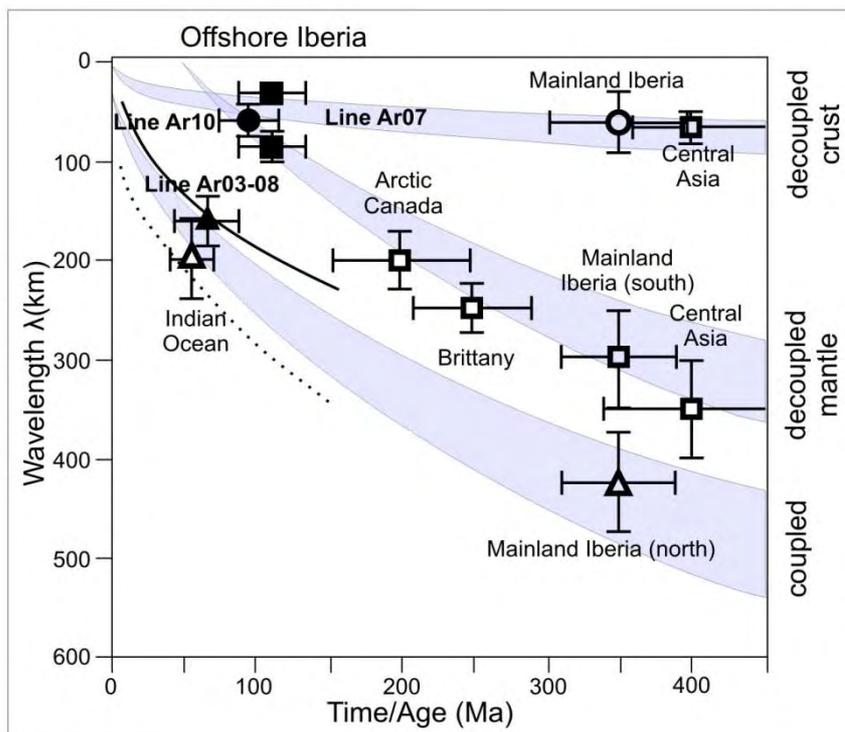
Zitellini et al., Figure 2, Zitellini_Fig_2.tif
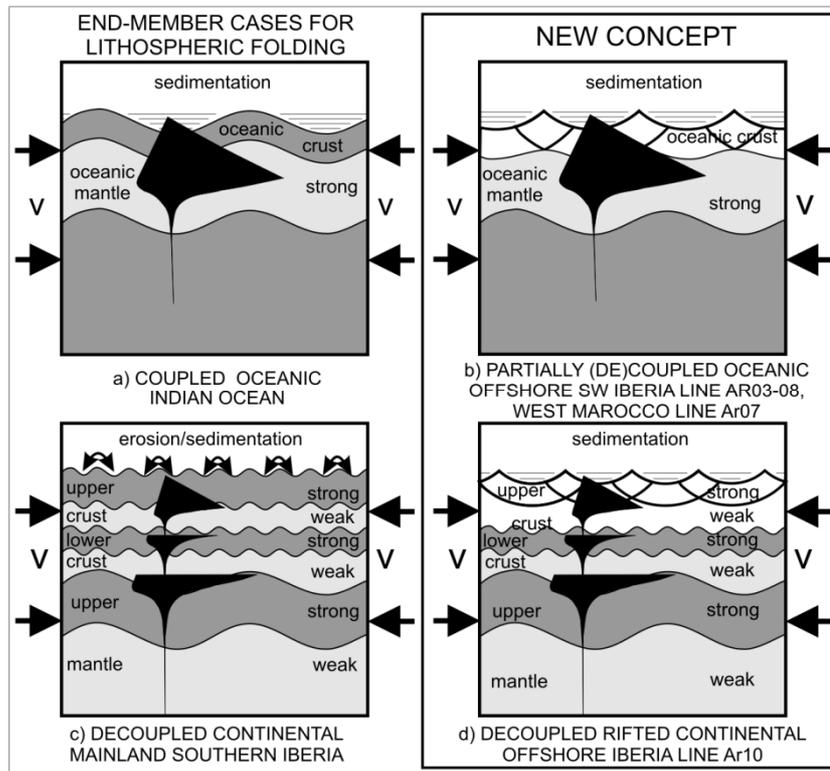
Zitellini et al., Figure 3, Zitellini_Fig_3.tif

topography (m)

$$\log(\sigma/\dot{\varepsilon})$$
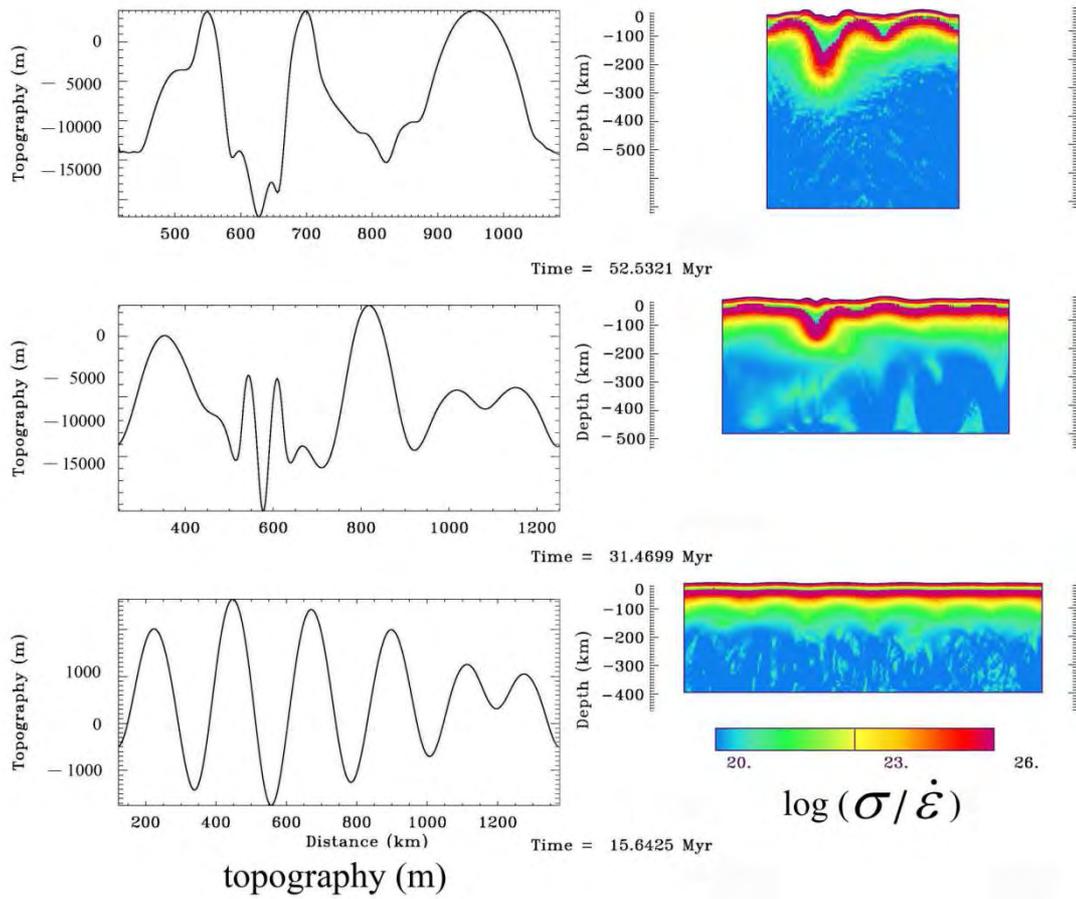
Zitellini et al., FigureDR-1, Zitellini_FigDR-1.tif

55

TABLE 1 CHARACTERISTICS INTRAPLATE DEFORMATION				
		Line AR07	Line AR10	Line AR03-08
1	Age Lithosphere (Ma)	160	150	150-120
2	Timing Compressional Reactivation (Ma)	55-2	55-0	55-15
3	Thermo-Mechanical Age at onset of Deformation (Ma)	105	65	65
4	Timing Trascurrent Motion Initiation (Ma)	2	2	2
5	Wavelength λ (km)	82 / 25	63	165
6	Shortening (km)	8 / 3		20
7	Strain-Rate (s-1)			2·10 -15
8	Mechanical Thicness H (km)	9	18	10
9	Max Thicness Sediments (km)	3	3	3
10	Ratio λ/H	9/3	3.5	16

Zitellini et al., Table DR-1, Zitellini_Table_1.tif

5 Recent development of the Eurasia-Africa Plate Boundary offshore Morocco

5.1 Introduction

The Iberia Africa plate boundary was interpreted as a diffuse plate boundary in the last 15 years (Sartori et al., 1994 ; Zitellini et al., 1999; Maldonado et al., 1999; Gutscher et al., 2002; Gracia et al., 2003; Gutsher, 2004; Zitellini et al., 2001, 2004; Medialdea et al., 2004). Recent high-resolution swath bathymetry compilation of the Gulf of Cadiz (Fig. 5.1.1 and Plate 1, Zitellini et al., 2009)
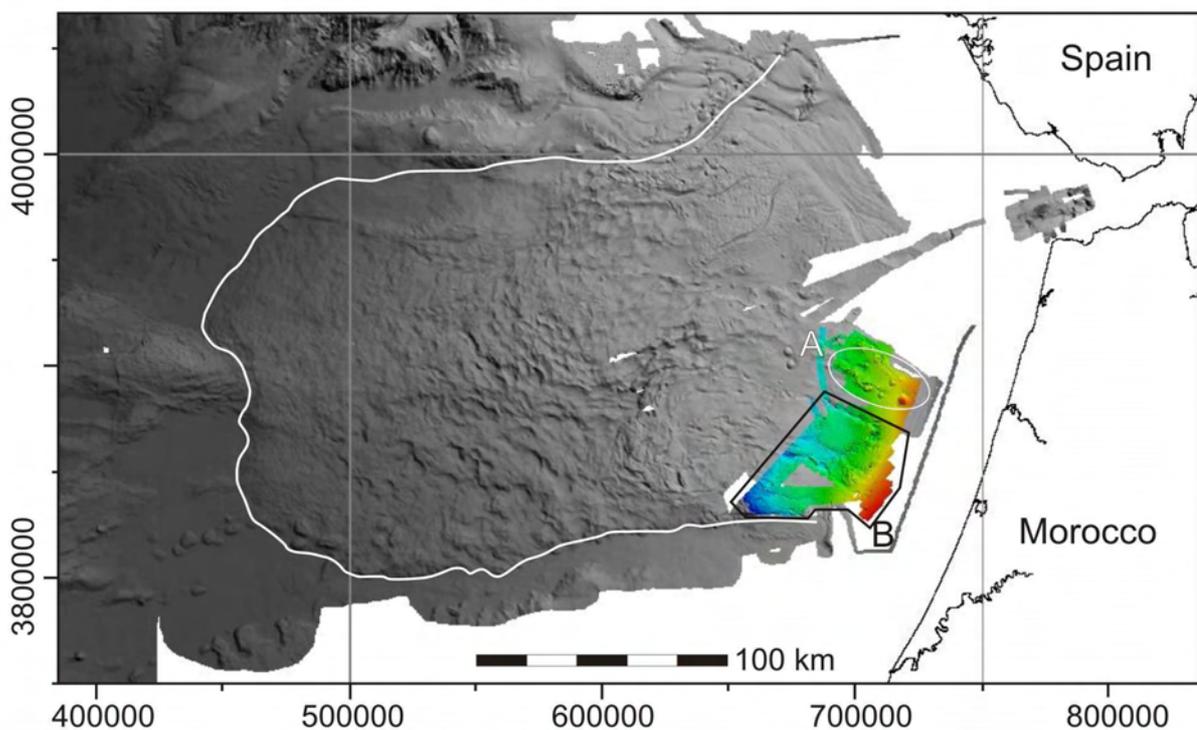
Figure 5.1.1 Gibraltar accretionary prism shaded relief; A: El Arraiche mud volcano fiel; B: NEAREST 2008 survey acquired and processed during this work. UTM 29 Projection.

provided new data that may solve the nature of the plate boundary. Zitellini et al. (2009) documented a series of tectonic lineaments cross-cutting the whole margin from the eastern termination of the Gloria fracture zone to the Moroccan continental shelf. Seismic multichannel lines from Horseshoe abyssal plain reveal that these lineaments are sub vertical faults.
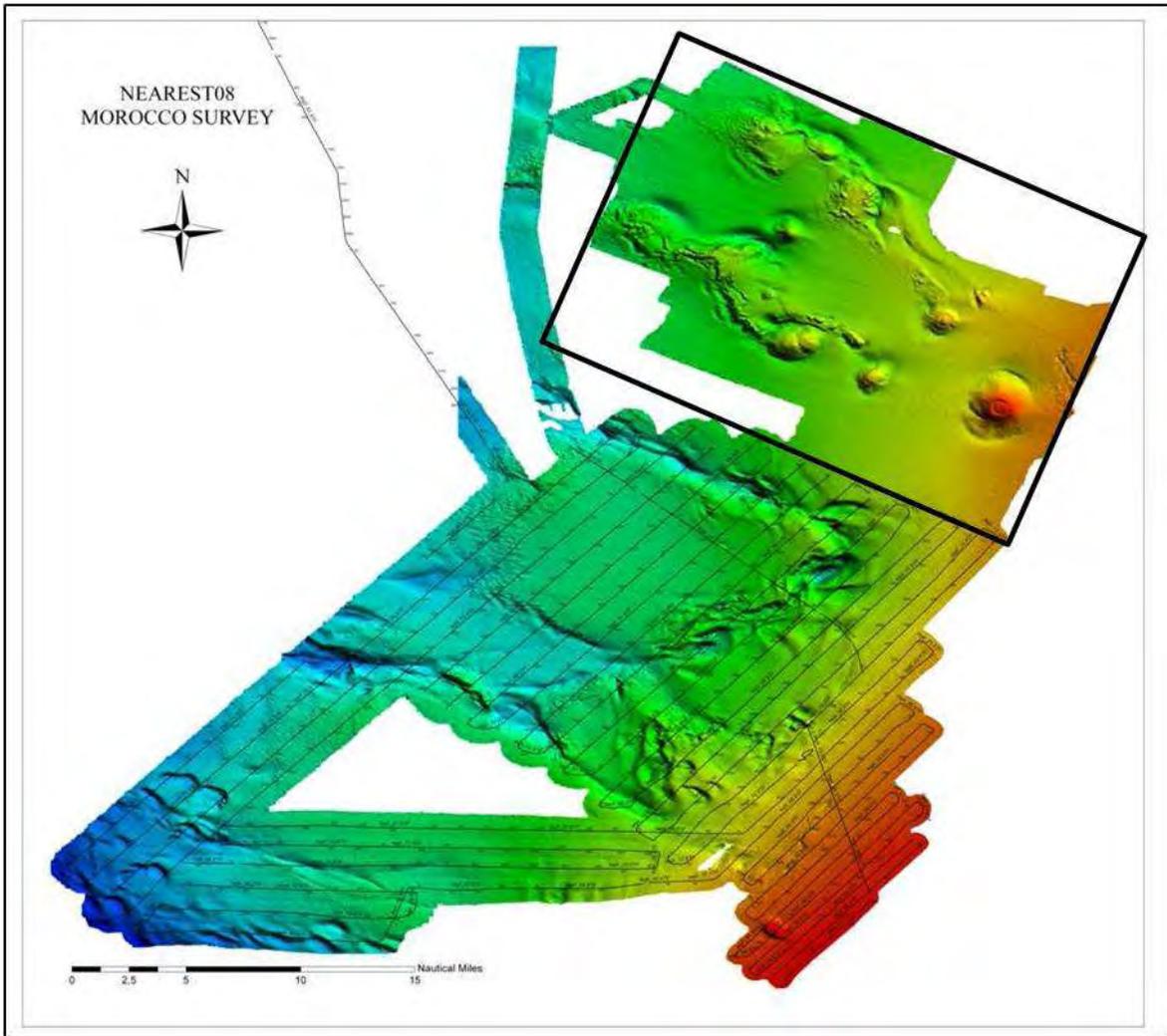
Figure 5.1.2 NEAREST08 (this work) and, in the box, R/V Belgica 2002 (Van Rensbergen et al., 2005), bathymetric surveys, shaded relief. Thin black line, CHIRP navigation tracks.

The presence of pop up structures, flowers geometries and the linearity prove their trascurrent nature (Line AR08 Plate 2). Eastward to the Horseshoe plain, these lineaments intersect the toe of the Gibraltar accretionary prism few kilometers North of Coral Patch Ridge. In this sector the morphological deformation associated to the lineaments are well recognized. Rosas et al. (2009) performed analogue modeling experiment to reproduce the mode of deformation associated to the lineaments as their interaction with the shallow soft sediment.

The experiment showed that the lineaments are related to crustal dextral trascurrent deformation started in the Late Pliocene at 1.8 Ma (Fig. 5.1.3).
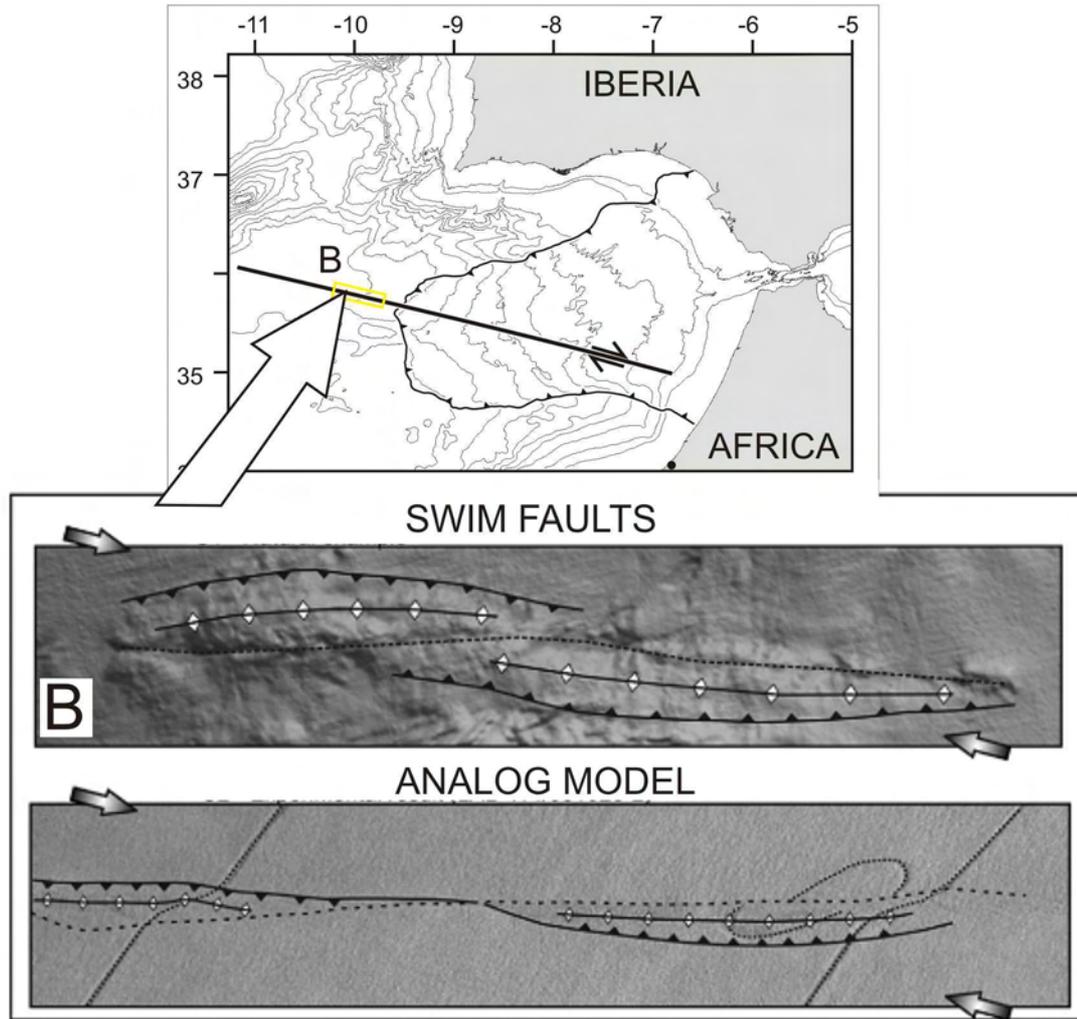
Figure 5.1.3 Analog modeling of the SWIM lineaments, modified after Rosas et al., (2009).

During the NEAREST 2008 R/V *Urania* cruise offshore Gibraltar, 1500 km^2 of multibeam high-resolution swath bathymetry were acquired together with high-resolution CHIRP seismic (Fig 5.1.2 and Plate 3). The survey was planned to map the eastern end of the SWIM lineaments on the Moroccan shelf. New bathymetric data provide grid image of the seabottom with the resolution of 25 x 25 m, this resolution allows to study also the small-scale elements of the lineaments and the interaction with the top of the accretionary prism.

The Gibraltar accretionary prism (Fig. 5.1.1), the offshore expression of the Betic Rifean orogenic arc extends for 350 km westward of Gibraltar Strait and is 150 km wide, in the North – South direction. To the North, it is bounded by the Guadalquivir Bank, an outcrop of

Hercinian Iberian basement. To the South, the prism is bounded by the Rharb submarine valley, the offshore extent of the Rharb basin, in Morocco. The frontal part of the prism ends against the Coral Patch Ridge which divided it in two lobes, one laying on the Seine and one laying on Horseshoe abyssal plains. These two frontal lobes present a markedly rough slope deformed by the high gravitational sliding of the prism.

The internal portion of the Gibraltar arc is characterized by a series of curvilinear ridge and troughs (Gutscher et al., 2009). The lower portion, at depth ranging from 3000 m bsl to 4300 m bsl, presents short wavelength (2-5 km), sub-parallel ridges, while in the shallower parts, up to 1000 m bsl, the ridges bound larger sub-rounded troughs. These ridges often are elongated parallel to the arcuate front of the prism. Offshore Morocco, the top of the prism has a very low slope, ≥1° and is flatter than its deeper parts.
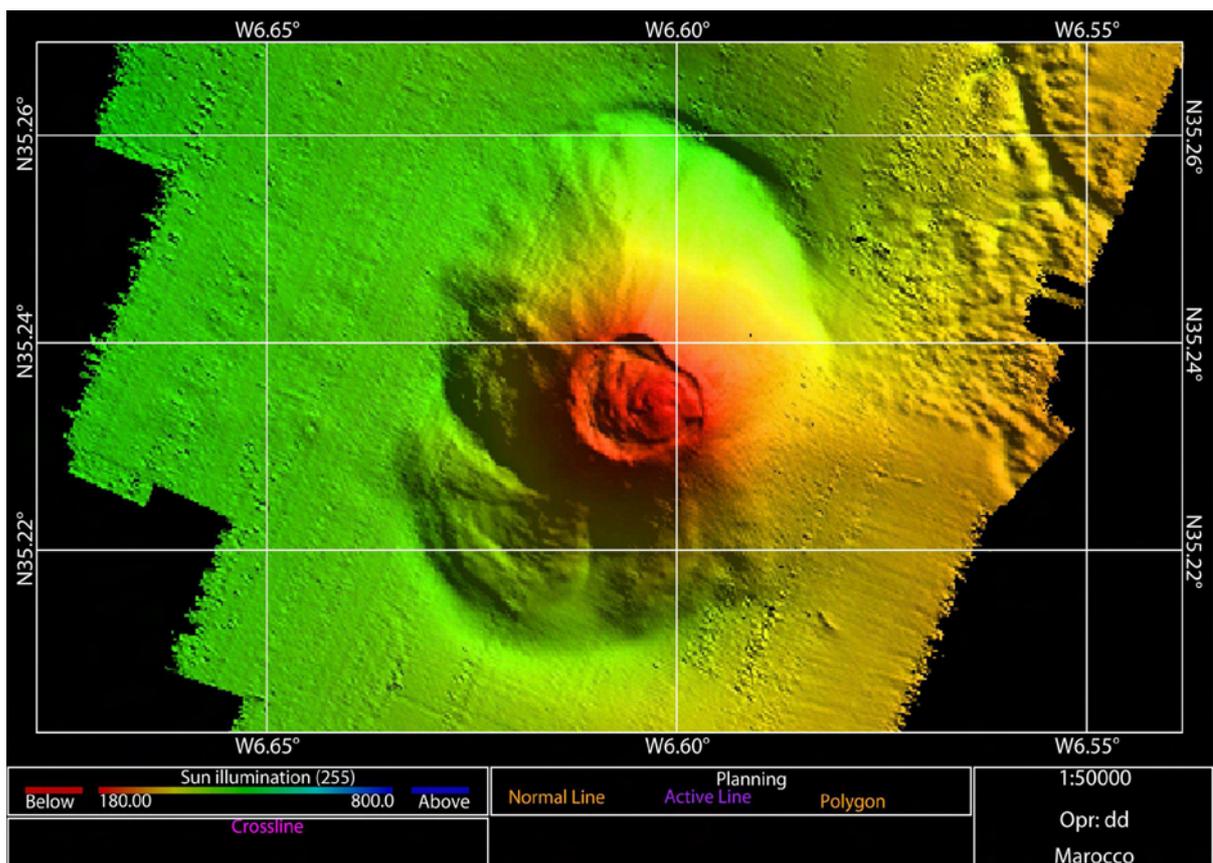
Figure 5.1.4 Al Idrissi mud volcano, located at the eastern termination of the Al Arraiche field, Shaded relief map, 25 x 25 m grid resolution. Image from NEPTUNE (Konsberg) multibeam data. Mercator projection.

The top of the prism presents several mud volcanoes clusters, frequently located at depth $\geq$ 1000 m. For example the El Arraiche field (Fig 5.1.1 and 5.1.2), North of the NEAREST2008 survey, consists of 8 mud volcanoes of various size and shape just below the Moroccan shelf edge. The largest mud volcano, Al Idrissi mud volcano (Fig. 5.1.4), is 225 m high and 5.3 km in diameter, the smallest observed mud volcano is only 25 m high and 500 m wide (Van Rensbergen et al., 2005). This area is cross cut by elongated sub linear features interpreted by Zitellini et al., 2009 as the eastern end of the SWIM lineaments. This linear features often correspond to two parallel ridges separated by deep narrow trough (Gutscher et al., 2009)

5.2 NEAREST2008 offshore Morocco survey

The investigated area is located on the continental slope offshore the Rharb basin, North Western Morocco, at depth variable from 170 m bsl down to 1100 m, in the South Western part (Fig. 5.1.2).

This sector is located on the Gibraltar prism terminating on the southern part on the Rharb submarine valley. At regional scale the area present very low slope value $\geq 1°$ but, in the study area, higher slope values are associated to gravitative phenomena and mud volcanism. The largest features the Mekness Mud volcano (Van Rensberg et al., 2005), is located in the South western part of the Nearest survey, in a zone mapped by the R/V *Belgica* 2002 cruise (Fig. 5.1.2).
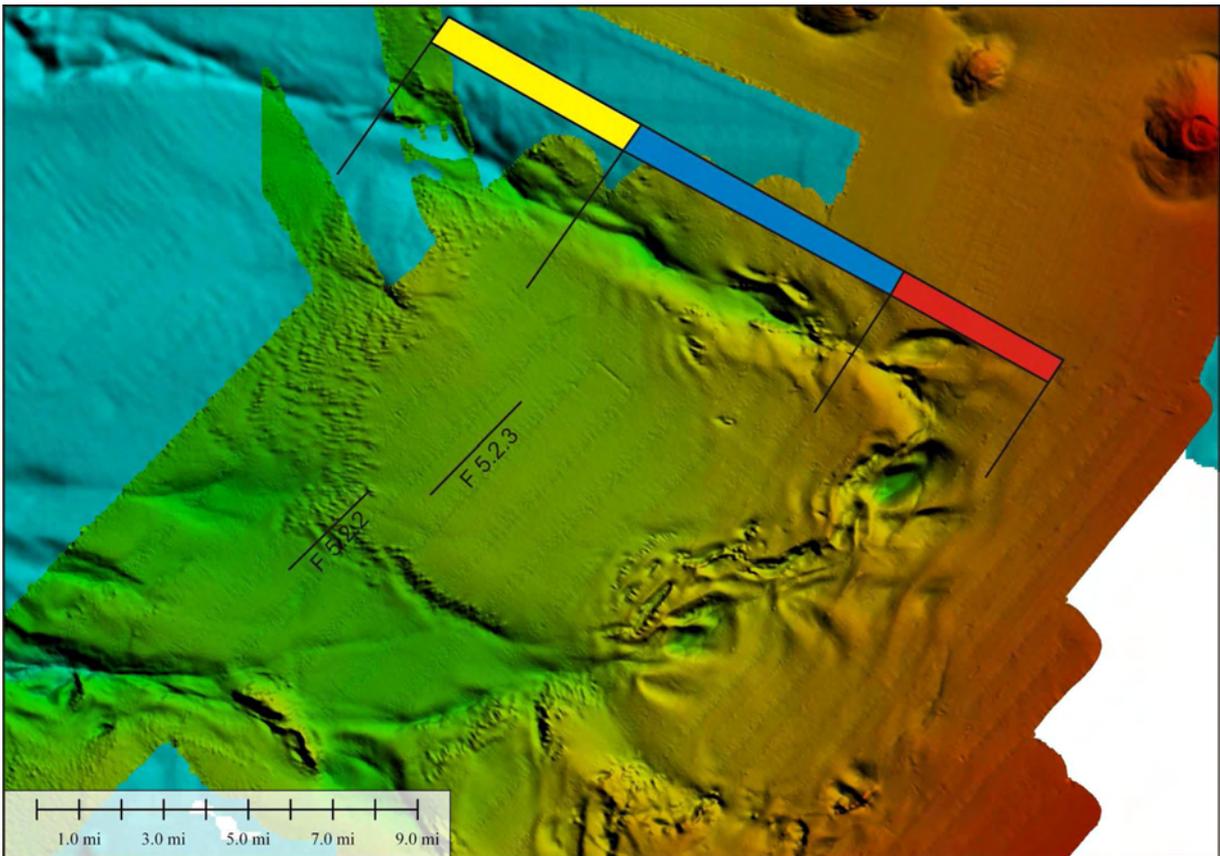
Figure 5.2.1 Landslide bathymetric shaded relief in the northern part of the Morocco survey. For location see Fig. 5.1.2, in Red is remarked the head domain, in Blue the translational zone and in yellow the toe deposits and track of the chirp line in Fig. 5.2.2 and 5.2.3.

The Nearest 2008 survey area presents many remarkable morphological features that denote the complex processes acting on top of the accretionary wedge. The North sector of the survey is characterized by a 20 km long and 10 km wide slide. All the three domains of the slide are well imaged from East to West, the headwall domain, the translational and the toe domain. The landslide present a very clear headwall domain zone with well developed graben-type deep valleys (Fig. 5.2.1). The headwall valleys are elongated from SW to NE where they are connected with a deep WNW - ESE deep submarine valley marking the Northern end of the slide. To the South, the headwall domain is connected with a set of lineaments elongated in the same direction. The valley reach a depth of 300 m in the northern sector while in the southern part it is at maximum 100 m deep. The sliding plane is not imaged in the Chirp line because of the presence of pervasive reflective hyperboles, in

correspondence of the head valleys, which mask the reflectors (Fig. 5.2.2) while in the translational domain the maximum penetration is a few tens of meters, so that, also in this sector, the bottom shear surface is not imaged.

The translational and toe domains are not well distinguished one from the other because the amount of translation of the landslide is very low. In fact, the slide moved downhill for a maximum of some hundreds of meters. Total displacement calculation in the head sector gives an estimate value decreasing from the Northern sector (with a maximum displacement of about 2.5 km) to the Southern margin (about 500 m). Uphill to the head valleys a series of extensional faults, driven by the opening of the head deep valleys, are present.
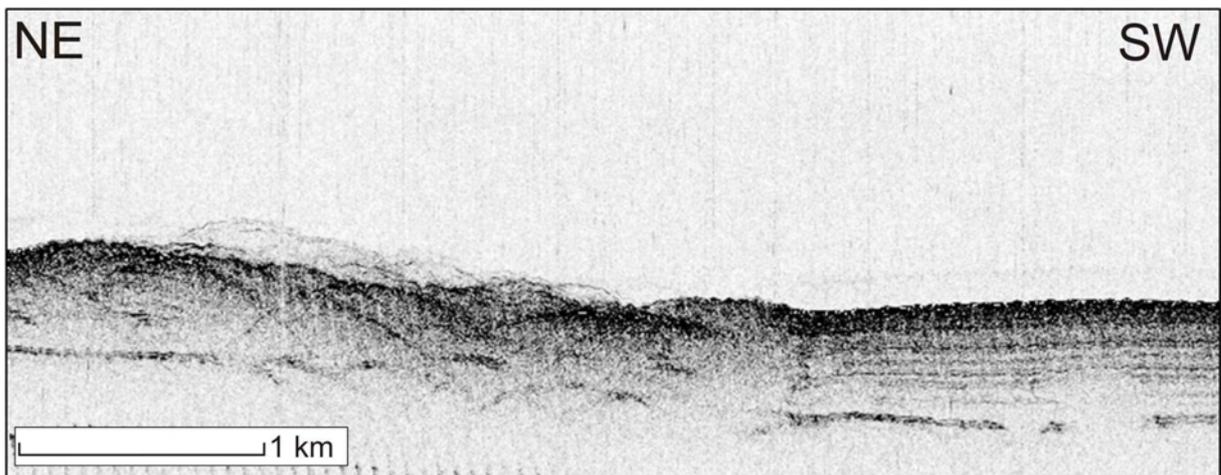
Figure 5.2.2 CHIRP seismic line LEG3_68. Vertical scale x2. Reflection hyperbole from the slide front.

The translational domain is connected in continuity with the head domain. The Northern lateral margin presents a deep incised valley corresponding with a long regional structural lineament. This valley presents a series of sigmoidal deep incisions suggesting a right lateral movements. A series of arcuate folds are present in this sector of the translational domain, which are interpreted as push ridge caused by the deformation of the higher head sector in to the translational domain. Chirp lines on the Western end of the translational domain of the slide show that the lateral continuity of the reflector is periodically interrupted every few km (Fig. 5.2.3). The reflectors are almost undeformed, quite horizontal, but are shifted along

vertical discontinuities, this pattern of blocks of truncated reflectors can be interpreted as longitudinal shear band in the sense of Bull et al., (2009). due to different slide velocity

The toe scarp of the landslide presents a series of downhill elongated scour and small ridges (Fig. 5.2.2). These features are elongated for a maximum of 1 km and wide some tens of meters Chirp lines downhill the toe domain show how the toe area is the source for dense turbidites like fluxes deposited few hundred of meters downhill. These fluxes can be triggered by the occurrence of a slope increment at the toe of the landslide together with fluid expulsion and consequent reduction of internal strength of the sediment.

A 100 m high scarp, with rough surface, delimits southward the landslide body. This limit corresponds to another regional lineament, probably bounding the gravitational movement of the landslide as the Northern lineament.
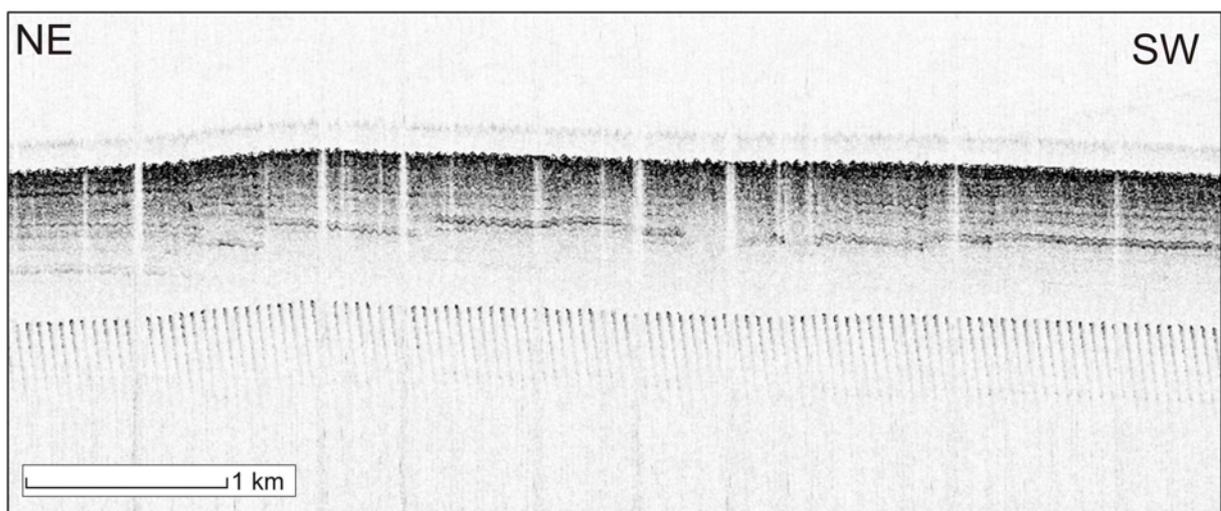
Figure 5.2.3 CHIRP line Leg3_81. Vertical exaggeration x5. Dislocated reflector in the translational domain of the landslide.

The sector of the survey, South of the landslide, is characterized by several lineaments that cut its Western sector. This is a flat continuous plain bounded by the slide body to the North and by a series of deep - incised valley to the South. To the East the plain prolongs into a slope between 500 m bsl and 800 m. On this slope several ridges and incisions are present, caused by gravitational creeping of the sea bottom.

Two order of lineaments can be recognized in the sector. First-order lineaments (WNW – ESE trending), are deep valleys with several sigmoidal depressions and pressure ridges, suggesting right-lateral movements. Second-order lineaments, branching out from the first order one and are elongated preferentially SW – NE; one of these second-order lineaments extends to the North and is in correspondence with the head domain area of the North Slide. This SW – NE lineaments cause weakening of the slope, likely triggering the onset of gravitative deformation. Chirp lines cutting the lineaments did not solve the deep structure of this for the poor penetration of the seismic high resolution signal and because of the hyperbolas.
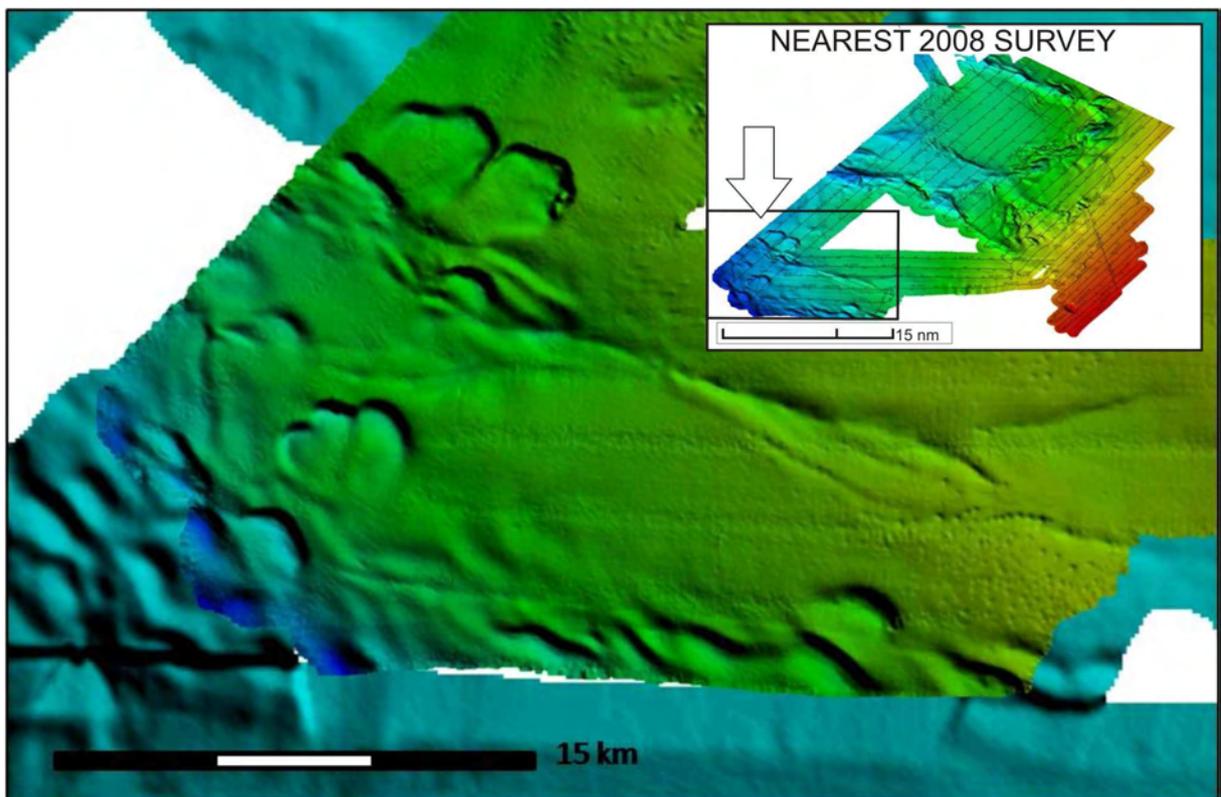
Figure 5.2.4 Particular of the NEAREST08 survey, shaded relief. It is recognizable on the wenstern margin the rounded scour. A set of lineaments marked with popmarcs are visible in the central and eastern sector.

The South sector of NEAREST 2008 survey presents principal lineaments elongated from the western margin toward ESE from which a series of small lineaments starts, often marked by pockmarks. Also in this case, as in the Northern sectors, the Chirp profiles didn't show clearly

the nature of the lineaments. Several round scours are present at the Southwestern end of the surveyed zone (Fig. 5.2.4). These are from 1km to 4 km wide and present the uphill side deeper than the downhill one. Chirp lines show how these gravitative fenomena are associated with the tectonic lineament. The erosional features are probably due to the interaction of sea bottom current and gravitative phenomena.
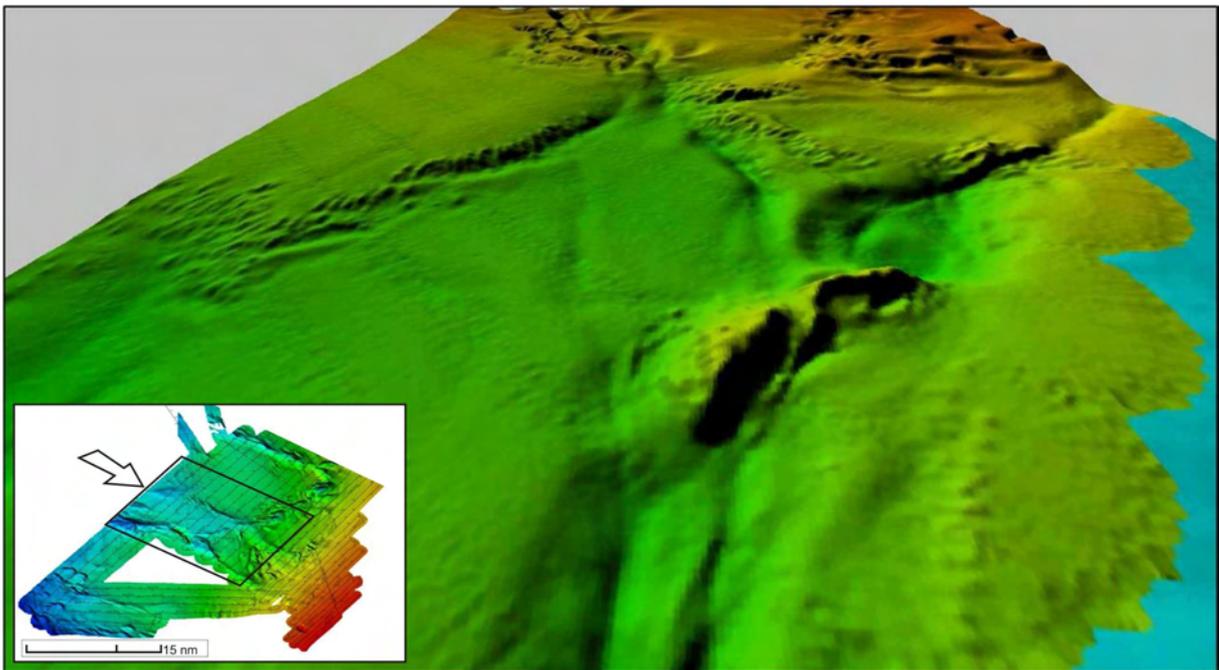
Figure 5.2.5 3D prospective of the lineaments in the central sector of the NEAREST 08 survey. On the top left side is present the landslide shows in Fig. 5.2.1.

Summarizing, this zone is characterized by the presence of four main NW-SE lineaments cross cutting the whole area. These elongated lineaments are frequently connected with a number of subsidiary and secondary lineaments. To the West, in the shallower part of the area, often these lineaments are not well recognized both by multibeam bathymetry and CHIRP seismic profiles. This is probably due to the high sedimentary rate which masks the deformation. Available seismic MCS line parallel, 15 nm to the Moroccan coast, evidenced that there is a extention of this discontinuities landwards. Despite the fact that the Rharb Basin is well studied in the deep portions by oil and gas well (Flinch, 1993), it is not sufficiently

investigated near the surface to find the presence of structures that can be related to this lineaments.

6 Cenozoic magmatic events in the Gulf of Cadiz

Coral Patch seamount as signature of the Monchique – Madeira hot Spot, Eastern Atlantic Sea.

Filippo D'Oriano[1,2], Lorenzo Angeletti[2], Lucilla Capotondi[2], Marinella A. Laurenzi[3], Marco Taviani[2], Luigi Torelli[4], Teresa Trua[4], Nevio Zitellini[2].

[1]Dipartimento di Scienze della Terra e Geologico - Ambientali, Università di Bologna, Piazza di Porta S. Donato 1, 40127, Bologna, Italy.

[2]Istituto di Scienze Marine, CNR, Area della Ricerca di Bologna, via Gobetti 101, 40129, Bologna, Italy.

[3]Istituto di Geoscienze e Georisorse, CNR, Area della Ricerca di Pisa, via G. Moruzzi 1, 56124, Pisa, Italy.

[4]Dipartimento di Scienze della Terra, Università degli studi di Parma, Viale G.P. Usberti 157, 43100, Parma, Italy.

Abstract

New detailed swath bathymetry, high resolution seismics and dredged samples from Coral Patch and Ormonde seamounts, SW Iberia, provide constraints on the emplacement of the Monchique-Madeira hotspot in the Eastern Atlantic Sea.

Swath bathymetric data document that Coral Patch is a composite structure, made up by at least nine distinct volcanic centers. Lithified pelagic carbonates, infilling fissures in lava blocks and hosting planktonic foraminifers permit to date at the Early Miocene the first documentation of Coral Patch acting as an offshore terrigenous-starved seamount. This setting extends to recent times. At Coral Patch seamount, similarly to what already observed at the Ormonde seamount, volcanism was emplaced on the top of a pre-existing relief and was

strongly affected by the regional tectonic compressive regime active, on this sector of the Africa Eurasia plate boundary, since the Oligocene.

Introduction

In the eastern Atlantic, a 700 km long belt of irregularly spaced seamounts stretches from SW Iberia to the Madeira archipelago (Fig.1). This feature is late Mesozoic to Recent in age and thought to represent the trace of the Monchique-Madeira hotspot (Morgan, 1981; Geldmacher *et al*., 2000).

Rocks representing initial and later stages of the Monchique – Madeira hotspot outcrop at the Serra de Monchique complex (~72 Ma, Miranda *et al*., 2009), in southern Portugal, and at the Madeira and Porto Santo islands (14-0 Ma, Geldmacher *et al*., 2000), respectively. The knowledge of the submerged portion of the hotspot track is quite scarce, due to the paucity of related samples. Previously collected volcanic samples from the Madeira hotspot related seamounts are alkaline in affinity, displaying a NE-SW decreasing age. Ages around 62-67 Ma (Ormonde seamount: Feraud *et al*., 1982, 1986), 31 Ma (Ampère seamount: Geldmacher *et al.*, 2000), 27 and 22 Ma (Unicorn and Seine Seamounts, respectively: Geldmacher *et al*., 2005), 11-14 Ma (Porto Santo Island) and < 5 Ma Madeira/Desertas volcanic complexes (Geldmacher *et al*., 2000) are known.

Various aspects concerning style of emplacement, spatial distribution and alignment of these volcanic seamounts are still debated (Geldmacher *et al*. 2005). Indeed, the emplacement of seamounts, particularly those lying eastward to the proposed hotspot track (i.e. Coral Patch and Ormonde) can either be related to (1) a volcanism locally controlled by lithospheric discontinuities or (2) magmatism related to a weak pulsating plume (Merle *et al*, 2006; Geldmacher *et al*., 2005).

The hotspot emplacement took place between Iberia and Africa plates. Since the earliest phase of continental break-up, the region recorded complex plate boundary interactions.

Nowadays, relative movement between Iberia and Africa is 4 mm/yr (DeMets *et al.*, 1994). The rifting-drifting stage was accompanied by sub-crustal mantle exhumation and scarce volcanic products (Boillot *et al.*, 1995; Whitmarsh and Wallace, 2001; Rovere *et al.*, 2004; Manatschal, 2004). From middle Cretaceous to late Oligocene, Iberia was part of the Africa Plate, and the Gulf of Cadiz was unaffected by any important tectonic stress. During the Oligocene, the counterclockwise rotation of Iberia respect to Africa produced a transtensive regime in the Bay of Biscay and intraplate diffuse compressive deformation in the Gulf of Cadiz (Sartori *et al.*, 1994; Galindo-Zaldivar *et al*, 2003). At about 2.0 Ma, the localization of the deformation started to be focused along ESE-WNW strike-slip faults (Zitellini *et al.*, 2009; Rosas *et al.*, 2009).

During this compressive stage, lithospheric folding developed in the area from Oligocene to Late Pliocene (Burov and Cloetingh, 2009; Zitellini *et al.*, submitted). Zitellini *et al.* (submitted) propose that lithospheric folding in the Gulf of Cadiz area caused the development of large synclines bounded by short thrust-top anticlines in the brittle crust, represented in this sector by the Coral Patch (CP) and the Gorringe Bank seamounts.

This work presents new marine geophysical and geological data collected it the Gulf of Cadiz area in the frame of the ESF SWIM project (SWIM04 and SWIM05 cruises) to better constrain the evolution of the Monchique-Madeira hotspot.

Materials and method

During the SWIM04 cruise of R/V *Urania* the navigation was done by the PDS2000 software linked with a DGPS Fugro satellite positioning system. High-resolution seismics was acquired by a 16 transducers 3.5kHz to 5 kHz BENTHOSII chirp sub bottom profiler. Sampling was performed by means of large volume (60 liters) grab and 200 kg heavy dredges.

During SWIM05 cruise of R/V *Explora*, 10000km^2 of swath bathymetric data have been acquired with a RESON 8150 multibeam system. The 12 kHz 234 beams echosouder was

mounted on the ship's keel and generated a swath of 150°. Daily CTD casts were performed during the survey from the surface down to 2000 m and integrated up to 5000m depth with available data from the Levitus Database (Locarnini *et al.*, 2005). The positioning and the navigation was performed with the PDS2000 software connected to a satellite DGPS LandStar MK Veripos.

The bathymetric data were processed on board with the PDS2000 and with the IFREMER Caraibes software, and at the ISMAR laboratory with the Konsberg NEPTUNE software to build a 50 x 50 m grid spacing digital terrain model (Fig.2) for elevation down to 1000 m bsl, 100 x 100 m under 1000 m bsl.

Volcanics (lavas and hyaloclastites) and sedimentary carbonates were recovered from the four sampling sites at the CP and Ormonde seamounts (Fig.3, Fig.4 and Appendix in Supplementary Material). The volcanic samples are strongly altered, thus precluding conventional geochemical whole rock analyses. The principal petrographical and mineralogical characteristics of the studied samples (thin sections and Electron Probe Microanalyses) are given in Appendix S2 and S3 (Supplementary Material). The major element composition of phenocrysts of the lava samples was analyzed by means of a CAMECA SX50 electron microprobe, equipped with four WDS, at the IGG-CNR, Padova.

^{40}Ar-^{39}Ar step-heating and single crystal analyses were performed on volcanic samples at the Ar-Ar laboratory, IGG-CNR, Pisa (details on analysis are in Supplementary Material). Errors are quoted at the $\pm$ 2σ level.

Biostratigraphical investigation has been performed on dredges SWIM29 and SWIM28, sampled from western part of the CP (Fig.3 and Fig.4). The analyses are based on the Foraminiferal content identified in thin section.

Morphobathymetry

71

The CP is a WSW-ENE elongated seamount that arises about 4000 m above the adjacent Horseshoe and Seine abyssal plains with a minimum depth of about 645 m (Fig.2). It is sub elliptical in shape, 120 km long and about 70 km wide.

Available seismic multichannel data (Hayward *et al.*, 1999; Contrucci *et al.*, 2004, Zitellini *et al.*, 2009) shows that CP, up to 2.500 m bsl, is sedimentary in nature. Nevertheless, at shallower levels volcanic rocks are present, as documented by ROV visual inspection (Hebbeln, 2008) and the sampling from the seamount (this study and Geldmacher and Hoernle, 2000).

On the CP top, swath bathymetry documents the presence of several coalescent volcanic edifices emplaced on the upper part of the seamount. Nine principal volcanic centers are recognizable, eight of which are clustered on the southwestern margin, while a single isolated cone (referred to as Vince volcano: Fig. 2) arises 450 m from the northeastern side. All the minor volcanic edifices have a mean width of about 3-5 km and a mean height of about 100-300 m. Instead the largest Vince volcano reaches a diameter of about 8 km. The volcanic edifices are recognized due to a sub-circular conic shape and well preserved morphology; at places, radial elongated lava flows are recognizable along their slopes (Fig.2).

On the western side, the CP declines gently joining the eastern slope of the Ampère Seamount. The southeastern slope is steeper with inclinations from 5° to 20°. This part is characterized by several straight scour erosional features; the biggest one, starting above a steep scarp near the summit, is 11 km in length with a mean slope of about 12°. East of Vince edifice, the slope becomes less steep and is characterized by several scarps elongated preferentially NNE-SSW. These scarps often are the head-scarps of important gravitative phenomena.

The North side of CP is more complex. On the eastern side, the slope declines gently toward the Horseshoe Abyssal Plain and only linear, small, scours are developed along it. The central sector is characterized by a flat topography in the shallower part and by a series of sub parallel north verging scarps on the deeper part, probably due to gravitational phenomena. A series of

sub parallel antiform ridges oriented NE-SW occurs westwards. These ridges run for 30 km and are usually 2-3 km wide terminating in the Horseshoe Abyssal Plain

Petrography

The samples dredged from the CP (station SWIM29) (Fig.3) and one sample from the Ormonde Seamount (station SWIM34) consist of large (up to 30 cm) blocks of fractured lavas, infilled by foraminiferal limestone, plus loose biogenic skeletal sediment. The other volcanic samples are hyaloclastites (CP) and lavas (Ormonde).

The high degree of alteration of the volcanic sample recovered from CP precludes conventional whole-rock analyses, necessary to properly classify the volcanic rocks, thus the magmatic affinity of this sample is only based on mineralogical criteria. The CP sample consists of three large blocks of olivine-phyric lavas cemented by biogenic limestone (Fig.3). The lava blocks, classified as basanites, have a mineralogical assemblage made of olivine (Fo_{83-81}), diopside (Wo_{47-50}-En_{29-39}) clinopyroxene. It is to note that the sampling of basanitic lavas from the CP improves our knowledge on the magmatism affecting this structure, since up to present only hawaiitic lavas were known (Geldmacher and Hoernle, 2000).

Four altered volcanic samples were recovered from the Ormonde Seamount (stations SWIM32 and 34), thus also for these samples, like the CP sample, the magmatic affinity is based on mineralogical criteria. These samples resemble the highly alkaline, silica-undersaturated volcanics previously recovered from the seamount (Corner, 1982; Geldmacher and Hoernle, 2000; Schärer *at al*., 2000). In detail, samples SWIM32/1, SWIM32/2 and SWIM32/3 show a mineralogical assemblage similar to the lamprophyric dikes cutting the north-eastern part of the seamount (Corner, 1982). These rocks are porphyric with altered olivine and diopsidic clinopyroxene (Wo_{47-52}-En_{26-41}) phenocrysts set in a groundmass consisting of these phases plus altered feldspar, phlogopite, opaque and altered glass. The other Ormonde sample (SWIM34) has rare phenocrysts of a mineral of the sodalite group and

resorbed biotite set in a microlitic fluidal groundmass consisting of these phases plus altered nepheline, feldspar, opaque and altered glass.

Biostratigraphy and geochronology

The micropaleontological analysis was performed on carbonate veins infilling fissures of the volcanic bedrock. A rich and well preserved planktonic foraminiferal fauna is present in CP sample SWIM29. Thin section study positively identified *Globoquadrina* aff. *dehiscens* (primitive forms), *Globorotalia* ex gr *opima nana/mayeri* (Fig.3) and especially the absence of *Globigerinoides* spp. documents the lowermost part of the Miocene Epoch. Following Bolli & Sauders 1985, this fauna is a characteristic element of the *Catapsydrax stainforthi* Zone correlable with the lower part of the M1 Zone of Berggren *et al*. 1995 spanning from 23.8 to 21.5 Ma.

^{40}Ar-^{39}Ar step-heating (SH) of the ground mass of sample (SWIM04-29/1) gives a disturbed age spectrum, with only a mini-plateau at 31.48 ± 1.98 Ma (28.4% of ^{39}Ar release, MSWD=0.24) (Fig.3). It is worth noting that the high degree of alteration of the sample allows considering the ^{40}Ar-^{39}Ar datum only as indicative.

At Ormonde, two biotites separated from station SWIM32 and SWIM34 give isochron ages of 63.31±0.87 Ma (SWIM04-32/3, SH, 41.7 % of ^{39}Ar release, MSWD=1.3) and 63.85±0.61 Ma (SWIM04-34, SH, 100% of ^{39}Ar release MSWD=2.0). Single crystal laser fusion (SCLF) analyses of SWIM04-34 biotites display a probability plot slightly asymmetric toward younger ages, likely due to alteration. See Supplementary Material for details on the analyses. These new Ormonde age data are all within the limits reported in literature (Feraud *et al.*, 1982, 1986).

Discussion and Conclusion

The geomorphological setting of CP seamount is quite complex as revealed by the detailed swath bathymetric data. Indeed, this new dataset shows that at the top of the seamount at least nine distinct volcanic coalescent cones are located. These were emplaced on a preexisting structural high and all of them have a well preserved morphology. The single volcanic sample recovered from one of the volcanic cones recognized on the western sector of the CP seamount is a strongly altered basanite whose groundmass suggests a middle Oligocene age (31 Ma). The Early Miocene age of the sediments infilling the basalt fractures further constrain the emplacement age of the volcanic complex at the CP. The combined petrologic evidence of our own data coupled with published data by Geldmacher *et al.* (2006) suggest that the magmatism affecting the CP seamount has a basanite-hawaiite range, comparable to that observed at the Ampère Seamount (Geldmacher and Hoernle, 2000). Geochemical composition from Ampère lavas permitted to relate their origin to different degrees of partial melting above discrete pulses of a mantle plume (Geldmacher and Hoernle, 2000). A similar process could control the basanite-hawaiite variation observed in the CP lavas, but more volcanic samples from this seamount are required to better constrain such an hypothesis.

Recently, Zitellini *et al*. (2009) showed that the whole sector of the Eurasia – Africa plate boundary was affected, since the Oligocene, by lithospheric folding. This implies an overlap of the two processes: oblique lithosphere collision and hotspot related volcanism. The ENE-WSW orientation of the major seamounts of the area, such as the Gorringe Bank and the CP Seamount, suggest that magmatism affecting these structures is also locally controlled by propagating lithospheric fractures.

Burov and Cloetingh (2009) showed how the impact of a mantle plume may result in a reduction of the folding wavelength of the overlying lithospheric plate. In the Gulf of Cadiz, lithospheric folding is manifested in a confined region near the plate boundary and above the hotspot track, thus folding and thrusting in this area were influenced by the plume

emplacement. Following the Burov and Cloetingh (2009) model, folding in a low convergence rate (< 1.5 cm/yr) area, having relatively young (<150 Ma) lithosphere, can only occur if an external perturbation such as a mantle plume, is also present.

Furthermore, as documented by our study, the volcanism affects pre-existing seamount structures suggesting that the lithospheric folding anticlines developed in the Gulf of Cadiz acted as preferential paths for the upwelling of mantle material. We suggest that the interaction between lithospheric folding and the hotspot emplacement can also be responsible for both the irregularly spaced hotspot seamounts, with large km-sized gaps in between, and for the WSW-ENE orientation of the volcanic centre at the CP and Ormonde seamounts. Finally, available seismic data integrated with new paleontological, and morphological evidences suggest that the CP was not affected by subsidence since early Miocene.

Acknowledgments

References

Berggren, W.A. Kent, D.V., Swisher, C.C. III, and Aubry, M.-P., 1995 A revised Cenozoic geochronology and chronostratigraphy, *Time Scales and Global Stratigraphic Correlation*. In: W.A. Berggren and D.V. Kent, Editors,*SEPM Spec. Publ.* **54** (1995), pp. 129–218.

Bolli H.M., Saunders J.B. 1985. Oligocene to Holocene low latitude planktic foraminifera. In:

Plankton Stratigraphy. Bolli H.M., Saunders J.B., Pearch Nielsen K., Editors, Cambridge University Press.

Boillot, G., Beslier, M.O. and Girardeau, J., 1995. Nature, structure and evolution of the ocean-continent boundary: the lesson of the West Galicia margin (Spain). In *Rifted Ocean-Continent Boundaries* (Banda, E., Torné, M. and Talawani, M., eds). NATO ASI Series, Kluwer Academic, Dordrecht.

Burov, E. and Cloetingh, S., 2009. Controls of mantle plumes and lithospheric folding on modes of Intraplate continental tectonics: differences and similarities *Geophysical Journal International*, **178**, 1691-1722

Contrucci, I., Klingelhöfer, F., Perrot, J. *et al.*, 2004. The crustal structure of the NW Moroccan continental margin from wide-angle and reflection seismic data. *Geophysical Journal International*, **159**, 117-128.

DeMets, C., Gordon, R. G., Argus, D. F. and Stein, S., 1994. Effect of recent revisions to the geomagnetic reversal time scale on estimates of current plate motions. *Geophysical Research Letters*, **21**, 2191-2194.

Féraud, G., Gastaud, J., Auzende, J.M., et al., 1982. G. Féraud, J. Gastaud, *et al.*, 1982. ^{40}Ar/^{39}Ar ages of the alkaline volcanism and the basement of Gorringe Bank, North Atlantic ocean. *Earth Planet. Sci. Lett.***57**, 211–226.

Féraud,G., York, D., Mével, C. et al., 1982. Additional ^{40}Ar-^{39}Ar dating of the basement and the alkaline volcanism of Gorringe Bank (Atlantic Ocean) *Earth and Planetary Science Letters*, **79**, 255-269.

Galindo-Zaldivar, J., Maldonado, A. and Schreider, A.A., 2003. Gorringe Ridge gravity and magnetic anomalies are compatible with thrusting at a crustal scale *Geophysical Journal International*, **153**, 586-594.

Geldmacher, J., Hoernle, K., Klugel, A., et al., 2006. Origin and geochemical evolution of the Madeira-Tore Rise (eastern North Atlantic) *Journal of Geophysical Research*, **111**, B09206, 1-19.

Geldmacher, J., Hoernle, K., Bogaard, P.v.d. *et al.,* 2005. New ^{40}Ar/^{39}Ar age and geochemical data from seamounts in the Canary and Madeira volcanic provinces: Support for the mantle plume hypotesis *Earth and Planetary Science Letters*, **237**, 85-101.

Geldmacher, J., and Hoernle, K., 2000, The 72 Ma geochemical evolution of the Madeira Hotspot (eastern North Atlantic); recycling of Paleozoic (≤500 Ma) oceanic lithosphere *Earth and Planetary Science Letters*, **183**, 73-92.

Hayward, N., Watts, A.B. Westbrook, G.K. and Collier, J.S. 1999. A seismic reflection and GLORIA study of compressional deformation in the Gorringe Bank region, eastern North Atlantic. *Geophysical Journal International*, **138**, 831–850.

Hebbeln, D., 2008. Short Cruise Report, Expedition 64PE284 R/V Pelagia. Online *http://www.ifm.zmaw.de* [checked 4 November 2009]

Locarnini, R. A., Mishonov, A. V. *et al*., 2006. World Ocean Atlas 2005, Volume 1: Temperature. Levitus, Ed. NOAA Atlas NESDIS 61, U.S. Government Printing Office, Washington, D.C., 182 pp.

Manatschal, G., 2004, New models for evolution of magma-poor rifted margins based on a review of data and concepts from West Iberia and the Alps. *International Journal of Earth Sciences*, **93**, 432-466.

Merle, R., Schrarer, U., Girardeau, J. and Corner, G., 2006. Cretaceous seamounts along the continent – ocean transition of Iberian margin; U –Pb ages and Pb – Sr – Hf isotopes. *Geochimica et Cosmochimica Acta*, **70**, 4950 – 4976.

Miranda, R., Valadares, V., Terrinha, P., *et al*, 2009. Age constraints on the Late Cretaceous alkaline magmatism on the West Iberian Margin. *Cretaceous Research*, **30**, 575-586.

Morgan, W.J., 1981. Hotspot tracks and the opening of the Atlantic and Indian Oceans. In: *The Sea: Oceanic Lithosphere* (Emiliani, C., ed). **7**, 443-487, John Wiley, New York.

Rosas, F.M., Duarte, J., Terrinha, *et al*., 2009. Major bathymetric lineaments and soft sediment deformation in NW Gulf of Cadiz (Africa–Iberia plate boundary): new insights from high resolution multibeam bathymetry data and analogue modelling experiments. *Marine Geology,* **261**, 33-47.

Rovere, M., Ranero, C.R., Sartori, *et al*., 2004, Seismic images and magnetic signature of the Late Jurassic to Early Cretaceous Africa-Eurasia plate boundary off SW Iberia. *Geophysical Journal International*, **158**, 554-568.

Srivastava, S.P., Roest, W.R., Kovacs, L.C., Oakey, G., Levesque, S., Verhoef, J., and Macnab, R., 1990, Motion of Iberia since the Late Jurassic; results from detailed aeromagnetic measurements in the Newfoundland Basin. Tectonophysics, **184**, 229-260.

Sandwell, D.T. and Smith, W.H.F., 1997. Global sea floor topography from satellite altimetry and ship depth soundings. *Science*, **277**, 1956–1962.

Whitmarsh, RB, Wallace, P.J., 2001. The rift-to-drift development of the West Iberia non volcanic continental margin: A summary and review of the contribution of ocean drilling program leg 173. In: Beslier, M.O., Whitmarsh, R.B, Wallace, P.J., Girardeau,

J., (eds) Proceedings of the Ocean Drilling Program, Scientific Results. CollegeStation, TX, **173**, 1–36

Zitellini, N., Gràcia E., Matias L., *et al*., 2009. The quest for the Iberia-Africa Plate boundary west of Gibraltar. *Earth and Planetary Science Letters*, **280**, 13-50.

Zitellini, N., Rovere, M., Terrinha, P., *et al*., 2004. Neogene through Quaternary Tectonic reactivation of SW Iberian Passive Margin. *Pure and Applied Geophyscs*, **161**, 565–585.

Zitellini, N., Cloetingh, S., D'Oriano, F. and Burov, E., submitted. Synclinal deformation as prime expression of compressional deformation of the lithosphere: the Atlantic segment of the Iberia-Africa Plate Boundary. *Geology* Submitted.

Figure Caption

D'Oriano et al., Figure 1
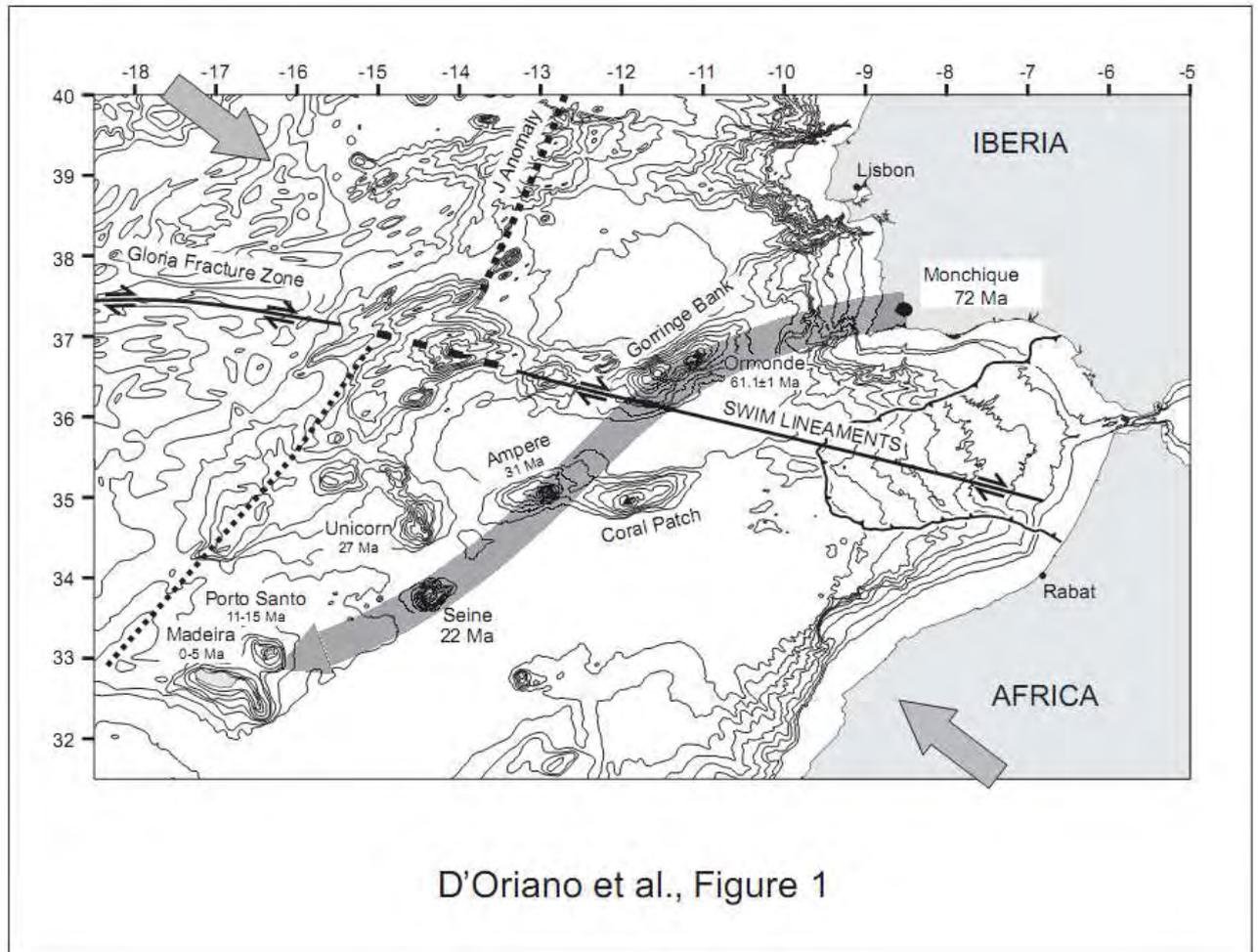
Figure 1

Bathymetry of the Central Eastern Atlantic Sea (Sandwell and Smith, 1997); thin black line: Gibraltar accretionary prism; thick black line: Iberia – Africa plate boundary proposed by Zitellini et al., (2009); transparent arrow: Monchique Madeira hot spot track; black triangle: SWIM sample on the Coral Patch and Ormonde seamounts; date of the seamount after Geldmacher et al., 2006.
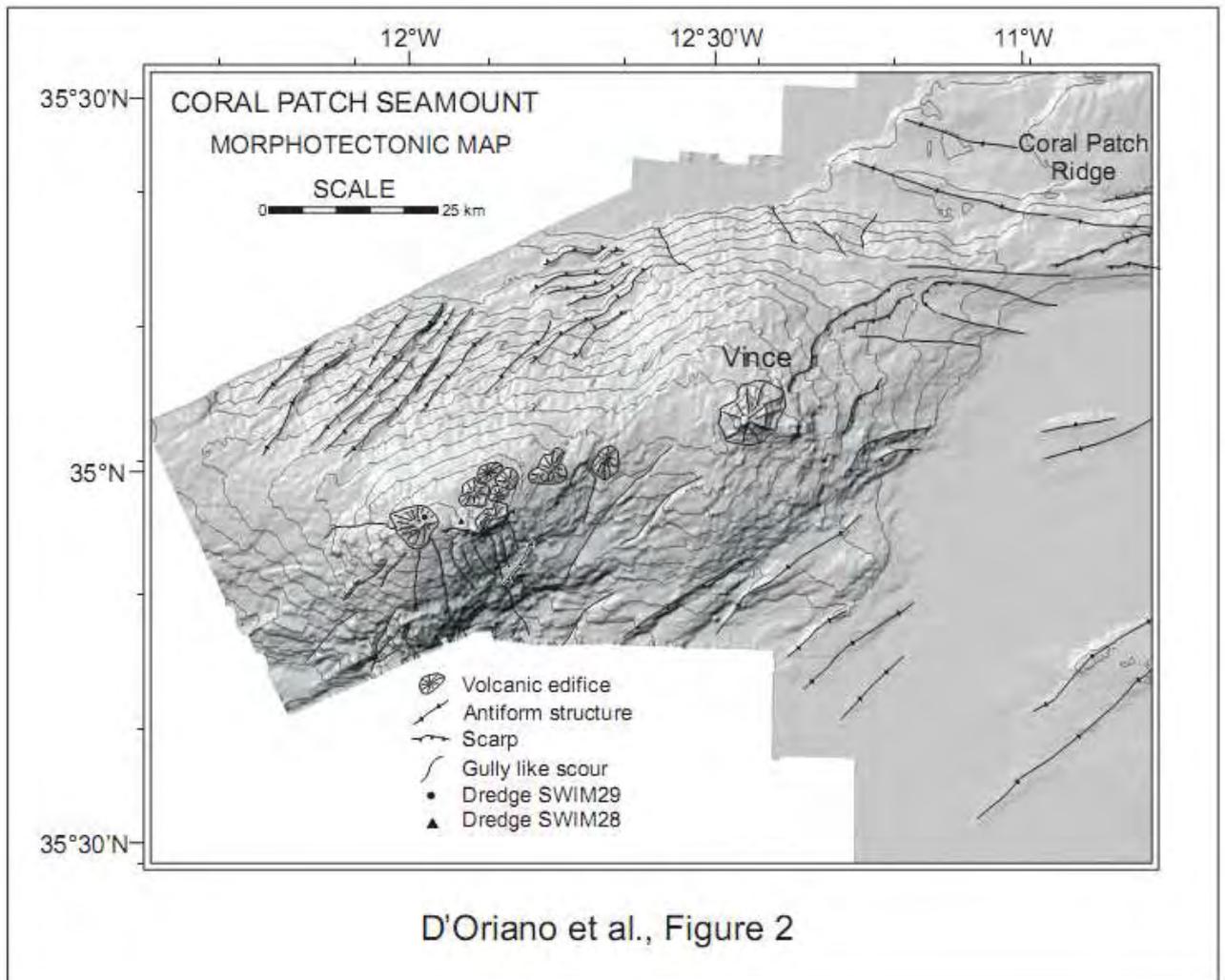
Figure 2

a) Shaded relief of the SWIM 05 survey, contour lines step 100m. b) Morphological and structural interpretation.
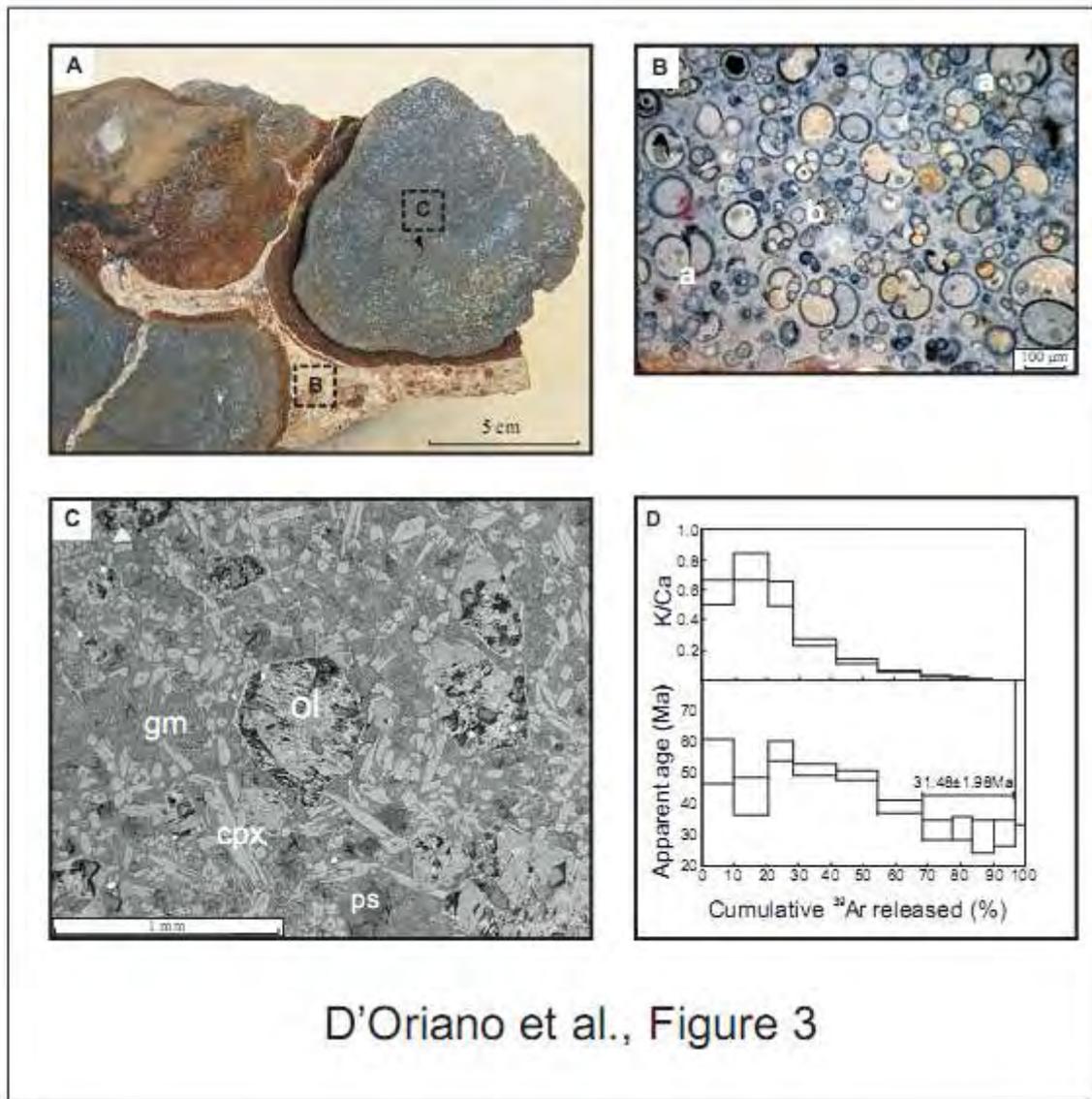
Figure 3

Sample SWIM 29 dredged on the Coral Patch seamount (coordinates in Table 1 supp. mat.).
A lava blocks infilled by bioclastic sediments; **B** planktic assemblage, **a** *Globoquadrina aff.*
dehiscens (primitive forms), **b** *Globorotalia* ex *gr opima nana/mayeri;* **C** SEM photo (in
back-scattered electrons) of one lava block. ol=olivine, cpx=clinopyroxene; (ps)=
pseudomorphs, having the shape of feldspathoids, composed of aggregate of zeolites and
carbonate; gm=groundmass ; **D** [40]Ar-[39]Ar step-heating age and K/Ca spectrum of the ground
mass separated from sample SWIM 29-1. Horizontal bar indicates plateau steps and error box
are ±2σ. See Supplementary Material for analytical details.

D'Oriano et al., Figure 4
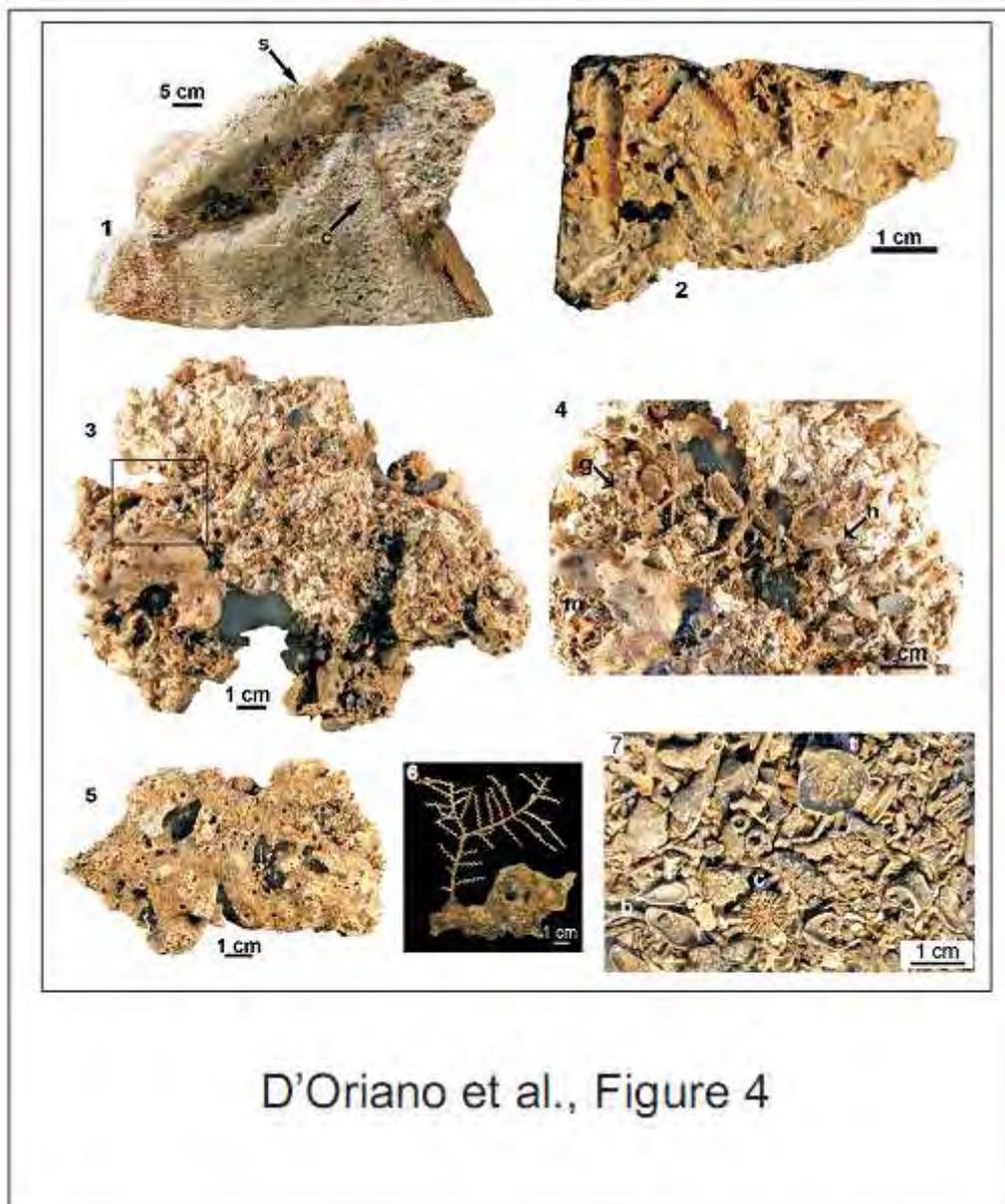
Figure 4

Various types of sedimentary products sampled from Coral Patch seamount: 1. Sliced slab of the olivine-phyric sample (St. SWIM29) reported in Fig.3A; note fouling recent epifauna, including serpulid tubes (s) and indetermined solitary coral base (c). 2. Carbonate hardground from St. SWIM28,958/725m; the fresh cut shows many elongated vugs due to dissolution of former deep-water coral branches; the external surface is blakneded by Mn-Fe oxide coating and affected by intense bioerosion (*Trypanites* - ichnofacies). 3. Carbonate hardground recovered at St. SWIM28, showing different stages of lithification. 4. Close-up of same sample in Fig. 4.3 displaying coarse skeletal component entrapped in poorly lithified matrix, including (g) benthic (*Amphissa acutecostata*) and holoplanktonic (h) gastropods, (m) deep-water branching corals (*Madrepora oculata*) and others. 5. Coarse coral frame bearing

hardground made up by degraded and bioeroded *Madrepora*, st. SWIM028. 6. Living hydroid (*Sertularella* sp.,identification courtesy of G. Bavestrello) growing on carbonate coral rubble (st. SWIM28). 7. Palimpsest skeletal assemblage from St. SWIM28; coarse coral-mollusc hash is mostly composed by more or less degared shell material, including molluscs (b= the bivalve *Asperarca*), brachiopods (t=*Terebratula*), corals (c=*Deltocyathus* sp.), barnacles, serpulids, echinoids etc.

The supplementary material of the paper is presented as Appendix of this work

Appendix S1: Sampling site, typology of sampling and recovery sample used in this work from SWIM 2004 cruise.
Appendix S2: Petrographical semples description.
Appendix S3: Petrographical analysis .
Appendix S4: ^{40}Ar-^{39}Ar Dating.
Appendix S5: 3D shaded relief of the Coral Patch Seamount.

7 Conclusion

The Gulf of Cadiz lies at the eastern end of the Azores Gibraltar plate boundary. It was considered in the last 15 years as a diffuse plate boundary, characterized by scattered seismicity and active tectonic structures (Sartori et al., 1994). recently, an high resolution bathymetric map, compiled by Zitellini et al. (2009) and built up in the frame of the ESF SWIM project by 12 European Institution, permitted to clarify the recent tectonic setting of this area. Zitellini et al. (2009) proposed that the deformation of the plate boundary, starting about 2 Ma ago, focused on a set of right trascurrent lineaments, cross cutting the whole Gulf of Cadiz from the eastern end of the Gloria Fracture Zone to the Moroccan margin.

One of the main task of this thesis was to investigate the deformation style offshore Gibraltar in the Eocene to late Pliocene time interval: It is here proposed that during this time the stress related to the compression between Africa and Eurasia caused lithospheric folding. Seismic lines interpretation and gravity data analysis permitted to develop a new concept on the mode of deformation caused by lithospheric folding in the upper lithosphere. In particular, the deformation is expressed by the development of large wavelength (8 – 130 km) "crustal scale" synclines bounded by short wavelength top thrust anticlines (2 – 40 km). This new concept predict that horizontal stress in the lithosphere do not form periodic anticlines and synclines, but develops asymmetric structures as large synclines and short anticlines. Further on, seismic multichannel data show that folding and faulting start both at the onset of the compression.

The lithospheric folding processes interact in the Gulf of Cadiz with the Monchique Madeira hot spot emplaced in the area from the 72 Ma old Monchique volcanic complex to recent Madeira Archipelago, and testified by a 700 km long series of abyssal volcanic seamounts. In this work it is the characterized, for the first time, a 31 Ma old basanitic volcanism related to the upwelling of mantle plume material at the Coral Patch seamount, and it is shown how it

interacts with the lithospheric folding. This seamount has been completely mapped by high resolution swath bathymetry, revealing that is more complex than previously thought. At least nine volcanic edifices are described and one of this has been sampled, giving an ^{40}Ar-39Ar age of 31.4±1.98 Ma, dating for the first time the top of the Coral Patch seamount. Analysis of bathymetry, seismic lines and paleontological samples testify that Coral Patch was not affected by subsidence since Chattian (28 Ma). This suggests that the tectonic horizontal stress and mantle plume thermal bulging are acting on this seamount since Oligocene.

During Late Pliocene, at the plate boundary, compression focused on the SWIM lineaments, a series of right lateral trascurrent faults. The interaction of these lineaments with the Gibraltar accretionary prism was studied in the last part of this thesis, after an oceanographic cruise that acquired new bathymetric and geophysical data offshore Moroccan in 2008. The bathymetric and high-resolution seismic survey was focused on the acquisition of new data at the eastern end of the SWIM lineaments, near the Moroccan shelf. The new dataset provide evidence about the interaction of the relatively young trascurrent faults and the Mio-Pliocene arc. In particular, it illustrates how the SWIM lineaments interact with the Pleistocene to Recent gravitative and fluid escape phenomena characterizing the top of the Gibraltar arc in the Moroccan offshore.

10 References

Argus, D.F., Gordon, R.G., DeMets, C., and Stein, S., 1989, Closure of the Africa-Eurasia-North America plate motion circuit and tectonics of the Gloria Fault: Journal of Geophysical Research, B, Solid Earth and Planets, 94, 5585-5602.

Bally, A.W., (ed). Atlas of Seismic Stratigraphy, 1987, AAPG studies in geology n°27, p.126, AAPG, Tulsa, Oklaoma, USA.

Banda, E., Torne, M., Sibuet, J.C., et al., 1995, Iberian Atlantic Margins Group investigates deep structure of ocean margins: Eos, Transactions, American Geophysical Union, 76, 25.

Boillot, G., Beslier, M.O., Krawczyk, et al., 1995, The formation of passive margins: constraints from the crustal; structure and segmentation of the deep Galicia margin, Spain: The tectonics, sedimentation and paleoceanography of the North Atlantic Region. Geological Society Special Publications, 71-91.

Bull, S., Cartwright, J., Husse, M., 2009. A review of kinematic indicators from mass-transport complexes using 3D seismic data. Marine and Petroleum Geology, v. 26, p.1132-1151.

Caratori Tontini, F., Cocchi, L. and Carmisciano, C., 2008. Potential-field inversion for a layer with uneve thickness: The Tyrrhenian Sea density model. Physics of the Earth and Planetary Interiors. 166, 105 – 111.

Caress, D.W. and Chayes, D.N., 2009.Dave Caress and Dale Chayes, MB-System, Mapping the Seafloor, Software for the Processing and Display of Swath Sonar Data, 2009, V5.1.1,www.ldeo.columbia.edu/res/pi/MB-System.

Contrucci, I., Klingelhöfer, F., Perrot, J. et al., 2004. The crustal structure of the NW
    Moroccan continental margin from wide-angle and reflection seismic data. Geophysical
    Journal International, 159, 117-128.

DeMets, C., Gordon, R. G., Argus, D. F. and Stein, S., 1994, Effect of recent revisions to the
    geomagnetic reversal time scale on estimates of current plate motions. Geophysical
    Research Letters, 21, 2191-2194.

Flinch, J.F., 1993. Tectonic evolution of the Gibraltar Arc. P.h.D. Thesis. Rice University,
    Huston, Texas, USA. 450pp.

Gasperini, L. and Stanghellini, G., 2009. SEISPRHO: An interactive computer program for
    processing and interpretation of high-resolution seismic reflection profiles. Computers
    & Geosciences, 35, 1497-1507.

Geldmacher, J., Hoernle, K., Bogaard, P.v.d. et al., 2005. New ^{40}Ar/^{39}Ar age and geochemical
    data from seamounts in the Canary and Madeira volcanic provinces: Support for the
    mantle plume hypotesis Earth and Planetary Science Letters, 237, 85-101.

Geldmacher, J., and Hoernle, K., 2000, The 72 Ma geochemical evolution of the Madeira
    Hotspot (eastern North Atlantic); recycling of Paleozoic ($\leq$500 Ma) oceanic lithosphere
    Earth and Planetary Science Letters, 183, 73-92.

Gracia, E., Danobeitia, J., Verges, J., 2003. Mapping active faults offshore Portugal (368N–
    388N): Implications for seismic hazard assessment along the southwest Iberian margin.
    Geology, .31, 83–86.

Grimison, N.L., and Chen, W.P., 1986, The Azores-Gibraltar plate boundary: Focal
    mechanisms, depths of earthquakes and their tectonic implications: Journal of
    Geophysical Research, 91, 2029–2047.

Gutscher, M., The Delila and DelSis Scientific Teams, 2009, Tectonic shortening and
    gravitational spreading in the Gulf of Cadiz accretionary wedge: Observations from

multi-beam bathymetry and seismic profiling. Marine and Petroleum Geology, 26, 647-659.

Gutscher, M.A., Malod, J., Rehault, J.P., et al., 2002, Evidence for active subduction beneath Gibraltar: Geology (Boulder), 30, 1071-1074.

Gutscher, M.-A., 2004. What Caused the Great Lisbon Earthquake? Science, 305.

Hayes, D.E., Pimm, A.C., Benson, W.E., et al., 1972, Shipboard site reports, Site 135: Initial Reports of the Deep Sea Drilling Project. 14, 15-25.

Hayward, N., 1996. Marine Geophysical Study of the Eurasian-Africa Plate Boundary in the Vicinity of the Gorringe Bank. PhD thesis. Exter College & Dept. of Earth Sciences, Oxford. p. 225.

Henkart, P., 2009. Chirp Sub-Bottom Profiler Processing-A Review. Sea Technology.

Hinz, K., Winterer, E.L., Baumgartner, P.O., et al., 1982. Preliminary result from DSDP Leg 79 seaward of the Mazagan Plateau off central Morocco. In Geology of the Northwest African continental margin. Von-Rad, U., Hinz, K., Sarthein, M. and Seibold, E. (eds.). Springer-Verlag. Berlin. 1982, 22, 23.

Maldonado, A., Somoza, L., and Pallares, L., 1999, The Betic orogen and the Iberian-African boundary in the Gulf of Cadiz; geological evolution (central North Atlantic): Marine Geology. 155, 9-43.

Martinez-Solares, J.M., López Arroyo, A., 2004. The great historical 1755 earthquake:effects and damage in Spain. J. Seismol. 8, 275–294.

Medialdea, T., Vegas, R., Somoza, L., et al., 2004, Structure and evolution of the "Olistostrome" complex of the Gibraltar Arc in the Gulf of Cadiz (eastern Central Atlantic): evidence from two long seismic cross-section: Marine Geology. 209, 173-198.

Merle, R., Schrarer, U., Girardeau, J. and Corner, G., 2006. Cretaceous seamounts along the continent – ocean transition of Iberian margin; U –Pb ages and Pb – Sr – Hf isotopes. Geochemica et Cosmochimica Acta. 70, 4950 – 4976.

Mitchum, R.M., Vail, P.R. and Sangree, J.B., 1997. Stratigraphic interpretation of seimsmic reflection patterns in depositional sequences. Page 117, 133. In Payton, C.E. (ed), Seismic Stratigraphy – applications to hydrocarbon exploration. Tulsa, Oclaoma, USA. The American Association of Petroleum Geologists.

Morgan, W.J., 1981. Hotspot tracks and the opening of the Atlantic and Indian Oceans. In: The Sea: Oceanic Lithosphere (Emiliani, C., ed). 7, 443-487, John Wiley, New York.

NEAREST PROJECT http://nearest.bo.ismar.cnr.it

Payton, C.E. (ed). Seismic Stratigraphy – applications to hydrocarbon exploration. AAPG, 1977, Houston, Texas.

Pinheiro, L.M., Ivanov, M.K., Sautkin, A., et al., 2002. Mud volcanismin the Gulf of Cadiz: results from the TTR-10 cruise. Marine Geology. 3269, 1 – 21.

Purdy, G.M., 1975, The eastern end of the Azores-Gibraltar plate boundary: The Geophysical Journal of the Royal Astronomical Society, v. 43, p. 973-1000.

Rosas, F.M., Duarte, J., Terrinha, et al., 2009. Major bathymetric lineaments and soft sediment deformation in NW Gulf of Cadiz (Africa–Iberia plate boundary): new insights from high resolution multibeam bathymetry data and analogue modelling experiments. Marine Geology, 261, 33-47.

Rosenbaum, G., Lister, G.S., and Duboz, C., 2002, Relative motions of Africa, Iberia and Europe during Alpine Orogeny: Tectonophysics, v. 359, p. 117-129.

Rovere, M., Ranero, C.R., Sartori, R., Torelli, L., and Zitellini, N., 2004, Seismic images and magnetic signature of the Late Jurassic to Early Cretaceous Africa-Eurasia plate boundary off SW Iberia: Geophysical Journal International, v. 158, p. 554-568.

Rovere, M., 2002, PhD thesis, Saturazione del margine atlantico iberico ed inversione miocenica in prossimità del limite di placca Eurasia-Africa, Dip. Scienze Geologiche e Ambientali, Università di Bologna.

Ryan, W.B.F., Hsue, K.J., Cita, M.B., et al., 1973, Gorringe Bank; Site 120: Initial Reports of the Deep Sea Drilling Project, 13, Part 1, 19-41.

Sandwell, D.T. and Smith, W.H.F., 1997. Global sea floor topography from satellite altimetry and ship depth soundings. Science, 277, 1956–1962.

Sartori, R., Torelli, L., Zitellini, N., et al., 1994, Eastern segment of the Azores-Gibraltar line (central-eastern Atlantic); an oceanic plate boundary with diffuse compressional deformation: Geology (Boulder), v. 22, p. 555-558.

Schettino, A., and C. R. Scotese, 2005. Apparent polar wander paths for the major continents (200 Ma - Present Day): A paleomagnetic reference frame for global plate tectonic constructions,Geophysical Journal International, v.163(2), p. 727-759.

Searle, R., 1980. Tectonic pattern of the Azores spreading centre and triple junction, Earth and Planetary Science Letters; 51, 415 – 434.

Sawyer, D.S., Whitmarsh, R.B., Klaus, A., et al., 1994, Site 897: Proceedings of the Ocean Drilling Program, Part A: Initial Reports. 149, 41-113.

Smith, W.H.F., Sandwell, D.T., 1997. Global sea floor topography from satellite altimetry and ship depth soundings. Science. 277 (5334), 1956–1962.

Srivastava, S.P., Roest, W.R., Kovacs, L.C., et al., 1990, Motion of Iberia since the Late Jurassic; results from detailed aeromagnetic measurements in the Newfoundland Basin: Tectonophysics. 184, 229-260.

Terrinha et al, 1998. Structural Geology and Tectonic Evolution of the Algarve Basin, South Portugal. P.h.D. Thesis. Imperial College, London. 400 pp.

Van Rensbergen P., Depreiter. D., Pannemans. B., et al., 2005.The El Arraiche mud volcano field at the Moroccan Atlantic slope, GulfofCadiz. Marine Geology, 219, 1 – 17.

Whitmarsh, R.B., Beslier, M.-O., Wallace, P.J., et al., 1998, Site 1065: Proceedings of the Ocean Drilling Program, Part A: Initial Reports, 173, 65-104.

Wessel P. and Smith W.H.F., New version of the Generic Mapping Tool released, EOS Trans. AGU, p.329, 1995,

Wessel and Smith, 1998. New, improved version of the Generic Mapping Tools released. EOS Transaction. AGU, 79, 579.

Zitellini, N., Gràcia E., Matias L., et al., 2009. The quest for the Iberia-Africa Plate boundary west of Gibraltar. Earth and Planetary Science Letters. 280, 13-50.

Zitellini, N., Rovere, M., Terrinha, P., et al., 2004. Neogene through Quaternary Tectonic reactivation of SW Iberian Passive Margin. Pure and Applied Geophyscs. 161, 565–585.

Zitellini, N., Cloetingh, S., D'Oriano, F. and Burov, E., submitted. Synclinal deformation as prime expression of compressional deformation of the lithosphere: the Atlantic segment of the Iberia-Africa Plate Boundary. Geology Submitted.

Zitellini, N., Mendes, L.A., Cordoba, D., et al., 2001, Source of 1755 Lisbon earthquake and tsunami investigated: Eos, Transactions, American Geophysical Union, 82, 285.

Zitellini, N., Chierici, F., Sartori, R., and Torelli, L., 1999, The tectonic source of the 1755 Lisbon earthquake and tsunami: Annali di Geofisica, v. 42, p. 49-56.

Acknowledgements

Il primo dei tanti ringraziamenti che dovrei fare va sicuramente a Nevio Zitellini che mi ha dato l'opportunità di svolgere questo bellissimo dottorato e mi ha introdotto con passione ai segreti della Geologia Marina di cui 3 anni ero assolutamente digiuno.

Per conformità con l'incipit passo subito a ringraziare tutte le persone con cui ho avuto l'opportunità di "lavorare" a ISMAR: i mie coinstanzini Luca e Francesco e Gabri (ex coinstanzina), tutti gli altri del secondo piano e in particolare ovviamente GB e ML pietre miliari della Geologia a ISMAR e perché non *scirocco, tornado, vega, bora aldebaran* con cui mi sono divertito a impallar.

Ovviamente tutti gli amici felsinei e non e in particolare i ragazzi del corner of uncostructive criticism, quello allargato anche alle persone che non hanno potuto esserci fisicamente.

Ovviamente per ultimo ma non in ordine di importanza, un ringraziamento speciale alla mia famiglia che ho trascurato in questi anni di fortunato esilio in pianura e che non lo ha fatto pesare….
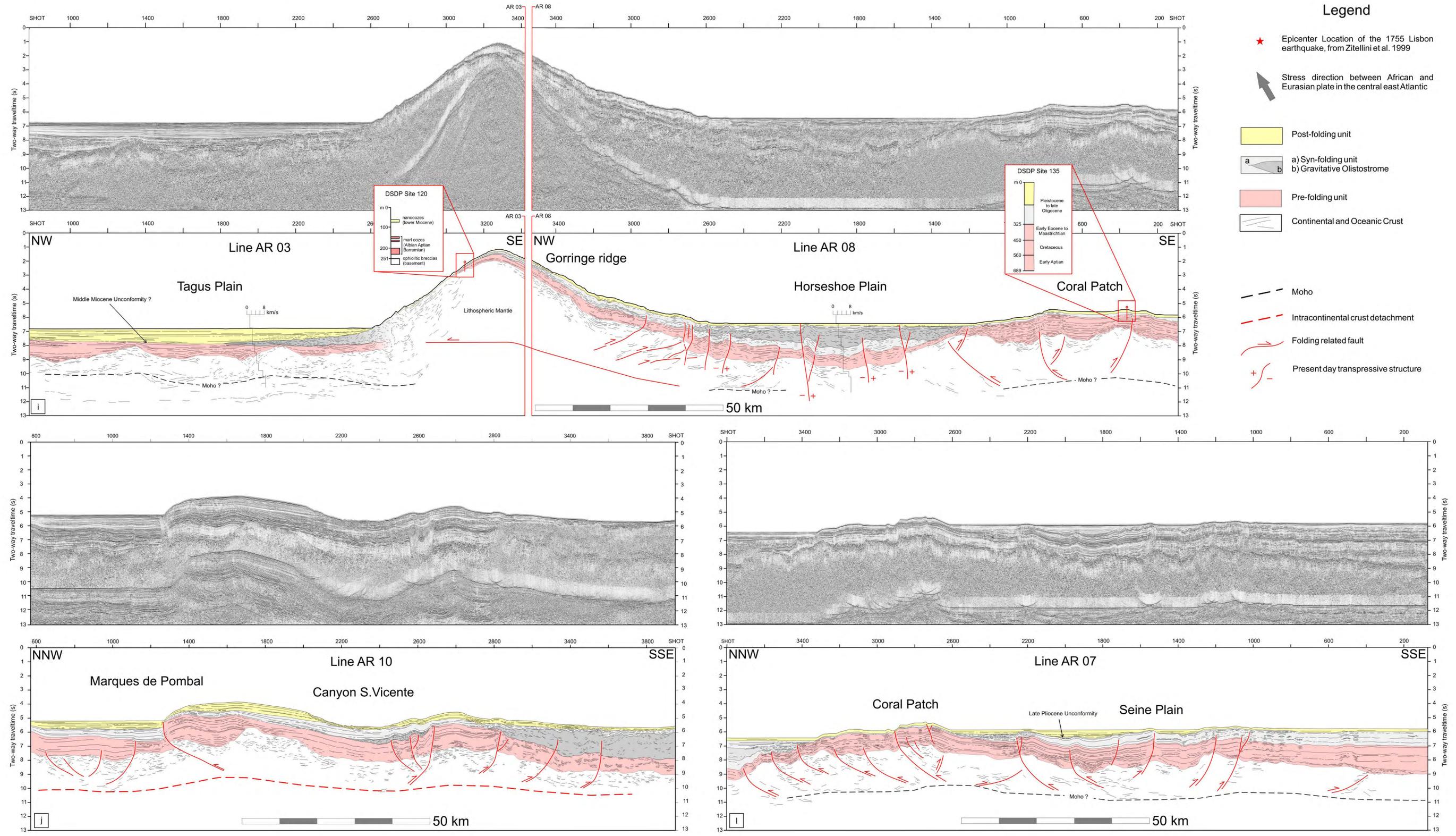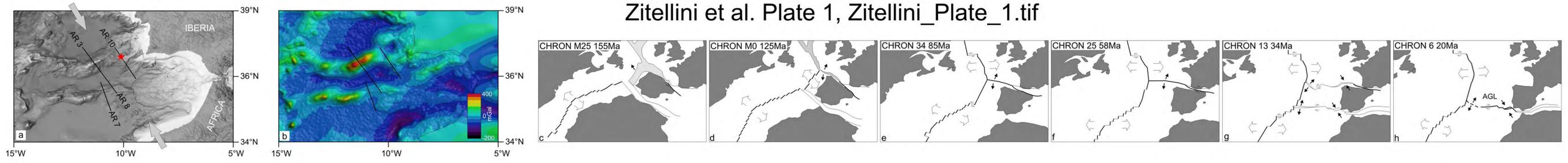
BATHYMETRY OF THE GULF OF CADIZ, NORTH-EAST ATLANTIC: THE SWIM MULTIBEAM COMPILATION

SPAIN

PORTUGAL

MOROCCO

Cadiz

Gibraltar

Lisbon Canyon

S. Vicente Canyon

Portiméo Canyon

TAGUS ABYSSAL PLAIN

GORRINGE BANK

HIRONDELLE SEAMOUNT

CORAL PATCH RIDGE

HORSESHOE ABYSSAL PLAIN

CORAL PATCH SEAMOUNT

SEINE ABYSSAL PLAIN

AMPERE SEAMOUNT

Terrain pixel size: 100 meters
Bathymetric contour lines from GEBCO digital atlas 2003
Isobath spacing: 250m (250m)
Background bathymetry from GEBCO digital atlas 2003
Coastlines and rivers from World Vector Shoreline, US National Image and Mapping Agency
Topography from SRTM 3" (Shuttle Radar Topography Mission 3 arc-second grid), NASA

Not to be used for navigation

10.3 Supplementary material of the Paper submitted to Terra Nova (see Chapter 6)
Appendix S1

	Station	Latitude	Longitude	Depth m	Type	Recovery
Coral Patch	SWIM28	34,95336	-11,91209	958/725	dredge	Sediments and volcanics
	SWIM29	34,96606	-11,95575	1011/742	dredge	Sediments and volcanics
Ormonde	SWIM32	36,74908	-11,05070	317	grab	Sediments and volcanics
	SWIM34	36,73478	-11,05161	103	grab	Volcanics

Appendix S2

Sample	Rock type	Texture	Mineralogical assemblage	Notes
CORAL PATCH				
29/1 **Microprobe analyses (EMPA)**: ol, cpx	basanite	Almost aphyric, microvesicular, intersertal	**Phenocrysts**: rare of olivine (*ol*) totally or largely pseudomorphically replaced by iddingiste and calcite, and pseudomorphs (*ps*) having the shape of feldspathoids but composed of aggregate of zeolites and carbonate. **Groundmass**: *ol*, clinopyroxene (*cpx*), *ps* (totally replaced by zeolites), dendritic crystals, brown glass	Secondary minerals (zeolite and calcite) partially or totally infill the vesicles.
29/2, 29/3, 29/4, 29/5	hyaloclastites	Basic shards totally altered to palagonite and cemented by calcite		
29/6	Granulite-facies metadiorite	Polygonal granoblastic	Plagioclase +K-feldspar +Ti-pargasite + Orthopyroxene+ Clinopyroxene + Fe-Ti oxides + Biotite	Slightly retrogressed rock (sericite, chlorite). Thin retrograde mylonitic to cataclastic shear zones.
29/7, 29/8	sediments			
ORMONDE				
32/1, 32/2, 32/3	lamprophyre (*var. monchiquite*)	Porphyric, intersertal	**Phenocrysts**: *ol*, totally pseudomorphically replaced by iddingiste and calcite; rare	Secondary minerals (zeolite and calcite)

			zoned *cpx* sometime with a greenish core. **Groundmass**: *ol, cpx, ps* (having rectangular or rounded shape and different extinction), biotite, opaques, totally altered glass.	partially or totally infill the vesicles. In sample 32/3, an ocello made of brown cpx + biotite + glass is present.
microprobe: cpx				
34 **microprobe**: cpx, k-fd, noseana, flogopite	phonolite	Porphyric, fluidal	**Phenocrysts**: rare *feldspatoids* of the sodalite group (noseana); *ps* having the shape of nephelina but replaced by zeolites; resorbed microphenocrysts of biotite. **Groundmass**: feldspar, *ps*, opaques and glass.	

Sample	29/1						
Phase	Ol	Ol	Ol	Ol	Ol	Ol	Ol
	2a8	3a6	3a7	3a9	3a10	3a14	4a1
SiO_2	39.79	39.99	39.99	40.11	40.08	51.11	39.86
TiO_2	0.00	0.00	0.11	0.05	0.04	1.65	0.00
Al_2O_3	0.00	0.04	0.06	0.02	0.03	3.08	0.04
Cr_2O_3	0.07	0.07	0.00	0.00	0.10	0.34	0.00
FeO	16.28	16.36	16.70	17.23	16.84	6.07	16.26
MnO	0.23	0.31	0.30	0.25	0.24	0.12	0.17
MgO	43.70	43.81	43.65	43.48	43.37	15.02	43.44
CaO	0.46	0.31	0.26	0.33	0.25	22.68	0.26
Na_2O	0.01	0.00	0.00	0.00	0.01	0.36	0.06
Totale	100.54	100.89	101.08	101.47	100.97	100.42	100.08
Fo%	82.50	82.41	82.06	81.59	81.90	81.23	82.50

Sample							
Phase	Ol	Ol	Ol	Ol	Ol	Ol	Ol
	5a1	5a8	5a10	5a12	6a2	6a5	6a11
SiO_2	39.49	40.48	40.25	40.04	39.48	40.74	40.58
TiO_2	0.17	0.03	0.06	0.04	0.02	0.00	0.02
Al_2O_3	0.40	0.02	0.02	0.02	0.00	0.00	0.00
Cr_2O_3	0.04	0.00	0.01	0.07	0.03	0.00	0.00
FeO	17.54	17.31	16.01	16.23	16.66	16.72	16.48
MnO	0.22	0.25	0.16	0.27	0.29	0.20	0.22
MgO	42.43	43.01	43.90	43.90	43.49	43.41	43.72
CaO	0.34	0.28	0.24	0.29	0.35	0.28	0.26
Na_2O	0.02	0.05	0.04	0.00	0.00	0.00	0.00
Totale	100.67	101.44	100.70	100.86	100.33	101.35	101.29
Fo%	80.98	81.36	82.87	82.58	82.06	82.05	82.35

Seamount: Ormonde

Sample 32/1

Phase	cpx	cpx	cpx	cpx	cpx	cpx	cpx	cpx	cpx	cpx	cpx
	2b1	2b2	2b3	2b4	2b7	2b9	4b2	4b3	4b5	4b6	4b7
SiO_2	47.04	46.00	46.14	46.61	47.47	46.48	52.63	50.55	51.92	42.43	48.76
TiO_2	2.93	3.24	3.59	3.62	2.76	2.98	0.71	1.50	0.99	4.78	2.30
Al_2O_3	6.36	7.28	6.95	6.97	6.21	6.39	2.54	4.65	3.33	9.39	5.16
Cr_2O_3	0.00	0.06	0.05	0.00	0.07	0.04	0.41	0.60	0.07	0.05	0.02
FeO	6.67	7.21	6.38	5.92	6.75	6.92	7.22	5.97	6.16	7.67	6.29
Mno	0.13	0.12	0.07	0.08	0.08	0.05	0.29	0.09	0.17	0.21	0.25
MgO	13.34	12.31	12.71	12.79	12.91	13.14	12.95	13.24	14.58	11.65	13.84
CaO	24.33	23.26	24.27	24.38	23.91	24.04	22.70	23.35	23.29	23.82	24.23
Na_2O	0.31	0.66	0.32	0.38	0.41	0.30	1.26	0.79	0.77	0.48	0.47
K_2O	0.03	0.00	0.03	0.00	0.00	0.00	0.00	0.00	0.00	0.00	0.00
Totale	101.14	100.14	100.50	100.75	100.57	100.34	100.70	100.73	101.27	100.49	101.32
Wo	50.01	49.28	51.10	51.33	49.94	49.82	46.69	48.78	46.79	50.80	49.20
En	38.15	36.27	37.22	37.47	37.52	37.87	37.05	38.50	40.76	34.56	39.12
Fs	10.70	11.93	10.48	9.74	11.00	11.19	11.59	9.74	9.65	12.77	9.97

Sample 32/2

Phase	cpx	cpx	cpx	cpx	cpx	cpx
	1d3	322s9	322s10	322s11	322s13	322s14
SiO_2	46.44	47.21	39.57	51.83	50.97	47.46
TiO_2	2.61	2.78	6.01	1.33	1.83	2.17
Al_2O_3	5.92	6.07	11.04	2.58	3.36	5.92
Cr_2O_3	0.04	0.02	0.00	0.05	0.00	0.00
FeO	6.11	6.04	8.00	6.20	7.09	12.38
Mno	0.11	0.14	0.06	0.28	0.16	0.29
MgO	13.44	13.69	10.50	14.08	13.63	8.94
CaO	24.35	23.71	23.49	23.52	23.77	22.00
Na_2O	0.24	0.32	0.41	0.73	0.69	1.61
K_2O	0.01	0.03	0.03	0.03	0.01	0.00
Totale	99.27	100.00	99.11	100.63	101.51	100.78
Wo	50.46	49.36	52.10	47.74	48.00	46.80
En	38.75	39.64	32.41	39.76	38.29	26.45
Fs	9.88	9.81	13.86	9.83	11.18	20.56

Sample 32/3

Phase	cpx	cpx	cpx	cpx	cpx	cpx	cpx	cpx	cpx	cpx	cpx	cpx	cpx	cpx
	3a1	3a2	3a3	3a4	3a5	3a6	3a9	3a17	3a19	3a23	3a24	3a25	3a26	3a28
SiO_2	51.25	48.27	48.59	46.53	45.48	46.67	46.48	43.45	46.20	47.04	49.70	49.43	49.65	46.63
TiO_2	1.19	2.33	2.19	3.35	3.04	2.61	2.94	4.27	2.72	2.44	1.78	1.75	1.79	2.54
Al_2O_3	2.44	4.86	4.42	5.76	6.56	5.77	6.21	8.24	6.04	6.92	4.33	4.61	4.52	6.70
Cr_2O_3	0.08	0.05	0.01	0.00	0.01	0.06	0.00	0.00	0.07	0.06	0.07	0.06	0.11	0.22
FeO	6.24	7.17	7.36	6.22	6.52	6.21	6.41	6.44	6.94	5.89	5.80	5.81	5.95	6.49
Mno	0.19	0.06	0.26	0.10	0.10	0.13	0.10	0.10	0.07	0.13	0.07	0.08	0.11	0.04
MgO	14.57	13.73	12.94	13.26	13.19	13.78	13.17	12.20	13.40	12.61	14.03	14.26	14.27	12.89
CaO	23.21	23.65	23.29	23.77	24.38	24.50	24.16	24.03	23.91	23.70	23.85	23.72	23.38	23.21
Na_2O	0.61	0.37	0.70	0.38	0.27	0.36	0.28	0.42	0.30	0.70	0.55	0.54	0.47	0.75
K_2O	0.00	0.00	0.01	0.00	0.00	0.00	0.03	0.02	0.00	0.01	0.02	0.00	0.00	0.00
Totale	99.78	100.51	99.77	99.37	99.55	100.08	99.77	99.17	99.65	99.50	100.20	100.27	100.25	99.46
Wo	46.92	48.24	48.21	49.78	50.46	49.84	50.34	51.36	49.28	50.32	48.78	48.32	47.98	48.80
En	40.98	38.97	37.27	38.63	37.99	38.99	38.19	36.27	38.43	37.25	39.92	40.43	40.75	37.71
Fs	9.85	11.42	11.90	10.17	10.53	9.86	10.43	10.74	11.17	9.75	9.26	9.24	9.54	10.65

Seamount: Coral Patch

Sample 29/1

Phase	cpx	cpx	cpx	cpx	cpx	cpx	cpx	cpx	cpx	cpx	cpx	cpx	cpx	cpx
	b	1a1	1a2	1a3	1a5	1a6	1a8	2a5	2a10	2a11	3a1	3a2	3a4	3a5	3a13
SiO_2	42.56	41.08	41.84	41.31	41.88	42.71	41.55	41.47	40.60	44.68	41.93	42.08	47.48	41.23	42.19
TiO_2	5.48	6.48	5.16	6.20	5.02	5.31	5.56	5.29	5.38	3.90	5.24	5.17	2.63	5.38	5.32
Al_2O_3	9.37	10.20	9.53	10.01	9.91	8.84	9.79	9.53	10.10	7.17	9.21	9.15	5.79	9.44	8.86
Cr_2O_3	0.01	0.01	0.11	0.11	0.00	0.05	0.03	0.05	0.05	0.07	0.01	0.05	0.39	0.00	0.15
FeO	9.66	9.72	10.41	9.52	9.87	9.13	10.25	10.35	10.40	9.20	10.47	9.14	6.90	11.40	9.35
Mno	0.21	0.10	0.16	0.13	0.15	0.11	0.11	0.12	0.11	0.12	0.12	0.12	0.15	0.10	0.10
MgO	10.51	9.90	10.14	10.18	10.02	10.79	10.04	10.07	9.65	12.31	10.19	10.45	13.34	9.69	10.87
CaO	22.10	22.08	21.94	22.00	22.18	22.22	21.57	21.56	22.22	22.12	21.67	22.25	22.97	21.43	22.03
Na_2O	0.44	0.56	0.64	0.56	0.59	0.58	0.65	0.61	0.53	0.53	0.59	0.61	0.33	0.69	0.58
K_2O	0.02	0.04	0.01	0.00	0.03	0.00	0.00	0.00	0.03	0.01	0.02	0.00	0.00	0.00	0.03
Totale	100.36	100.18	99.94	100.02	99.66	99.75	99.60	99.05	99.10	100.11	99.46	99.02	99.94	99.40	99.49
Wo	49.04	49.68	48.42	49.31	49.41	48.91	48.24	48.18	49.68	46.67	48.06	49.41	48.34	47.57	48.40
En	32.45	30.99	31.12	31.75	31.06	33.07	31.25	31.32	30.02	36.14	31.44	32.29	39.08	29.92	33.24
Fs	16.73	17.07	17.92	16.66	17.17	15.69	17.89	18.05	18.15	15.15	18.12	15.85	11.33	19.76	16.04

Sample

Phase	cpx	cpx	cpx	cpx	cpx	cpx	cpx	cpx	cpx	cpx	cpx	cpx	cpx
	4a2	4a3	5a3	5a11	5a14	5a15	5a16	6a1	6a8	6a9	291s2	291s4	291s5
SiO_2	44.16	41.34	41.94	45.96	43.05	42.30	42.18	42.84	41.72	42.06	40.22	41.19	45.19
TiO_2	4.00	5.80	5.70	3.44	5.34	5.25	5.43	5.22	5.56	5.56	5.92	5.89	3.83
Al_2O_3	8.19	9.34	9.82	7.18	8.85	9.52	9.20	9.03	10.34	9.50	9.94	9.69	6.86
Cr_2O_3	0.10	0.00	0.01	0.30	0.08	0.01	0.02	0.00	0.00	0.04	0.01	0.00	0.30
FeO	9.03	10.15	10.11	7.76	8.91	10.24	9.26	9.68	9.40	10.91	11.24	10.71	8.12
Mno	0.15	0.14	0.03	0.08	0.08	0.08	0.12	0.18	0.02	0.13	0.08	0.15	0.08
MgO	11.67	10.02	10.04	12.57	11.00	9.98	10.56	10.34	10.27	9.85	9.48	9.76	12.73
CaO	21.79	21.95	22.22	22.77	21.97	21.87	21.75	22.45	22.30	22.02	21.88	21.75	21.95
Na_2O	0.44	0.54	0.58	0.44	0.60	0.58	0.48	0.62	0.59	0.51	0.63	0.62	0.50

K$_2$O	0.00	0.02	0.00	0.02	0.03	0.06	0.02	0.00	0.00	0.00	0.02	0.02	0.00
Totale	99.51	99.30	100.56	100.46	99.90	99.87	99.03	100.35	100.39	100.59	99.42	99.78	99.59
Wo	47.51	49.00	49.24	48.34	48.49	48.83	48.83	49.32	49.57	48.74	48.65	48.54	46.79
En	35.40	31.13	30.95	37.12	33.77	31.00	32.98	31.60	31.76	30.35	29.32	30.30	37.76
Fs	15.36	17.68	17.49	12.86	15.35	17.84	16.22	16.61	16.31	18.86	19.51	18.65	13.51

Seamount Ormonde

Sample	34	
Phase	Noseana	Noseana
SiO2	36.82	37.55
TiO2	0.00	0.00
Al2O3	33.30	33.97
Cr2O3	0.00	0.00
FeO	0.12	0.18
MnO	0.00	0.01
MgO	0.00	0.03
CaO	2.32	1.98
Na2O	18.90	17.86
K2O	0.77	0.62
SO3	6.96	6.73
Totale	99.19	98.93

Seamount: Ormonde

Sample	34				
Phase	flogopite	flogopite	flogopite	flogopite	flogopite
SiO2	35.28	34.63	34.74	35.52	35.47
TiO2	4.88	4.78	4.63	4.52	4.42
Al2O3	13.00	13.09	13.05	12.73	12.93
Cr2O3	0.00	0.05	0.00	0.00	0.01
FeO	24.16	23.68	24.44	23.40	23.40
MnO	1.07	1.03	1.09	0.95	0.86
MgO	8.62	8.49	8.65	8.83	8.70
CaO	0.00	0.01	0.04	0.02	0.00
Na2O	0.59	0.62	0.52	0.50	0.59
K2O	8.37	8.34	8.34	8.16	8.28
SO3					
Totale	95.97	94.72	95.50	94.63	94.86

Sample	34		
Phase	K-fd	K-fd	K-fd
	microlite	microlite	microlite
SiO_2	67.69	65.06	66.95
TiO_2	0.00	0.09	0.00
Al_2O_3	18.83	19.11	18.64
Cr_2O_3	0.00	0.02	0.00
FeO	0.39	1.17	0.42
MnO	0.02	0.01	0.06
MgO	0.03	0.36	0.01
CaO	0.11	0.11	0.12
Na_2O	5.77	5.29	5.95
K_2O	7.70	7.02	7.32
Totale	100.53	98.25	99.46
Ab %	52.96	53.06	54.90

An %	0.55	0.59	0.63
Or %	46.49	46.35	44.48

APPENDIX: ^{40}Ar-^{39}Ar DATING

Samples

Three samples were considered for ^{40}Ar-^{39}Ar dating: a lava block from Coral Patch seamount (SWIM04-29/1) and two small volcanic fragments from Ormonde seamount (SWIM04-32/3 and SWIM04-34). Coral Patch lava is heavily altered and full of empty cavities. The sample was cut in slices and the less altered inner parts were chosen for grinding, sieving and ground mass separation. The fraction chosen for the analysis (>180 μm) was leached in ultrasonic bath at 30 °C with HCl 3.5N (60 minutes) and HNO$_3$ 1N (60 minutes) and then thoroughly washed with deionised water. Biotites of Ormonde seamount samples were separated with conventional magnetic and gravimetric methods followed by hand picking. SWIM04-34 biotites appeared fresh, while the few biotite crystals obtained from SWIM04-32/3 were relatively dirty. Biotites were washed with methanol and de-ionized water in ultrasonic bath.

Method

Samples were packed in Al foil and piled in a quartz tube along with multiple samples of the neutron fluence monitor FCT sanidine (28.03 Ma, Jourdan & Renne, 2007). The package was irradiated for 8 hours in the core of the 250 kW TRIGA reactor of Pavia University.

All samples were step-heated (SH) and single crystals total fusion (SCTF) experiments were performed on both micas. In step-heating experiments the defocused beam of a diode-pumped Nd-YAG infra-red (IR) continuous wave laser was used as heating device at progressively higher power levels. The defocused laser beam passed through a faceted lens that produces an even spatial distribution of the beam power. When the laser beam surface was smaller than the sampled area, the beam was slowly rastered over the entire sample. The evolved gas was cleaned with two SAES AP10 getters held at ~400 °C and one SAES GP50 getter held at room temperature. Argon was measured with a Mass Analyser Products (MAP) 215-50 mass spectrometer, operated in electron multiplier mode. System blanks were measured every two-four analyses. The mass discrimination was monitored using an on-line air pipette. The steps ages were corrected for system blanks, mass discrimination, radioactive decay of ^{37}Ar and ^{39}Ar and nuclear interferences through the ArArCALC software (Koppers, 2002) (see the Analytical Table). ^{40}Ar-^{39}Ar plateau ages were calculated on at least three consecutive steps that yield concordant ages at the 2σ level. In fact these samples never satisfy the criterion of Fleck et al. (1977) that requires at least 50% of the total K-derived ^{39}Ar for a reliable plateau and their age computation is discussed below. Unlike plateau ages, where an atmospheric initial isotopic ratio is assumed, isochron ages calculations correct for

the initial ^{40}Ar/^{36}Ar ratio of the system, whichever its value. Isochron ages were calculated using ISOPLOT (Ludwig, 2003).

Results

SWIM04-29/1 ground mass displays a disturbed age spectrum, with older ages at low laser power (i.e. temperature) and younger ages at higher temperatures. The K/Ca shows a monotonic decrease from the second step, compatible with the progressive degassing of pyroxene. The only K-bearing phase in the sample is glass (see main text for further discussion).

SWIM04-32/3 mica SH analysis was performed on a population of variable grain-size and limited weight (~1 mg). The sample displays a slightly disturbed age spectrum, with apparent ages slowly decreasing towards higher laser powers (i.e. temperatures) (Fig. 1). The majority of the age spectrum is also characterized by relatively low K/Ca ratios for a biotite. Five steps, equivalent to 41.7 % of ^{39}Ar release give a weighted plateau age of 64.02±0.48 Ma (MSWD=2.6), and K/Ca ratios varying from 23 to 7. The same steps identify an isochron age of 63.31±0.87 Ma (MSWD=1.3), with a poorly defined initial ^{36}Ar/^{40}Ar intercept (453±180) (Fig. 1). The limited amount of ^{39}Ar release and the overall shape of the age spectrum question the validity of the obtained age.
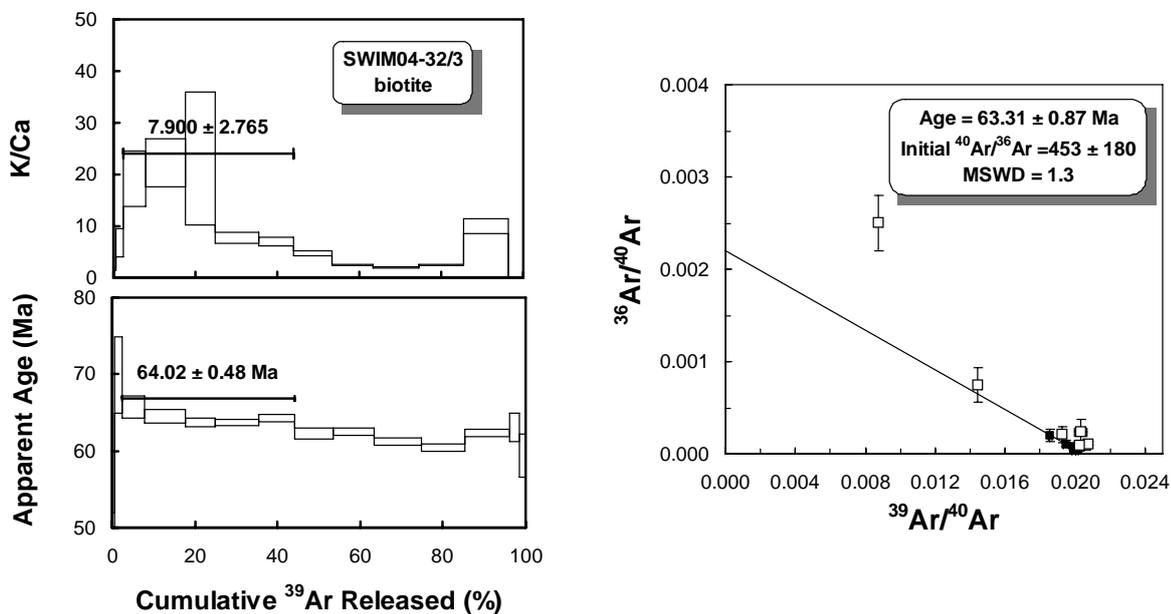
Fig. 1. SWIM04-32/3- Left: age and K/Ca spectrum. Error boxes are ± 2 σ. The horizontal bar indicates the steps used to calculate the plateau age and the average K/Ca ratio. Right: Isotope correlation diagram: solid squares represent the plateau steps and have been used to calculate the isochron age, empty squares are all the other points.

The four single crystal total fusion analyses might suggest an explanation for the age spectrum shape, although the data are affected by high uncertainties due to the low analytical signal. Two crystals have almost no Ca, high [40]Ar radiogenic yields (>95%) and ages of 63-64 Ma; two crystals have K/Ca ratios <1, lower [40]Ar radiogenic yields (66-88%) and younger ages (~ 58 Ma). The shape of the SH age spectrum might derive by the mixing of two population of micas, an older pristine one, and a younger altered one. The yield of the overall sample (95.7 %, see the Analytical Table) allows to consider that pristine micas prevail in the analysed population. The isochron age of 63.31±0.87 Ma is considered the best estimate of the age of this sample.

SWIM04-34 mica SH analysis evidences a flattish age spectrum, with an overall plateau age hampered by a low age intermediate temperature step (1.3 W). Two mini-plateau are calculated on steps 1-8, 64.03±0.39 Ma (MSWD=1.8, 45.8 % of [39]Ar release) and steps 10-14, 64.07±0.32 Ma (MSWD=1.39, 44.9 % of [39]Ar release) (Fig. 2). The data obtained on the two groups of steps are equivalent and overlap within error to the integrated age of 63.95±0.25 Ma. All data points identify an isochron 63.85±0.61 Ma (MSWD=2.0, initial [36]Ar/[40]Ar intercept =286±26) (Fig. 2).
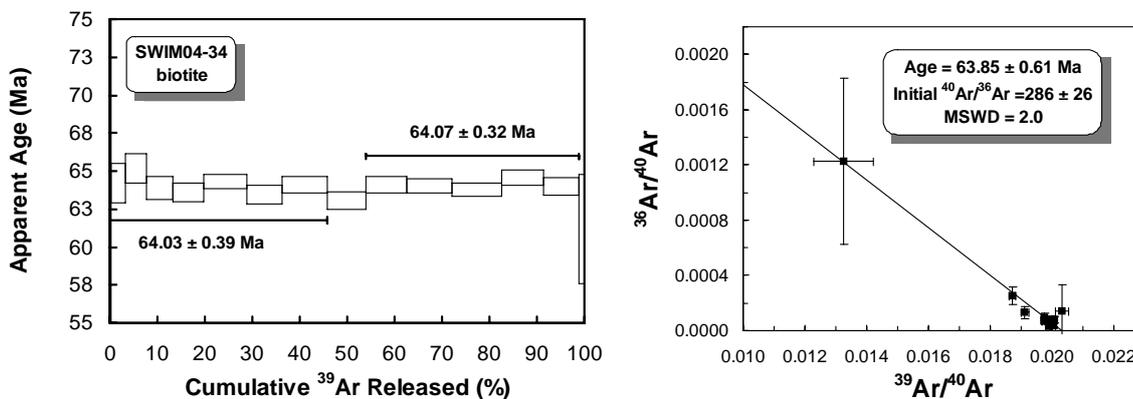
Fig. 2. SWIM04-34- Left: age spectrum. Right: Isotope correlation diagram. Legend as in figure 1.

Eight SCTF analyses on relatively big crystals of SWIM04-34 evidence the presence of a unique population, with a weighted average age of 64.18±0.42 Ma (Fig. 3) (see main text). Both SH and SCTF analyses of this biotite give concordant ages and the isochron age is chosen as more representative.
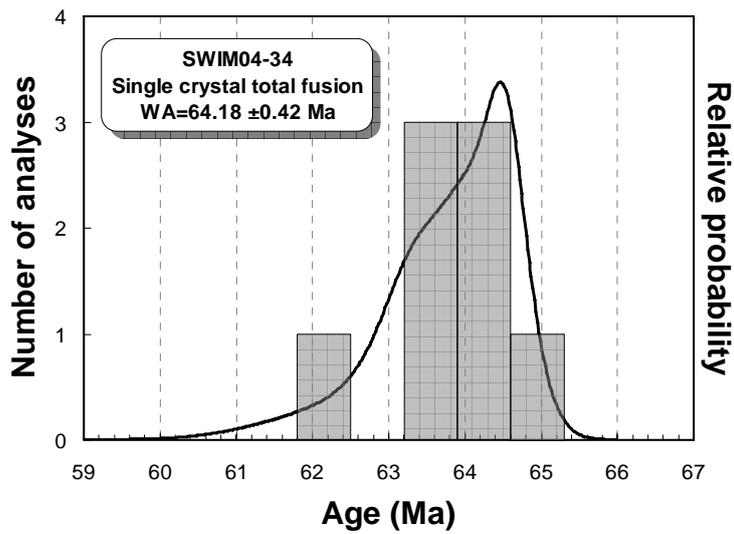
Fig. 3. SWIM04-34. Age probability plot of single crystal laser total fusion experiments.WA= Weighted Average.

References

Fleck, R.J., Sutter J.F., Elliot D.H., 1977. Interpretation of discordant [40]Ar/[39]Ar age-spectra of Mesozoic tholeiites from Antarctica. *Geochimica et Cosmochimica Acta,* **41**, 15-32.

Jourdan, F. & Renne, P.R. (2007). Age calibration of the Fish Canyon sanidine [40]Ar/[39]Ar dating standard using primary K-Ar standards. *Geochimica et Cosmochimica Acta,* **71**, 387-402.

Koppers, A.A.P., 2002. ArArCALC – software for [40]Ar/[39]Ar age calculations. *Computers & Geosciences*, **28**, 605-619.

Ludwig, K.R., 2003. Isoplot 3.00. A geochronological Toolkit for Microsoft Excel. *Berkeley Geochronology Center Special Publication*, 4, 71 pp.

Analytical Table

Legend: Argon isotopes are in moles.

Steps used to calculate plateau and isochron ages are in bold. SH= Step-heating analysis; SCTF= Single crystal laser fusion analysis.

Columns headings are as follows: $^{36}Ar_{(atm)}$ = atmospheric ^{36}Ar; $^{38}Ar_{(Cl)}$ = Cl-derived ^{38}Ar; $^{39}Ar_{(K)}$ = K-derived ^{39}Ar; $^{40}Ar_{(rad)}$ = radiogenic ^{40}Ar; $^{40}Ar_{(rad)}(\%)$ = percentual ratio of radiogenic ^{40}Ar over total ^{40}Ar.

Total fusion age is calculated summing the isotopic measurements of all steps, and its error includes uncertainty on J value. Errors quoted for individual analyses ages include analytical error only.

SWIM04-32/3 biotite SH   J=0.0007318±0.0000011 (±1σ)

Laser power W	$^{36}Ar_{(atm)}$	$^{37}Ar_{(Ca)}$	$^{38}Ar_{(Cl)}$	$^{39}Ar_{(K)}$	$^{40}Ar_{(rad)}$	$^{39}Ar_{(K)}$ %	Age Ma	± 2σ	$^{40}Ar_{(rad)}$ %	K/Ca	± 2σ
0.2	1.64E-17	1.80E-17	6.79E-19	5.76E-17	1.71E-15	0.63	38.82	13.14	26.1	1.70	0.29
0.4	8.14E-18	1.21E-17	1.40E-18	1.56E-16	8.44E-15	1.71	69.93	5.01	77.8	6.84	2.72
0.6	**5.49E-18**	**1.41E-17**	**1.36E-18**	**5.08E-16**	**2.57E-14**	**5.57**	**65.69**	**1.47**	**94.1**	**19.14**	**5.27**
0.75	**4.63E-18**	**2.10E-17**	**1.91E-18**	**8.83E-16**	**4.39E-14**	**9.68**	**64.54**	**0.88**	**97.0**	**22.29**	**4.64**
0.9	**1.35E-18**	**1.51E-17**	**2.22E-18**	**6.54E-16**	**3.21E-14**	**7.18**	**63.70**	**0.55**	**98.8**	**23.03**	**12.81**
1.05	**3.87E-18**	**6.53E-17**	**3.20E-18**	**9.60E-16**	**4.72E-14**	**10.53**	**63.75**	**0.44**	**97.6**	**7.80**	**1.07**
1.2	**1.75E-18**	**6.01E-17**	**3.30E-18**	**7.95E-16**	**3.94E-14**	**8.71**	**64.29**	**0.54**	**98.7**	**7.01**	**0.91**
1.35	3.72E-18	9.66E-17	4.05E-18	8.60E-16	4.13E-14	9.44	62.29	0.66	97.4	4.72	0.40
1.55	3.65E-18	1.87E-16	4.40E-18	9.01E-16	4.35E-14	9.88	62.58	0.47	97.6	2.55	0.17
1.7	4.93E-18	2.62E-16	4.78E-18	1.03E-15	4.86E-14	11.31	61.21	0.51	97.1	2.08	0.10
1.9	5.35E-18	2.08E-16	3.76E-18	9.83E-16	4.58E-14	10.78	60.41	0.47	96.6	2.51	0.14
2.2	4.49E-18	5.25E-17	3.19E-18	9.84E-16	4.73E-14	10.79	62.37	0.52	97.3	9.93	1.43
2.5	2.40E-18	b.d.l.	9.46E-19	2.20E-16	1.07E-14	2.41	63.14	1.85	93.8	n.d.	
fuse	1.47E-18	b.d.l.	1.47E-19	1.25E-16	5.71E-15	1.37	59.41	2.77	92.9	n.d.	
TF							62.80	0.29	95.7	4.78	0.20

SWIM04-32/3 biotite SCTF   J=0.0007318±0.0000011 (±1σ)

# ID	$^{36}Ar_{(atm)}$	$^{37}Ar_{(Ca)}$	$^{38}Ar_{(Cl)}$	$^{39}Ar_{(K)}$	$^{40}Ar_{(rad)}$	Age Ma	± 2σ	$^{40}Ar_{(rad)}$ %	K/Ca	± 2σ
Fuse	3.52E-18	1.07E-16	9.18E-19	1.77E-16	7.88E-15	57.96	2.99	88.3	0.87	0.10
Fuse	3.45E-18	1.01E-16	3.71E-19	4.41E-17	1.98E-15	58.31	13.3	66.1	0.23	0.04
Fuse	1.40E-18	2.19E-18	5.89E-19	1.69E-16	8.20E-15	62.86	3.12	95.2	40.94	208.58
Fuse	1.08E-18	b.d.l.	7.87E-19	3.49E-16	1.72E-14	63.97	1.6	98.2	n.d	

SWIM04-34 biotite SH   J=0.0007318±0.0000011 (±1σ)

Laser power W	$^{36}Ar_{(atm)}$	$^{37}Ar_{(Ca)}$	$^{38}Ar_{(Cl)}$	$^{39}Ar_{(K)}$	$^{40}Ar_{(rad)}$	$^{39}Ar_{(K)}$ %	Age Ma	± 2σ	$^{40}Ar_{(rad)}$ %	K/Ca	± 2σ
0.3	**3.36E-18**	**3.48E-18**	**1.43E-19**	**3.64E-17**	**1.75E-15**	**0.21**	**62.51**	**17.73**	**63.8**	**5.54**	**10.58**
0.5	**7.07E-18**	**b.d.l.**	**1.86E-18**	**5.29E-16**	**2.62E-14**	**3.09**	**64.21**	**1.33**	**92.6**	**n.d.**	
0.65	**5.02E-18**	**b.d.l.**	**1.50E-18**	**7.34E-16**	**3.69E-14**	**4.28**	**65.17**	**0.95**	**96.1**	**n.d.**	

0.8	4.52E-18	b.d.l.	3.01E-18	9.61E-16	4.73E-14	5.61	63.86	0.75	97.2	n.d.
0.9	4.26E-18	b.d.l.	2.70E-18	1.14E-15	5.60E-14	6.66	63.6	0.63	97.8	n.d.
1	5.46E-18	b.d.l.	4.23E-18	1.53E-15	7.58E-14	8.92	64.32	0.49	97.9	n.d.
1.1	4.64E-18	b.d.l.	3.88E-18	1.27E-15	6.21E-14	7.41	63.45	0.64	97.8	n.d.
1.2	6.82E-18	b.d.l.	4.02E-18	1.65E-15	8.14E-14	9.61	64.1	0.52	97.6	n.d.
1.3	5.58E-18	b.d.l.	3.43E-18	1.39E-15	6.78E-14	8.14	63.07	0.56	97.6	n.d.
1.4	4.13E-18	b.d.l.	3.86E-18	1.46E-15	7.21E-14	8.51	64.12	0.55	98.3	n.d.
1.55	3.34E-18	b.d.l.	4.06E-18	1.67E-15	8.24E-14	9.74	64.02	0.45	98.8	n.d.
1.7	4.37E-18	b.d.l.	1.66E-18	1.77E-15	8.69E-14	10.32	63.8	0.43	98.5	n.d.
1.9	2.60E-18	b.d.l.	4.21E-18	1.51E-15	7.52E-14	8.82	64.57	0.51	99.0	n.d.
2.2	3.78E-18	b.d.l.	3.46E-18	1.29E-15	6.38E-14	7.55	63.97	0.57	98.3	n.d.
fuse	1.33E-18	b.d.l.	5.81E-19	1.89E-16	8.93E-15	1.11	61.18	3.61	95.8	n.d.
TF							63.95	0.25	97.7	

SWIM04-34 biotite SCTF   J=0.0007318±0.0000011 (±1σ)

# ID	$^{36}Ar_{(atm)}$	$^{37}Ar_{(Ca)}$	$^{38}Ar_{(Cl)}$	$^{39}Ar_{(K)}$	$^{40}Ar_{(rad)}$	Age Ma	± 2σ	$^{40}Ar_{(rad)}$ %
Fuse	2.66E-18	b.d.l.	9.03E-19	2.55E-16	1.25E-14	63.55	1.36	94.1
Fuse	3.02E-18	b.d.l.	2.58E-18	1.05E-15	5.25E-14	64.53	0.45	98.3
Fuse	1.75E-18	b.d.l.	1.21E-18	5.97E-16	2.92E-14	63.43	0.77	98.2
Fuse	2.03E-18	b.d.l.	1.94E-18	7.26E-16	3.59E-14	64.01	0.60	98.3
Fuse	1.47E-18	b.d.l.	b.d.l.	1.94E-16	9.34E-15	62.41	1.94	95.5
Fuse	2.12E-18	b.d.l.	1.74E-18	4.37E-16	2.18E-14	64.63	0.69	97.2
Fuse	1.51E-18	b.d.l.	8.47E-19	3.22E-16	1.57E-14	63.41	1.16	97.2
Fuse	1.43E-18	b.d.l.	3.93E-18	1.14E-15	5.67E-14	64.43	0.70	99.2

SWIM29/1 g.m.   J=0.0007318±0.0000011 (±1σ)

Laser power W	$^{36}Ar_{(atm)}$	$^{37}Ar_{(Ca)}$	$^{38}Ar_{(Cl)}$	$^{39}Ar_{(K)}$	$^{40}Ar_{(rad)}$	$^{39}Ar_{(K)}$ %	Age Ma	± 2σ	$^{40}Ar_{(rad)}$ %	K/Ca	± 2σ
0.2	1.29E-16	1.59E-16	4.97E-18	1.75E-16	7.25E-15	9.76	53.87	7.06	16.0	0.5840	0.0799
0.4	6.02E-17	1.35E-16	7.23E-18	1.92E-16	6.31E-15	10.69	42.97	6.09	26.2	0.7529	0.0854
0.55	1.08E-17	1.33E-16	1.57E-17	1.44E-16	6.42E-15	8.06	57.77	3.35	66.8	0.5734	0.0818
0.7	9.95E-18	4.93E-16	3.30E-17	2.35E-16	9.30E-15	13.12	51.46	1.81	76.0	0.2527	0.0209
0.85	9.49E-18	9.26E-16	2.77E-17	2.30E-16	8.78E-15	12.85	49.61	1.69	75.8	0.1318	0.0100
1	8.88E-18	2.00E-15	1.96E-17	2.49E-16	7.52E-15	13.90	39.41	2.19	74.1	0.0660	0.0047
1.15	9.45E-18	2.43E-15	9.85E-18	1.66E-16	4.02E-15	9.25	31.69	3.19	59.0	0.0362	0.0024
1.3	6.46E-18	2.61E-15	4.36E-18	1.05E-16	2.60E-15	5.85	32.44	3.71	57.6	0.0213	0.0015
1.6	6.57E-18	4.84E-15	4.84E-18	1.21E-16	2.76E-15	6.73	29.94	5.31	58.7	0.0132	0.0009
2	5.75E-18	1.31E-14	4.94E-18	1.17E-16	2.76E-15	6.55	30.76	4.47	61.9	0.0048	0.0003
fuse	4.17E-18	6.03E-14	3.82E-18	5.79E-17	2.59E-15	3.23	58.13	24.55	67.7	0.0005	0.0001
TF							43.88	1.45	43.9	0.011	0.001

Age monitor for the second set of samples: FCT sanidine, 28.03 Ma (Jourdan & Renne, 2007).
The correction factors for reactor induced interfering reactions were: $^{39}Ar/^{37}Ar$ (Ca) = 0.00075 ± 0.000075; $^{36}Ar/^{37}Ar$ (Ca) = 0.00024 ± 0.00002; $^{40}Ar/^{39}Ar$ (K) = 0.00925 ± 0.0009.

APPENDIX S5

Coral Patch Seamount

Vince volcano

W12°

W11°40'

N35°20'   W11°

D'Oriano et al., Appendix S5 Supplementary Material

3D shaded relief of the Coral Patch Seamount, vertical exageration 10X, view from NE to SW. Note the Vince volcano in the East part and the coalescent smaller volcanic edifices in the shallow part.